

# The Prodiabatic Elimination: A Method Beyond the Adiabatic Elimination

Master Thesis



University of Basel  
Department of Physics

submitted by  
Jan Neuser  
February 2025

Supervisors  
Marcelo Janovitch  
Dr. Matteo Brunelli  
Prof. Patrick P. Potts

## Abstract

Solving nonlinear coupled differential equations is often challenging and, in some cases, even impossible. Consequently, rather than pursuing exact solutions, it is common to focus on obtaining reliable approximations. In the field of open quantum systems, the method of adiabatic elimination is a well-established approach to obtain such an approximation. This thesis introduces the *prodiabatic elimination*, a novel technique designed to extend beyond the limitations of the adiabatic elimination. To establish a testing field, we consider a driven cavity that is linearly coupled to a two-level system, described by the driven Jaynes-Cummings Hamiltonian. Additionally, both the cavity and the two-level system are subject to dissipation, where we model the overall dynamics by a Lindblad master equation. In the adiabatic elimination, the dynamics are solved in the two-level subspace and subsequently mapped to the cavity. While this approach is relatively straightforward, it also has inherent limitations. Primarily, it is unable to account for the initial dynamics and cannot incorporate higher-order corrections. The prodiabatic elimination simplifies the formal solution through the application of a Taylor expansion to the adiabatically eliminated cavity operator, resulting in an approach analogous to the adiabatic elimination, but including higher-order effects. Compared to the adiabatic elimination, a notable enhancement in the accuracy of the  $g^{(2)}$ -function and various other quantities could be observed. In addition, we investigated how standard perturbation techniques perform on this problem, using the method of multiple scales. While the method can include initial conditions and higher-order corrections, the required calculations are tedious and do not consistently outperform the adiabatic elimination. The prodiabatic elimination offers a stepping stone for future research, potentially enabling more precise control and understanding of quantum systems in diverse scenarios.

## **Acknowledgments**

I want to thank everyone who supported me in any way during the composition of this thesis. Firstly, I would like to thank my supervisors, Patrick P. Potts, Marcelo Janovitch, and Matteo Brunelli. Not only did they make this project possible, but they also taught me how to approach physics research and consistently supported me in the best possible ways. I am deeply grateful for the time they invested to make the process so enjoyable and the patience they had with me. I also have to thank my friends who listened to me when I needed to vocalize my thoughts to sort them out and were always there for me: Joëlle Broch, Joel Zumbach, Van Do, Alex Merstetter, Danial Chughtai, Jannik Wyss, Dominique Trüssel, and Oliver Wicki. I also have to thank my girlfriend Kyra Stalder, for calming me in times of discouragement and listening to me when I was stuck with a problem. Lastly, my family, not only did they make it possible for me to study physics, but they also helped me so much by just being the greatest support I could wish for. Some say you do not choose family, but for me, even a choice would not have led to a different outcome. Thank you so much, Mama, Papa, and Nicole.

## **Disclaimer**

In the course of composing this thesis, we utilized AI tools (mainly ChatGPT and DeepL Write) primarily to refine sentence structure, improve the clarity of expression and enhance overall readability. It is important to emphasize that the core ideas, research findings and analytical insights contained within this work are the result of our own efforts. The use of AI was strictly confined to aiding in the articulation of these ideas, ensuring that the content was communicated as clearly as possible.

# Contents

<b>1. List of Symbols</b>	
<b>2. Introduction</b>	<b>1</b>
2.1. Motivation . . . . .	1
2.2. Summary . . . . .	2
<b>3. Background</b>	<b>3</b>
3.1. The System . . . . .	3
3.2. Obtaining Equations of Motion . . . . .	6
3.3. The Second Order Photon Correlation Function . . . . .	7
3.4. Materials and Methods . . . . .	9
<b>4. Adiabatic Elimination</b>	<b>10</b>
4.1. Overview and Principles of Adiabatic Elimination . . . . .	10
4.2. Two-Level Dynamics . . . . .	12
4.2.1. Effective Lindblad Master Equation . . . . .	12
4.2.2. Analyzing Two-Level System Dynamics . . . . .	12
4.3. Cavity Dynamics . . . . .	13
4.3.1. Average Cavity Field $\langle a(t) \rangle$ . . . . .	13
4.3.2. Determination of the $g^{(2)}(t)$ -Function . . . . .	16
4.4. Limitations of Adiabatic Elimination and Importance of Normal Ordering . . . . .	18
<b>5. Prodiabatic Elimination</b>	<b>21</b>
5.1. General Procedure of the Prodiabatic Elimination . . . . .	21
5.1.1. Obtaining the Cavity Field Operator . . . . .	21
5.1.2. Obtaining the Two-Level Dynamics . . . . .	22
5.2. Two-Level System . . . . .	24
5.2.1. Effective Lindblad Master Equation . . . . .	24
5.2.2. Steady State . . . . .	28
5.2.3. Analyzing the Two-Level System Dynamics . . . . .	30
5.2.4. Numerical Comparisons . . . . .	31
5.3. Cavity Dynamics . . . . .	33
5.3.1. Steady State . . . . .	33
5.3.2. Average Cavity Field $\langle a(t) \rangle$ . . . . .	35
5.3.3. Obtaining the $g^{(2)}(t)$ -Function . . . . .	37
<b>6. Method of Multiple Scales</b>	<b>41</b>
6.1. Minimal Example of the Method of Multiple Scales . . . . .	41
6.2. Application to the Cavity-Atom System . . . . .	42
<b>7. Conclusion &amp; Outlook</b>	<b>47</b>
<b>A. Appendix</b>	<b>51</b>
A.1. Rotating Frame . . . . .	51

*Contents*

A.2. Analysis of Exponential Matrix of Adiabatic Elimination . . . . .	51
A.3. $g^{(2)}(0)$ -Function in the Adiabatic Elimination . . . . .	52
A.3.1. Low Drive Expansions of $g^{(2)}(0)$ -Function . . . . .	54
A.4. Derivation of the Master Equation for the Prodiabatic Elimination . . . . .	55
A.5. Additional Notable Methods . . . . .	58
A.5.1. Low Photon Number Elimination . . . . .	58
A.5.2. Boundary Layer Theory . . . . .	58

# 1. List of Symbols

Symbol	Description
$\kappa$	Dissipation strength of the cavity.
$\gamma$	Dissipation strength of the two-level system.
$g$	Coupling strength between cavity and two-level system.
$E, \epsilon\sqrt{\kappa}$	Strength of the coherent drive coupled to the cavity.
$\epsilon^2$	Incoming photon flux per second.
$\Delta_c$	Detuning between drive and cavity frequency.
$\Delta_d$	Detuning between drive and two-level system frequency.
$a$	Bosonic ladder operator of the cavity.
$\sigma$	Fermionic annihilation operator $ 0\rangle\langle 1 $ of the two-level system.
$\sigma_z, Z$	Pauli $z$ -matrix: $ 1\rangle\langle 1  -  0\rangle\langle 0 $ .
$\bullet^\dagger$	Hermitian conjugate of $\bullet$ .
$\bullet^*$	Conjugation of $\bullet$ .
$\langle \bullet \rangle_{ss}$	Steady state expectation value of $\bullet$ .
$\text{tr}\{\bullet\}$	Trace operation acting on $\bullet$ .

Operator Relations	
$[a^{(\dagger)}, \sigma^{(\dagger)}]$	$= 0$
$[a, a^\dagger]$	$= 1$
$[\sigma^\dagger, \sigma]$	$= \sigma_z$
$\sigma\sigma$	$= 0$
$\sigma^\dagger\sigma$	$=  1\rangle\langle 1  = (\sigma_z + 1)/2$
$\sigma\sigma^\dagger$	$=  0\rangle\langle 0  = (1 - \sigma_z)/2$
$\{\sigma, \sigma^\dagger\}$	$= 1$

## 2. Introduction

### 2.1. Motivation

The interplay between light and matter is a fundamental process that enables our perception of the world, including the ability to see colors. But these are not the only interesting properties of light, its nature and how it can be described in different scenarios is equally important to physicists. Consequently, the investigation of the interaction between light and matter based on quantum physics constitutes an area of significant importance [1–3]. Optical cavities, formed by two mirrors that confine light between them, are essential for studying these interactions in a controlled manner. The motivation for utilizing cavities in place of direct illumination is twofold. Firstly, they enhance the light-matter coupling through the Purcell effect, and secondly, they restrict the scattering of light to a single direction [4]. From this fundamental configuration, a multitude of intriguing phenomena can be explored. These include the development of lasers [5, 6], single-photon sources [7], and microcavities [8]. However, cavities are not only of great interest to physicists but also to biologists, who employ them as a tool in the detection and measurement of nanoparticles and viruses [9, 10].

A paradigmatic model to investigate light-matter coupling is provided by the Jaynes-Cummings model, which describes the interaction between a single light mode with a two-level system. In addition to that, we will also allow for dissipative terms and a drive. While this seems to be just a model to test theory on, it can also be realized experimentally in various different ways [11–14]. Our goal is to find a way to approximate the dynamics of both the cavity mode and the two-level system. This requires solving a system of nonlinear coupled differential equations. Solving these is a non-trivial problem; while analytical solutions exist for the non-driven, non-dissipative case [15], there is currently no analytical solution for the more complicated driven, dissipative scenario.

One of the standard techniques to obtain an approximation is the so-called, *adiabatic elimination*, which assumes the existence of different time scales in the problem and further assumes that the fast one can be removed. In our case, the cavity changes on a fast timescale, while the two-level system changes slowly in comparison. Therefore, we approximate that the cavity adapts infinitely fast to changes in the two-level system, i.e. the cavity is always in equilibrium with the two-level system. This allows for a description of the cavity dynamics solely based on the two-level system. Due to this simplification, the problem becomes linear and thus solvable. For this solution to be reasonable, one needs initial states that are consistent with the approximation, as well as system values that allow the cavity mode to adapt quickly, usually done by a high cavity dissipation. We believe that these restrictions are too harsh, hence we want to improve this technique in a way that we can include higher-order corrections as well as incorporate the initial conditions.

Once a description of the time dynamics is found, the next question is how the photons leave the cavity and are subsequently measured, this would provide a simple experimentally measurable quantity. A common quantifier is provided by the so-called second-order photon correlation function or  $g^{(2)}$ -function for short. It is one of the most important tools to distinguish classical from non-classical light sources [16]. This is of further interest because not only can

## 2. Introduction

one use cavities to study the object in the cavity, but one can also use known objects such that the setup becomes a generator of light with certain statistical properties.

While we relied on the proposed system in this motivation, we also want to emphasize that the adiabatic elimination is a widely applied technique. By finding an approximation that relaxes the underlying conditions we hope that this new technique can be adapted to other systems as well.

### 2.2. Summary

In the following Chap. 3 we introduce the theoretical framework of this thesis. We show how we model the system dynamics by the driven Jaynes-Cummings Hamiltonian with dissipation via a Lindblad master equation. Further, we outline how we obtain equations of motion in the Heisenberg picture and explain the second-order photon correlation function. The chapter concludes with a summary of the computational tools used to obtain the results of the later chapters.

How to use the adiabatic elimination to approximate the system dynamics is outlined in Chap. 4. The method reduces the problem to the subspace of the two-level system, as demonstrated in [17]. This offers a significant simplification, as it removes the need to solve for the cavity's dynamics directly. Adiabatic elimination is most effective when applied to a *bad cavity*, characterized by substantial cavity dissipation, minimal two-level dissipation and small drive strength. The main limitation of this approach is that it only keeps leading order terms, therefore making it only applicable in some scenarios.

Our most accurate approximation, the *prodiabatic elimination*, is presented in Chap. 5 and builds on the formal solution of the cavity field. This solution would require an analytic expression for the two-level dynamics at previous times to yield a definitive result, which is generally inaccessible. To tackle this issue, we assume that the two-level operators can be expanded in a truncated Taylor series. This leads to an analytical form for the cavity field operator, which is influenced by both the two-level behavior and the initial state of the cavity field. Unlike the adiabatic elimination, the Taylor series enables continued addition of corrections to the approximation, a feature unavailable in the adiabatic elimination framework. To get a final result, techniques similar to those in the adiabatic elimination are employed, ensuring a straightforward extension from the standard approach.

In Chap. 6 we test how the approximations of Chaps. 4 and 5 compare to standard singular perturbation techniques with our choice being the method of multiple scales. Similar to the adiabatic elimination it assumes different timescales affecting the problem and treats them independently of each other. Since it is a perturbative technique, it is possible to include arbitrarily high-order correction terms, but these terms become increasingly complicated and do not provide much further insight. Since the first few orders do not outperform the adiabatic elimination, we do not consider the approach to be a reasonable solution to the problem.

### 3. Background

The purpose of this chapter is to provide the necessary tools to understand the upcoming chapters. We start with a more physical approach to the considered system and will gradually increase the amount of math in order to understand the math, as well as the physics, used further on. Further, we use  $\hbar = 1$  throughout the whole thesis.

#### 3.1. The System

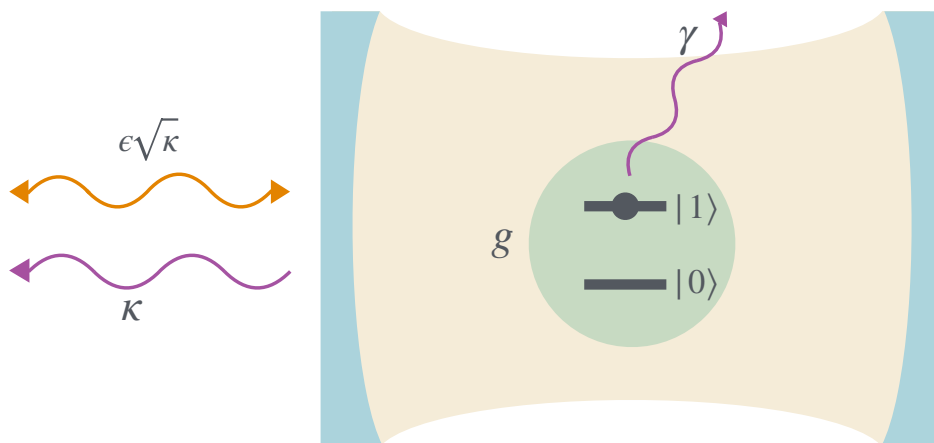


Figure 3.1.: Sketch of the system. Light blue mirrors form the cavity, with the left one partially transmissive and the right fully reflective. The two-level system is shown as a green circle. We have a coherent input with strength  $\epsilon\sqrt{\kappa}$ , the coupling between the cavity and the two-level system is denoted by  $g$ , dissipation out of the cavity with rate  $\kappa$  and two-level dissipation rate with  $\gamma$ .

The system shown in Fig. 3.1 consists of two mirrors that trap light between them. One mirror is perfectly reflecting (right), while the other is slightly transmissive. The transmissive mirror allows a coherent drive to couple to the cavity by directing a laser at its backside. Furthermore, we would like to place an object into the cavity, in this case, a two-level system. If we follow the path of a single incoming photon, it will first go through the left translucent mirror entering the cavity, now it is trapped in the cavity, which means it is bouncing back and forth in between the mirrors. Inside the cavity, it has the possibility of interacting with the two-level system. If the photon is in the cavity, it can also be sucked up by the drive or be dissipated through the translucent mirror. In addition, we omitted another possibility of losing photons, the two-level system can emit a photon in a way that they are not caught by the cavity. For example, it can emit one orthogonal to the mirrors, but since we want the emission to be restricted to a single direction it is favorable to have this rate as close to zero as possible.

### 3. Background

With a qualitative understanding of what happens in the set-up, we can connect it to a few variables. The laser that shines into the cavity enters with the strength  $\epsilon\sqrt{\kappa}$ , where  $\epsilon^2$  is the total incoming photon flux per unit of time. The coupling between the cavity and the two-level system is described by the parameter  $g$ , the dissipation rate of the two-level system by  $\gamma$  and the dissipation rate of the cavity by  $\kappa$ . One might ask why the drive strength is connected to the dissipation rate  $\kappa$ ; they have to be connected since a more translucent mirror would not only increase the dissipation, due to photons escaping the cavity more easily but would also increase the drive strength since it is easier to fill the cavity. The scaling of  $\sqrt{\kappa}$  can only be explained by input-output theory, which we will not focus on here [18].

When an atom is placed in a single-mode cavity, its interaction with the electromagnetic field is constrained to transitions resonant with the cavity mode, making it qualitatively analogous to a two-level system interacting with the cavity field. As such, the terms atom and two-level system will be used interchangeably during this thesis. Additionally, the cavity environment significantly modifies the spontaneous emission of the atom. The atom experiences the Purcell effect, where the spontaneous emission rate is enhanced by the Purcell factor

$$F_p = \frac{4g^2}{\gamma\kappa}, \quad (3.1)$$

and the total resulting emission rate is increased by

$$\Gamma = \gamma F_p, \quad (3.2)$$

to

$$\gamma(1 + F_p) = \gamma + \Gamma. \quad (3.3)$$

The Purcell factor  $F_p$  tells us how the emission of the two-level system is taking place.  $F_p$  can be defined as  $F_p = \frac{W_{cav}}{W_{free}}$ , where  $W_i$  is the rate at which photons are emitted either into free space or into the cavity [19]. Values of  $F_p > 1$  indicate that emission into the cavity mode dominates, while  $F_p < 1$  implies that free-space emission is more significant. Another important parameter to characterize cavities is the  $\beta$  factor, which tells us the fraction of photons emitted into the cavity to the total emitted photons, therefore giving the probability that a photon is emitted into the cavity. The  $\beta$  factor is given by

$$\beta = \frac{F_p}{F_p + 1}. \quad (3.4)$$

In the course of this thesis we will be dealing with the so-called *bad cavity limit*, one of the main approximations we will be considering, the adiabatic elimination, is highly dependent on it so we want to outline what it is and why it is important. For our system the bad cavity limit is defined by [17]

$$\kappa/\gamma \rightarrow \infty \quad (3.5) \quad \gamma/g \rightarrow 0 \quad (3.6) \quad \epsilon/\sqrt{\kappa} \rightarrow 0. \quad (3.7)$$

One can see from those expressions that it is sufficient to have a big  $\kappa$  and a small  $\gamma$ . The name of bad cavity can be misleading, as one could take the word *bad* by its face value and think that this is just due to bad engineering, but this is not the case. Having a bad cavity is a design choice and a wanted feature. Two perfectly reflective mirrors, resulting in  $\kappa = 0$ , would make measurements impossible because light would never escape the cavity. By using translucent mirrors we make the cavity *bad* which means it is not good at trapping light inside of it, but just this feature makes measurements possible. Additionally, a bad cavity allows for efficient coupling between the drive and cavity, by shining the laser at the translucent mirror we

### 3. Background

are able to put photons into the system. Of course, this paragraph is a bit one-sided, in reality, the design of a cavity depends on its intended use case, the absolute worst cavity is probably not desirable and neither is a perfect reflective one.

With a concrete picture in mind, we can have a more mathematical view of the system. The Hamiltonian is given by

$$H = \Delta_c a^\dagger a + \Delta_d \sigma_z + g \left( a^\dagger \sigma + \sigma^\dagger a \right) - \epsilon \sqrt{\kappa} \left( a + a^\dagger \right), \quad (3.8)$$

where  $\Delta_c, \Delta_d$  are the detunings between cavity/two-level system with the drive, which are present because this Hamiltonian is already in a rotating frame with the frequency of the drive. The rotating frame is also the reason why the driving term is time-independent, as the technique of moving into a rotating frame is widely applied, we have outlined how to do it in the appendix App. A.1. Additionally,  $a$  is the bosonic cavity annihilation operator, which means  $a$  follows the commutation relations

$$\left[ a, a^\dagger \right] = a a^\dagger - a^\dagger a = 1, \quad (3.9)$$

and  $\sigma_i$   $i = x, y, z$  are the Pauli matrices

$$\sigma_x = \begin{pmatrix} 0 & 1 \\ 1 & 0 \end{pmatrix} \quad (3.10) \quad \sigma_y = \begin{pmatrix} 0 & -i \\ i & 0 \end{pmatrix} \quad (3.11) \quad \sigma_z = \begin{pmatrix} 1 & 0 \\ 0 & -1 \end{pmatrix}, \quad (3.12)$$

and

$$\sigma = |0\rangle\langle 1| = \begin{pmatrix} 0 & 0 \\ 1 & 0 \end{pmatrix}, \quad (3.13)$$

is the lowering operator of the atom. Note that  $\sigma$  follows the anticommutation relations

$$\left\{ \sigma^\dagger, \sigma \right\} = \sigma^\dagger \sigma + \sigma \sigma^\dagger = 1, \quad (3.14)$$

which can be confusing since we are dealing with photons, so one would suspect a commutator instead of an anticommutator, but the nature of the two-level systems forbids it from having multiple excitations therefore it is described by anticommutation relations. We assume the cavity has sharp equally spaced energy levels, as can be seen by Eq. (3.8) where we essentially assume the cavity is a quantum harmonic oscillator. Because of the single mode of the cavity, we can assume that the atom is equivalent to a two-level system and therefore we use Pauli matrices to describe it.

Next, we take a look at the setup without a drive i.e.  $\epsilon = 0$  and no dissipation  $\kappa = \gamma = 0$ . The dynamics simplify to the Jaynes-Cummings model [20], which uses a linear coupling of the cavity and two-level system with strength  $g$

$$H = \Delta_c a^\dagger a + \Delta_d \sigma_z + g \left( a^\dagger \sigma + \sigma^\dagger a \right). \quad (3.15)$$

The idea behind the Jaynes Cummings model is to have a flip-flop interaction. The coupling term in Eq. (3.15), which is proportional to  $g$ , swaps one photon back and forth between the cavity and the two-level system. The interaction conserves the total number of excitations, as can be seen by the fact that the Jaynes-Cummings Hamiltonian commutes with the total photon number operator  $a^\dagger a + |1\rangle\langle 1|$ .

### 3. Background

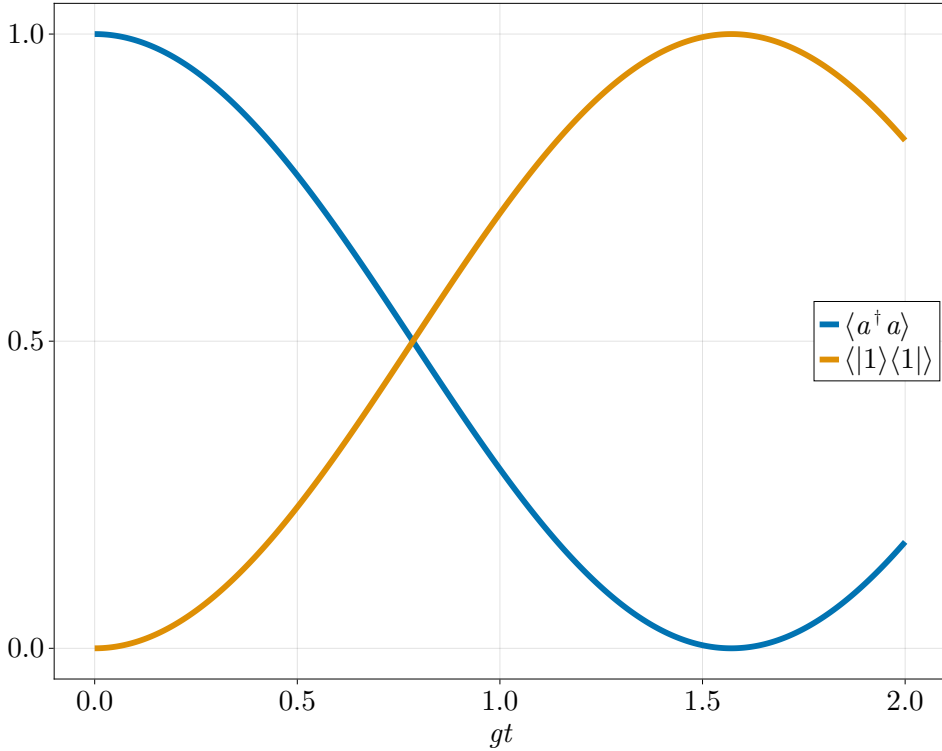


Figure 3.2.: Display of total excitation number in the cavity (blue) and two-level system (orange) as a function of time, starting in the pure Fock state of one photon in the cavity and none in the atom. For this simulation, we set  $\Delta_i/g = 0$ .

In Fig. 3.2 we see this exchange of photons from the cavity and two-level system and the reverse, done by  $H = g(a^\dagger\sigma + \sigma^\dagger a)$ . The initial state was chosen as one photon in the cavity and none in the two-level system  $|1\rangle_{cav} |0\rangle_{atom}$ . In this case, we first move the photon out of the cavity into the atom and then emit it back into the cavity. In addition to this simple scenario, we want to make it more realistic by introducing dissipation to the photons in the two-level system and cavity. But this would create a new problem since without an energy input we are always ensured that the steady state is the vacuum state  $|0\rangle_{cav} |0\rangle_{atom}$ . The reason is there would be an energy flow out of the system without an energy flow in, which means for long times we just empty the cavity and two-level system. Therefore, we want to also introduce a coherent drive with strength  $\epsilon\sqrt{\kappa}$ , the total Hamiltonian  $H$  is given by Eq. (3.8). It is the Jaynes Cummings Hamiltonian plus a driving term and the total dynamics are described by a Lindblad Master equation

$$\dot{\rho} = -i[H, \rho] + \kappa\mathcal{D}[a]\rho + \gamma\mathcal{D}[\sigma]\rho, \quad (3.16)$$

where  $\gamma$  is the the dissipation rate of the two-level system and  $\kappa$  the dissipation rate of the cavity and the dissipators  $\mathcal{D}[\bullet]$  are superoperators acting as

$$\mathcal{D}[A]\rho = A\rho A^\dagger - \frac{1}{2}\{A^\dagger A, \rho\}. \quad (3.17)$$

## 3.2. Obtaining Equations of Motion

To describe our dynamics, we use time-dependent operators instead of states, hence our framework is based on the Heisenberg picture. However, as we are not working with unitary dynamics,

### 3. Background

it is necessary to understand the meaning of a time-dependent operator in this context. This requires deriving the Heisenberg equation of motion from the Lindblad master equation. To do so, consider an arbitrary operator  $A$

$$\begin{aligned}\langle \dot{A} \rangle &= \frac{d}{dt} \text{tr}\{A\rho\} = \text{tr}\left\{A \frac{d}{dt}\rho\right\} \\ &= \text{tr}\left\{-i[A, H]\rho + \kappa\left(a^\dagger Aa - \frac{1}{2}\{A, a^\dagger a\}\right)\rho + \gamma\left(\sigma^\dagger A\sigma - \frac{1}{2}\{A, \sigma^\dagger \sigma\}\right)\rho\right\} \\ \Rightarrow \dot{A} &= -i[A, H] + \kappa\left(a^\dagger Aa - \frac{1}{2}\{A, a^\dagger a\}\right) + \gamma\left(\sigma^\dagger A\sigma - \frac{1}{2}\{A, \sigma^\dagger \sigma\}\right),\end{aligned}\quad (3.18)$$

where we mainly used the cyclic properties of the trace multiple times and assumed the operator  $A$  not to be explicitly time dependent. Solving Eq (3.18) will give us the wanted time-dependent operators.

It is important to note that for this type of time evolution, the product rule breaks down

$$\frac{d}{dt}o_1o_2 \neq \left(\frac{d}{dt}o_1\right)o_2 + o_1\left(\frac{d}{dt}o_2\right), \quad (3.19)$$

where  $o_1$  and  $o_2$  are some arbitrary operators. Note that the loss of the product rule also implies

$$(o_1o_2)(t) \neq o_1(t)o_2(t), \quad (3.20)$$

which means it makes a difference to consider a product of operators as a product of two time-dependent quantities or as a singular one. This can be a bit confusing, but remember our differential operator is defined by Eq. (3.18). To observe the breakdown of the product rule we consider  $\gamma = 0$ , therefore

$$\frac{d}{dt}(o_1o_2) = -i[o_1o_2, H] + \kappa\left(a^\dagger o_1o_2a - \frac{1}{2}\{o_1o_2, a^\dagger a\}\right) \quad (3.21)$$

$$\begin{aligned}\left(\frac{d}{dt}o_1\right)o_2 + o_1\left(\frac{d}{dt}o_2\right) &= -i[o_1o_2, H] + \kappa\left(a^\dagger o_1ao_2 + o_1a^\dagger o_2a\right. \\ &\quad \left. - \frac{1}{2}\{o_1, a^\dagger a\}o_2 - \frac{1}{2}o_1\{o_2, a^\dagger a\}\right),\end{aligned}\quad (3.22)$$

if now  $[a^{(\dagger)}, o_1] \neq 0$  or  $[a^{(\dagger)}, o_2] \neq 0$ , we will not end up with the same dynamics. One can also directly see that this behavior comes from the non-unitary part, which is to be expected since the product rule holds if we have a unitary time evolution. This can be seen by assuming we have a unitary  $U$  to move into the Heisenberg picture, leading to

$$(o_1o_2)(t) = U^\dagger o_1o_2U = U^\dagger o_1UU^\dagger o_2U = o_1(t)o_2(t), \quad (3.23)$$

which follows directly from the unitarity of  $U$ . But since our considered system does not have this nice property, we need to be very careful of how we treat the time dependencies of our operators, especially once we consider the products of operators.

### 3.3. The Second Order Photon Correlation Function

In this section, we assume that the right mirror is slightly translucent, enabling the detection of dissipated photons. This setup is crucial because photons dissipated through this mirror

### 3. Background

can be distinguished from photons reflected by the drive, a distinction that would otherwise be impossible if the dissipation occurred solely through the driven side. Furthermore, we consider the dissipation rate through this mirror to be minimal, ensuring that its impact on the overall cavity dynamics is negligible. This slightly changed setup can be seen in Fig. 3.3.

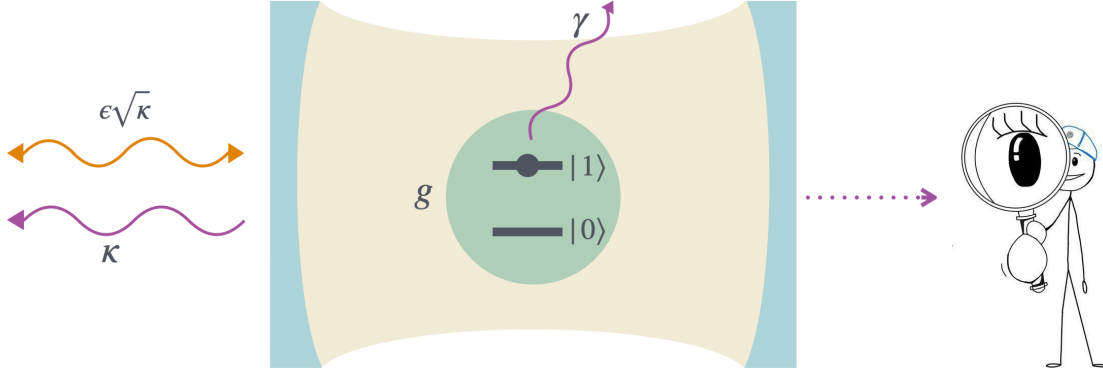


Figure 3.3.: Sketch as in Fig. 3.1, but with an included detector (guy with the magnifying glass) through the right mirror, we consider this dissipation rate to be so small that its effect on the overall dynamics is neglectable.

The central quantity of interest in this thesis is the  $g^{(2)}$ -function, also called the second-order photon correlation function. Consider the following scenario: a physicist takes a look at the photons coming out of their cavity setup and asks themselves "I just detected a photon, but when will I detect the next one?", knowing that they are working with something that follows a stochastic process, they are likely to refine their question to "I just detected a photon, how likely is it that at time  $\tau$  I will detect the next one?". The answer this scientist is looking for is the  $g^{(2)}$ -function. It is a measure of how we expect light to leave our cavity, when we are likely to measure a photon in the detector or when it is unlikely. But it gives also other insights, it is one of the main tools to distinguish classical from non-classical light sources [4, 21]. It is defined by

$$g^{(2)}(\tau) = \frac{\langle a^\dagger(t)a^\dagger(\tau)a(\tau)a(t) \rangle}{\langle a^\dagger(t)a(t) \rangle^2}, \quad (3.24)$$

where for future reference we will set the initial time  $t = 0$  [18]. Since we work with density matrices, we will replace the expectation value with a trace and further assume the initial state to be the steady-state  $\rho_{ss}$

$$g^{(2)}(\tau) = \frac{\text{tr}\{a^\dagger(\tau)a(\tau)a\rho_{ss}a^\dagger\}}{\text{tr}\{a^\dagger a\rho_{ss}\}^2}. \quad (3.25)$$

Here, one might ask how to connect this formula to the earlier mentioned picture of the scientist detecting photons. It is advantageous to first forget about the normalization, so we investigate

$$\text{tr}\{a^\dagger(\tau)a(\tau)a\rho_{ss}a^\dagger\} = \text{tr}\{a(\tau)a\rho_{ss}a^\dagger a^\dagger(\tau)\}, \quad (3.26)$$

where we just used the cyclic property of the trace once. Now, we dissect this formula into two parts, first, we have the  $a\rho_{ss}a^\dagger$  part and the  $a(\tau)a^\dagger(\tau)$  part that is applied to it. So initially, we remove a photon out of the system, by applying  $a$  from the left and  $a^\dagger$  from the right, this would be the first photon the scientist measures, and it also defines  $t = 0$  of our experiment.

### 3. Background

Next, we do the same again at time  $\tau$  by applying the same operator again, this is done by using the time-dependent cavity operators. Finally, we trace this expression to obtain the total amplitude of this process, which gives us something proportional to how likely it is to remove another photon at time  $\tau$ . It is important to note that this expression is greater than or equal to zero, but it has no upper bound, so an interpretation through probabilities is not directly possible. However, a high value will still give you the information that the scientist is expecting to detect a photon. Whereas if it is close to zero, the scientist would not expect to see a photon.

Next, we want to show that in the long time limit the  $g^{(2)}$ -function will converge to 1. For this, we identify the normalized state  $\rho' = \frac{a\rho_{ss}a^\dagger}{\text{tr}\{a^\dagger a\rho_{ss}\}}$ , which one can interpret as removing a photon of the cavity at time  $t = 0$ , therefore

$$g^{(2)}(\tau) = \frac{\text{tr}\{a^\dagger(\tau)\rho'a(\tau)\}}{\text{tr}\{a^\dagger\rho_{ss}a\}}, \quad (3.27)$$

which effectively quantifies the expectation value for removing an additional photon at time  $t = \tau$  in relation to the steady-state scenario. Evaluating the numerator of Eq. (3.27) for  $\tau \rightarrow \infty$  leads to

$$\lim_{\tau \rightarrow \infty} \text{tr}\{a^\dagger(\tau)\rho'a(\tau)\} = \text{tr}\{a^\dagger\rho_{ss}a\}, \quad (3.28)$$

directly implying

$$\lim_{\tau \rightarrow \infty} g^{(2)}(\tau) = 1. \quad (3.29)$$

We focused on the initial state being the steady state much in this section, the reason being that the earlier mentioned scientist can typically achieve this scenario quite easily; they set up the system, wait for a while and then assume that the system has reached steady-state conditions. At this point, the scientist begins to observe, detecting the first photon, which initiates the entire process. While this is one way to measure the  $g^{(2)}$ -function, it would be a tedious one, typically the easier route is to detect the output of the cavity for a long time and use the time in between each measurement to obtain the  $g^{(2)}$ -function. This works because in principle each measured photon can be thought of as the first detected one.

### 3.4. Materials and Methods

All simulations are done using the *Julia* programming language [22] using the *QuantumOptics.jl* package [23]. Plots are done using the *Makie.jl* package [24], where for higher inclusion we used the color map `:seaborn_colorblind`, which is optimized to have high contrast in color so that the interpretations are also easy to follow for color-blind people [25, 26]. The *QuantumAlgebra.jl* package [27] was also a great tool to find equations of motion of operators in the Heisenberg picture. While some calculations were performed using Mathematica [28], they could, in principle, have been completed manually.

## 4. Adiabatic Elimination

This chapter is primarily motivated by [17], which employs the quantum Langevin equation to analyze system dynamics. However, since our approach is based on the Lindblad master equation given in Eq. (3.16), we follow an alternative derivation. To establish a solid foundation, we begin with an overview of the general approach and key assumptions, providing a discussion to develop physical intuition. We then explore the analytical insights gained from this method and compare them with numerical simulations to assess its effectiveness.

### 4.1. Overview and Principles of Adiabatic Elimination

The adiabatic elimination can be a challenging method to grasp when it comes to deriving time dynamics. To start, we assume  $\dot{a} = 0$ . At first glance, this might seem confusing; after all, we aim to determine the  $g^{(2)}$ -function, which requires an expression for  $a(t)$ . But should setting  $\dot{a} = 0$  not eliminate all time dependence? The short answer is *no*. This is because  $\dot{a}$  depends on the two-level system operators, which we do *not* assume to be time-independent. By setting  $\dot{a} = 0$ , we derive an expression for the cavity field  $a$  as a function of the two-level system, which remains time-dependent. Thus,  $a$  itself becomes time-dependent, indirectly capturing the time dynamics through the two-level system. In making this assumption, we're effectively stating that the cavity field adapts so fast to any changes in the two-level system that it reaches steady-state conditions instantaneously. Since this change would happen without taking any time, it is nonphysical, but for fast adapting systems it is a reasonable assumption, yielding good results. Under this assumption, we may use  $\dot{a} \approx 0$ , redirecting our focus from the fast dynamics of the cavity field  $a$  to the slower dynamics of the two-level system, as can be further read in [29]. This shift simplifies the problem, making it solvable in a straightforward way by focusing on the effective dynamics of the two-level system while assuming that the cavity field continuously equilibrates to it. These assumptions can not be true in all cases, but for our system, they become justified in the *bad cavity* limit, defined by Eqs. (3.5), (3.6) and (3.7) for which the method is exact. The introduction above should help the reader with a basis for the following chapter to guide themselves on, but we will nonetheless outline whenever we use one of the described steps and assumptions.

For starters, we need to find the equations of motion of the system operators, this is done by employing Eq. (3.18), leading to

$$\dot{a} = -\left(i\Delta_c + \frac{\kappa}{2}\right)a - ig\sigma + i\epsilon\sqrt{\kappa} \quad (4.1)$$

$$\dot{\sigma} = -\left(i\Delta_d + \frac{\gamma}{2}\right)\sigma + ig\sigma_z a \quad (4.2)$$

$$\dot{\sigma}_z = -2ig(\sigma^\dagger a - a^\dagger \sigma) - \gamma(\sigma_z + 1). \quad (4.3)$$

The non-linear coupling between  $a$  and  $\sigma$ , by  $g\sigma_z a$ , prevents us from decoupling these equations and thus hinders us from finding a simple analytical solution. The non-linearity means that even small variations in one variable can significantly impact the others, making the overall behavior hard to capture. Since the non-linear terms cause these problems we would like to remove them,

#### 4. Adiabatic Elimination

for this we consider  $\dot{a} = 0$ , which leads to

$$a = a_{adb} = -\frac{2it_c}{\kappa} \left( g\sigma - \epsilon\sqrt{\kappa} \right), \quad (4.4)$$

where we introduce the parameter

$$t_c = \left( \frac{2i\Delta_c}{\kappa} + 1 \right)^{-1}. \quad (4.5)$$

This is the step where we assume that the cavity field equilibrates infinitely fast to the two-level system, which lets us assume that the derivative of the cavity field vanishes. We will call this new representation of  $a$  simply  $a_{adb}$ , where the subscript stands for *adiabatic*.

Our next step is to substitute each instance of  $a$  with  $a_{adb}$  in the equation of motion of the two-level system, given by Eqs. (4.2) and (4.3). It is important to note, that this substitution is not rigorously justified, as outlined in Sec. 3.2, instead products of operators must be treated as single, time-dependent entity. This also reveals the significance of normal ordering in this context. When replacing  $a$  with  $a_{adb}$ , the position of  $a_{adb}$  to the left or right of a two-level operator can become relevant. The justification for the replacement cannot be explained without addressing the role of noise operators, a detailed discussion on this topic is provided in Sec. 4.4. The breakdown of commutation relations can be seen by the commutator of  $a_{adb}$  and  $\sigma^\dagger$

$$[a_{adb}, \sigma^\dagger] = -\frac{2it_c}{\kappa} \left( g[\sigma, \sigma^\dagger] \right) = \frac{2it_c g}{\kappa} \sigma_z \neq 0, \quad (4.6)$$

which would be zero if we used  $a$  instead of  $a_{adb}$ , since  $a$  used to be in a different Hilbert space than  $\sigma^\dagger$ . The breakdown of commutation relations in the Heisenberg picture when using a Lindblad Master equation is further outlined in [18].

By doing this replacement for now and shifting the discussion to Sec. 4.4 and assuming that we are allowed to apply the commutation relations of the two-level system, we obtain a linear system of equations in the two-level subspace

$$\dot{\sigma} = -\frac{2g\epsilon t_c}{\sqrt{\kappa}} \sigma_z - \left( \frac{2g^2 t_c}{\kappa} + \frac{\gamma}{2} + i\Delta_d \right) \sigma \quad (4.7)$$

$$\dot{\sigma}_z = -\left( \frac{4g^2}{\kappa} \text{Re}\{t_c\} + \gamma \right) (\sigma_z + 1) + \frac{4g\epsilon}{\sqrt{\kappa}} \left( t_c^* \sigma + t_c \sigma^\dagger \right). \quad (4.8)$$

From here, we also see how we can obtain a time-dependent cavity field operator. Remember that  $\dot{a} = 0$ , but we will not be using  $a$  since we replace it by  $a_{adb}$  and from Eq. (4.7) one can see that  $\dot{a}_{adb} \propto \dot{\sigma} \neq 0$ , which gives us the wanted time dynamics of the cavity field. To solve the system of Eqs. (4.7) and (4.8), we first write it as a matrix equation

$$\frac{d}{dt} \vec{v}(t) = A \vec{v}(t),$$

where we used that  $\dot{\sigma}^\dagger = (\dot{\sigma})^\dagger$  and identify

$$A = \begin{pmatrix} -\left( \frac{2g^2 t_c}{\kappa} + \frac{\gamma}{2} + i\Delta_d \right) & 0 & -\frac{2g\epsilon t_c}{\sqrt{\kappa}} & 0 \\ 0 & -\left( \frac{2g^2 t_c^*}{\kappa} + \frac{\gamma}{2} - i\Delta_d \right) & -\frac{2g\epsilon t_c^*}{\sqrt{\kappa}} & 0 \\ \frac{4g\epsilon}{\sqrt{\kappa}} t_c^* & \frac{4g\epsilon}{\sqrt{\kappa}} t_c & -\left( \frac{4g^2}{\kappa} \text{Re}\{t_c\} + \gamma \right) & -\left( \frac{4g^2}{\kappa} \text{Re}\{t_c\} + \gamma \right) \\ 0 & 0 & 0 & 0 \end{pmatrix}, \quad (4.9)$$

## 4. Adiabatic Elimination

with the convention

$$\vec{v}(t) = \begin{pmatrix} \sigma(t) \\ \sigma^\dagger(t) \\ \sigma_z(t) \\ 1 \end{pmatrix}. \quad (4.10)$$

It is sufficient to use expectation values instead of operators in  $\vec{v}(t)$ , as we ultimately only need the expectation values. However, this distinction does not matter since the final results are linear combinations of operators and applying expectation values to these expressions will yield the same results. The system of linear equations is solved by an exponential matrix ansatz

$$\vec{v}(t) = e^{At}\vec{v}(0), \quad (4.11)$$

which gives us the final solution of the time-dependent two-level operators. This also concludes the main steps of the adiabatic elimination, as from that solution various quantities can be derived, including the  $g^{(2)}$ -function.

## 4.2. Two-Level Dynamics

### 4.2.1. Effective Lindblad Master Equation

This section aims to understand the dynamics in the two-level system after the adiabatic elimination was applied to the cavity. We ask the question whether there exists a Lindblad master equation (LME) that can create the same dynamics, so the task is to find an LME which naturally creates the differential equations of Eqs. (4.7) and (4.8). To reproduce those equations of motion, we see that using a Hamiltonian

$$H = \left( \frac{\Delta_d}{2} + \frac{g^2 \text{Im}\{t_c\}}{\kappa} \right) \sigma_z + \frac{2gei}{\sqrt{\kappa}} t_c (\sigma^\dagger - \sigma), \quad (4.12)$$

and a dissipator in  $\sigma$  creates the wanted dynamics. The total LME reads

$$\dot{\rho} = -i[H, \rho] + \gamma (\text{Re}\{t_c\} F_p + 1) \mathcal{D}[\sigma]\rho, \quad (4.13)$$

where the Hamiltonian  $H$  is given by Eq. (4.12). We notice that after the adiabatic elimination, the system dynamics reduce to the case of a driven two-level system that is objected to dissipation. The dissipation in  $\sigma$  is reasonable since we assume the cavity acts mainly like a sink, in which it absorbs the photons that are emptied into the cavity. This is because we assume  $\kappa$  to be a big parameter, as it is needed for the adiabatic elimination to work well, which implies a fast dissipation out of the cavity. Using this picture one can see the enhanced dissipation rate  $\gamma (\text{Re}\{t_c\} F_p + 1)$ . But we overlooked the other way in which the cavity can affect the two-level system, this is by using the Jaynes-Cummings term to move a photon from the cavity into the two-level system. This feature is captured by  $\sigma^\dagger$  of the drive term in Eq. (4.13). One could argue that the Hamiltonian has an imaginary drive amplitude, but by moving into a different frame, by  $\sigma \rightarrow i\sigma$  we can again make the drive strength real and positive, but this is not done in this chapter, as there is no further insight from that.

### 4.2.2. Analyzing Two-Level System Dynamics

From now on, we will assume that the drive is on resonance  $\Delta_c = \Delta_d = 0$ . In the Appendix App. A.2 we have a further look into the eigenvalues of the Matrix  $A$  of Eq. (4.9), which leads to

## 4. Adiabatic Elimination

a critical drive strength. If one exceeds this drive strength, we obtain imaginary eigenvalues of  $A$ , therefore one expects oscillatory behavior in the expectation values of the two-level operators. Imaginary eigenvalues are expected as soon as

$$\frac{\epsilon}{\sqrt{\kappa}} > \frac{g}{4\kappa\beta}, \quad (4.14)$$

with  $\beta$  given by Eq. (3.4). This allows us to define the critical drive strength

$$\epsilon_c = \frac{g}{4\beta\sqrt{\kappa}}, \quad (4.15)$$

for drives below this value, there should not be any visible oscillations for values above we would expect to see them. But this is only true if we assume the result of the adiabatic elimination also captures the real dynamics. In Chap. 5 we found an even tighter bound for possible oscillations and in Fig. 5.4 we see how increasing  $\epsilon$  above the critical drive strength leads to oscillations in the expectation value of  $\sigma_z$ .

### 4.3. Cavity Dynamics

#### 4.3.1. Average Cavity Field $\langle a(t) \rangle$

Since we have an analytic expression for  $\sigma(t)$ , we can also find one for  $a_{adb}(t)$  by Eq. (4.4), which we want to use to find an expression of the  $g^{(2)}$ -function. But first, let us test how well this approximation works on expectation values of  $a$ , instead of directly jumping into the case of multiple cavity operators. We are questioning whether the initial state affects the approximation on  $a$  and how we can tune system values for a higher alignment between numerics and the approximation. We will obtain all expectation values of  $a$  by

$$\langle a(t) \rangle = \langle a_{adb}(t) \rangle = -\frac{2i}{\kappa} (g \langle \sigma(t) \rangle - \epsilon\sqrt{\kappa}), \quad (4.16)$$

where  $\langle \sigma(t) \rangle$  is obtained through Eq. (4.11).

In the following, we assume that the initial state has no excitations, so the cavity, as well as the two-level system, are in the vacuum state  $|0\rangle$ . Our intuition tells us that the adiabatic elimination should perform badly for early times since the vacuum state should be too far away from the steady state, therefore we would expect that  $\dot{a} = 0$  is not a reasonable assumption in this case. But we also expect that at some point the adiabatic elimination should obtain a good approximation since the state has to evolve into the steady state.

#### 4. Adiabatic Elimination

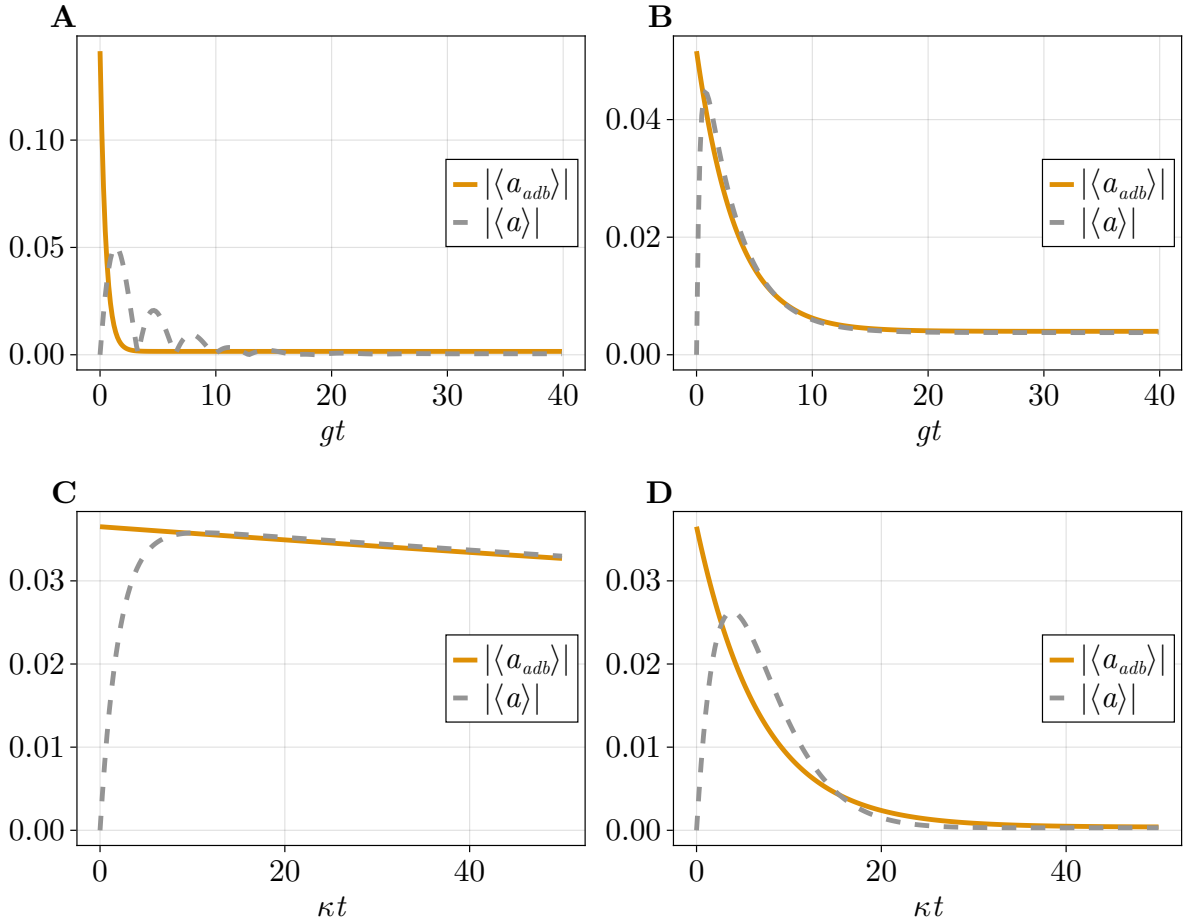


Figure 4.1.: Comparison between the numerical expectation value  $|\langle a \rangle|$  (dashed and gray) and the adiabatic elimination (full and orange). For this plot we assumed an initial vacuum state and further varied  $g$  and  $\kappa$ ,  $\kappa$  variations are in **A**, **B** and  $g$  variations in **C**, **D**. For the  $\kappa$  variations  $\kappa/g = 1, 15/2$  in **A**, **B** and for the  $g$  variations we used  $g/\kappa = 1/30, 8/30$  in **C**, **D**. For the  $g$  variation case we used  $\gamma/\kappa = 1/3000$  and  $\epsilon/\sqrt{\kappa} = 1/10\sqrt{30}$ . In the case of varying  $\kappa$  we used  $\gamma/g = 1/200$  and  $\epsilon/\sqrt{g} = 1/10\sqrt{2}$ .

In Fig. 4.1, we can see how well the adiabatic elimination works for longer timescales; it converges nicely to the numerical result after some time. We attribute this to the fact that at this point the assumption of the cavity being close to steady-state conditions is reasonable. By having a clear look at the subfigures **C**, **D** in Fig. 4.1, we can see that by increasing  $g$  the decay happens more rapidly. This is due to the enhanced decay factor  $2g^2/\kappa$ , seen in Eq. (4.7) scaling with  $g^2$ , so a bigger  $g$  will increase the total decay rate. Next, we can look at what happens if we increase  $\kappa$ ; this can be seen in subfigures **A**, **B**. We argue, that the adiabatic elimination is exact in the *bad cavity* limit, see [17]. Therefore, we should expect a larger  $\kappa$  to increase the alignment between adiabatic elimination and numerics. In Fig. 4.1, one can see this effect, since for larger  $\kappa$  the adiabatic elimination works fairly well. In subplot **A** we observe oscillations in the numerics, seen by the small jumps of the gray line. We explain this by an exchange of excitations between the cavity and two-level system, this effect can not be captured by the adiabatic elimination. The reason for this is that the added excitation to the cavity is removed

#### 4. Adiabatic Elimination

instantly by the adiabatic elimination, whereas in panel **A** it is reabsorbed. We can always observe a mismatch at  $t = 0$ , this is because the adiabatic elimination can not incorporate the initial conditions of the cavity field, but only the ones of the two-level systems. By using the vacuum as the initial state we use a state not closely related to the steady state, therefore this initial mismatch was to be expected.

Next, we show that by choosing an initial state closely related to the steady state, the adiabatic elimination can also work well on early timescales. For this, consider the initial state,

$$\rho = \frac{a\rho_{ss}a^\dagger}{\text{tr}\{a\rho_{ss}a^\dagger\}}, \quad (4.17)$$

which is the steady state after removing a single photon from the cavity, which we will call photon reduced steady-state further on. This initial state is of interest, not only because it is related closely to steady-state conditions, but also because it is the initial state when computing the  $g^{(2)}$ -function, see Eq. (3.25). For the following numerics, the initial values for the vector  $\vec{v}(t)$  of Eq. (4.11) are obtained from the simulation. In principle, one can also obtain them from the adiabatic elimination, but those are accompanied by the errors of this approximation, but since we are mainly interested in the overall behavior, we will use numerics to obtain the initial values.

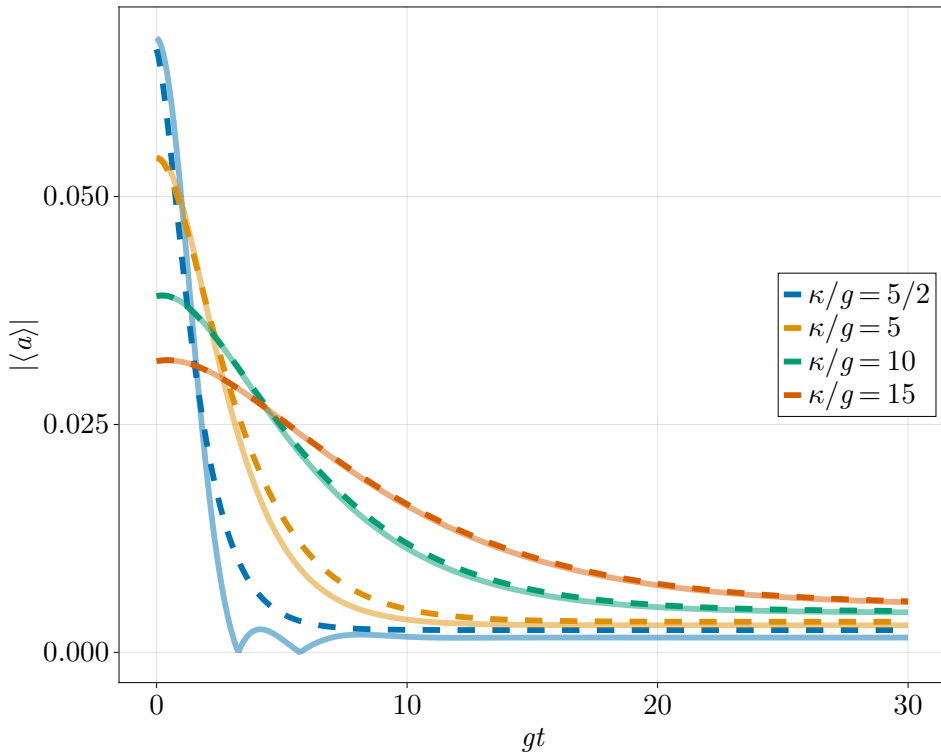


Figure 4.2.: Comparison between the numerical expectation value  $|\langle a \rangle|$  (full) and the adiabatic elimination (dashed). The initial state given by Eq. (4.17), we further varied  $\kappa$ , such that in  $\kappa/g = 5/2, 5, 10, 15$  the other system values are chosen as  $\gamma/g = 1/200$  and  $\epsilon/\sqrt{g} = 1/10\sqrt{2}$ .

In Fig. 4.2, we can now clearly see that for this state and increasingly high  $\kappa$  (lines in red and green) the approximation captures the dynamics very well at all times, therefore our assumptions seem to be justified. For low  $\kappa$  (blue) one can again see the presence of oscillations, due to the

#### 4. Adiabatic Elimination

exchange of photons between the cavity and two-level system, which are not captured by the adiabatic elimination.

##### 4.3.2. Determination of the $g^{(2)}(t)$ -Function

This subsection focuses on finding the  $g^{(2)}$ -function with the initial state chosen as the steady state, the reason for this being that in experiments one can usually assume the system to be in a steady state and then as soon as a photon is detected one starts the constant measurement of photons leaving the cavity. Analyzing the time between each measurement will result in the  $g^{(2)}$ -function. We note that the following steps are also applicable to an arbitrary initial state, but we are mainly interested in the case of an initial steady state.

To obtain an expression of the  $g^{(2)}$ -function, we want to start with the normalization constant  $\langle a^\dagger a \rangle_{ss}$ , which is given by Eq. (A.21) in the appendix, where we outlined how to obtain steady-state values from the adiabatic elimination as well as calculated  $g^{(2)}(0)$ . Since we found this normalization all that is left to do is find an expression of

$$\text{tr}\{a^\dagger(0)a^\dagger(\tau)a(\tau)a(0)\rho_{ss}\}, \quad (4.18)$$

to do this we first notice that we can find an operator description of  $a^\dagger(\tau)a(\tau)$  from the adiabatic elimination by

$$a_{adb}^\dagger(\tau)a_{adb}(\tau) = \left(\frac{2}{\kappa}\right)^2 \left(\frac{g^2}{2}(\sigma_z(\tau) + 1) - g\epsilon\sqrt{\kappa}(\sigma(\tau) + \sigma^\dagger(\tau)) + \epsilon^2\kappa\right), \quad (4.19)$$

where we used the identity  $\sigma^\dagger\sigma = \frac{1}{2}(\sigma_z + 1)$ . Note that this is the same expression as in Eq. (A.21), but instead of steady state values, we now use the time-dependent ones, obtained from Sec. 4.1. The  $g^{(2)}$ -function is just the measure of the average photon number over time, with the initial state being the normalized photon reduced steady state of Eq. (4.17). We will further use the quantum regression theorem to obtain the  $g^{(2)}$ -function [30]. But note that from the form of the  $g^{(2)}$ -function given by Eq. (4.18) we notice it would be sufficient to find an approximation of  $\langle a^\dagger(\tau)a(\tau) \rangle$  for the initial state  $a(0)\rho_{ss}a^\dagger(0)$ , which is another way to obtain the  $g^{(2)}$ -function.

To obtain a result we need to find  $\langle a^\dagger(0)a^\dagger(\tau)a(\tau)a(0) \rangle$ , but since  $a_{adb}^\dagger(\tau)a_{adb}(\tau)$  solely depends on the two-level expectation values it is sufficient to find  $\langle a^\dagger(0)\sigma_i(\tau)a(0) \rangle$ . To achieve this we first need to find the atom operator expectation values at time  $\tau = 0$  and then based on this we find the time evolution by the quantum regression theorem. This is done by changing  $\vec{v}(0)$  to

$$\vec{v}(0) = \begin{pmatrix} \langle a^\dagger\sigma a \rangle_{ss} \\ \langle a^\dagger\sigma^\dagger a \rangle_{ss} \\ \langle a^\dagger\sigma_z a \rangle_{ss} \\ \langle a^\dagger a \rangle_{ss} \end{pmatrix}, \quad (4.20)$$

where all expectation values are obtainable from within the adiabatic elimination. We will show how to do this for  $\langle a^\dagger\sigma a \rangle_{ss}$ , the other quantities then follow in the same manner

$$\begin{aligned} \langle a^\dagger\sigma a \rangle_{ss} &= \frac{4}{\kappa^2} \left\langle \left( g\sigma^\dagger - \epsilon\sqrt{\kappa} \right) \sigma \left( g\sigma - \epsilon\sqrt{\kappa} \right) \right\rangle_{ss} \\ &= -\frac{4\epsilon\sqrt{\kappa}}{\kappa^2} \left\langle \left( g\sigma^\dagger - \epsilon\sqrt{\kappa} \right) \sigma \right\rangle_{ss} \\ &= -\frac{4\epsilon}{\kappa\sqrt{\kappa}} \left( \frac{g}{2}(\langle \sigma_z \rangle_{ss} + 1) - \epsilon\sqrt{\kappa} \langle \sigma \rangle_{ss} \right). \end{aligned} \quad (4.21)$$

#### 4. Adiabatic Elimination

Then by inserting the steady state values from App. A.3 we obtain our initial values of  $\vec{v}(0)$ . By further applying Eq. (4.11) together with the quantum regression theorem [30], we see that we can find  $\langle a^\dagger(0)\sigma_i(\tau)a(0) \rangle$  through

$$\begin{pmatrix} \langle a^\dagger(0)\sigma(\tau)a(0) \rangle \\ \langle a^\dagger(0)\sigma^\dagger(\tau)a(0) \rangle \\ \langle a^\dagger(0)\sigma_z(\tau)a(0) \rangle \\ \langle a^\dagger(0)a(0) \rangle \end{pmatrix} = e^{A\tau}\vec{v}(0), \quad (4.22)$$

where  $\vec{v}(0)$  is given by Eq. (4.20). Now we see that

$$\begin{aligned} \langle a^\dagger(0)a_{adb}^\dagger(\tau)a_{adb}(\tau)a(0) \rangle &= \left(\frac{2}{\kappa}\right)^2 \left[ \frac{g^2}{2} \left( \langle a^\dagger(0)\sigma_z(\tau)a(0) \rangle + \langle a^\dagger(0)a(0) \rangle \right) \right. \\ &\quad \left. - g\epsilon\sqrt{\kappa} \left( \langle a^\dagger(0)\sigma(\tau)a(0) \rangle + \langle a^\dagger(0)\sigma^\dagger(\tau)a(0) \rangle \right) \right. \\ &\quad \left. + \epsilon^2\kappa \langle a^\dagger(0)a(0) \rangle \right], \end{aligned} \quad (4.23)$$

where all the expectation values are obtained from Eq. (4.22). Together with the normalization, given by Eq. (A.21), we have all the parts to compute the  $g^{(2)}$ -function by

$$g^{(2)}(\tau) = \frac{\langle a^\dagger(0)a_{adb}^\dagger(\tau)a_{adb}(\tau)a(0) \rangle}{\langle a^\dagger(0)a(0) \rangle^2}, \quad (4.24)$$

where we want to note that  $\langle a^\dagger(0)a(0) \rangle = \langle a^\dagger a \rangle_{ss}$ . A comparison of this expression to numerical simulations of the system can be seen in Fig. 4.3.

In principle we obtained an expression of the  $g^{(2)}(\tau)$ -function, but since the resulting expression is rather long and does not give much further insight we want to display it in the low drive limit by expanding it in  $\epsilon$  up to order  $\mathcal{O}(\epsilon^2)$

$$g^{(2)}(\tau) = \left(1 - F_p^2 e^{-\frac{\tau}{2}\gamma(F_p+1)}\right)^2 + \mathcal{O}(\epsilon^2), \quad (4.25)$$

where one can nicely see that for  $\tau \rightarrow \infty$  we will obtain  $g^{(2)} = 1$ . In the low drive limit, we also nicely see the dependence of the coherent decay factor  $F_p$ , which is given by Eq. (3.1). Additionally, we can obtain a simple expression of  $g^{(2)}(0)$  in the low drive limit, for this we simply set  $\tau = 0$  in Eq. (4.25) and obtain

$$g^{(2)}(0) = \frac{(1 - 2\beta)^2}{(1 - \beta)^4} + \mathcal{O}(\epsilon^2), \quad (4.26)$$

where  $\beta$  is given by Eq. (3.4), this expression of  $g^{(2)}(0)$  is the same as can be found in the appendix in Eq. (A.28). Having an expression of  $g^{(2)}(0)$  is of interest because it tells us when we expect photon bunching or antibunching. Photon bunching and antibunching describe how photons are expected to leave the cavity, photon bunching ( $g^{(2)}(0) > 1$ ) occurs when photons leave the cavity in groups. Antibunching ( $g^{(2)}(0) < 1$ ) signifies photons leave one at a time. From the simple expression of  $g^{(2)}(0)$ , we expect perfect bunching if  $\beta = 1$  and perfect antibunching if  $\beta = 1/2$ . Where we want to note that for  $\beta = 1$  we would need  $F_p \rightarrow \infty$ , under the assumption of nonzero dissipation rates  $\kappa, \gamma$ , this is not accessible with a finite coupling between two-level system and cavity.

Further on, we want to motivate the choice of the low drive limit, which allowed us to expand the  $g^{(2)}$ -function in orders of  $\epsilon$ . One of the primary reasons for using the low drive limit is that

#### 4. Adiabatic Elimination

a strong drive destroys coherence in the system. In quantum mechanical systems, coherence refers to the superposition and phase relationships between states, which are fundamental for observing quantum effects like entanglement or photon antibunching. Under strong driving conditions, the external field would dominate, but since we want to observe quantum mechanical effects the low drive limit is a reasonable assumption.

Next we want to take a look at how well the full approximation performs in comparison to numerics. Since we start with something related to the steady state, we would expect a good fit between approximation and full numerics.

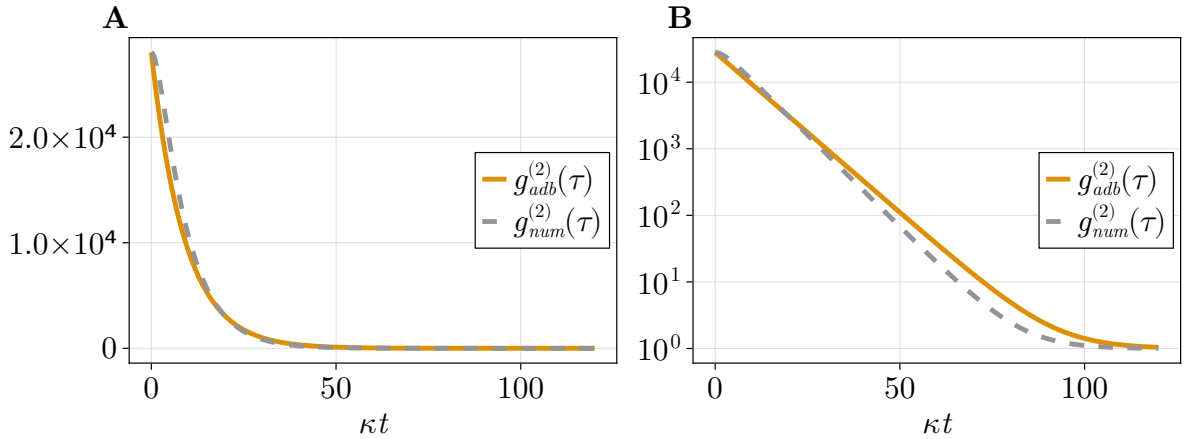


Figure 4.3.: Comparison between the  $g^{(2)}(\tau)$ -function between exact numerics (grey) and the full adiabatic approximation (orange) on a linear scale in panel **A** and on a logarithmic scale in panel **B**. System values are chosen as  $g/\kappa = 1/6$ ,  $\epsilon/\sqrt{\kappa} = 1/20\sqrt{30}$ .

In Fig 4.3 we can now see that the adiabatic elimination works fairly well, but we also get a glimpse of the motivation for this project, since the adiabatic elimination does not capture the early behavior very well. Because of this, we want to find additional terms or corrections to it, so that in total we get a description that effectively overlaps the dashed line in Fig. 4.3. We also see that qualitative features are missing, for example, the adiabatic elimination is not able to capture the early and later curvature of the  $g^{(2)}$ -function. From the *log*-plot, panel **B** in Fig. 4.3 we suspect the adiabatic elimination expects a simple exponential decay for early times, whereas the real behavior seems to be more complex than that. Additionally, we are still restricted to the regime of the *bad cavity* limit, since moving too far away from it will reduce the accuracy of the adiabatic elimination drastically.

#### 4.4. Limitations of Adiabatic Elimination and Importance of Normal Ordering

This section will explain why normal ordering is so important in the framework of the adiabatic elimination, the main steps are taken from [17]. We want to do this using the Langevin equation, in this framework the product rule and the commutation relations hold, thus making the analysis

#### 4. Adiabatic Elimination

independent of the normal ordering. In our case, the Langevin equations of motion read

$$\dot{a} = -\frac{\kappa}{2}(a - a_{adb}) + \hat{\xi}_1 \quad (4.27)$$

$$\dot{\sigma} = -\frac{\gamma}{2}\sigma + igZa + \hat{\xi}_2, \quad (4.28)$$

where  $\hat{\xi}_1$  and  $\hat{\xi}_2$  are noise operators with zero mean  $\langle \hat{\xi}_1 \rangle = \langle \hat{\xi}_2 \rangle = 0$  and  $a_{adb} = -2i/\kappa(g\sigma - \epsilon\sqrt{\kappa})$ . In principle, we are only interested in Eq. (4.27), so let's write down the formal solution of it

$$a(t) = e^{-\frac{\kappa t}{2}} a(0) + \frac{\kappa}{2} \int_0^t d\tau a_{adb}(t-\tau) e^{-\frac{\kappa}{2}\tau} + \int_0^t d\tau \xi_1(t-\tau) e^{-\frac{\kappa}{2}\tau}, \quad (4.29)$$

where we would like to outline that this whole equation is dependent on  $\hat{\xi}_2$  by the  $a_{adb}$ , so both noise operators influence the dynamics of  $a$ . Next, we use the formal limit of  $\kappa \rightarrow \infty$  leading to

$$a(t) = a_{adb}(t) + \frac{2}{\kappa} \xi_1(t). \quad (4.30)$$

Neglecting the influence of the  $\hat{\xi}_2$  operator, we can see that by using normal ordered operators, which means creation operators are to the left and annihilation operators are to the right, we are ensured that  $\hat{\xi}_1$  acts on the vacuum bath state  $|0\rangle_b$ , as well as  $\hat{\xi}_1^\dagger$  acts on  $\langle 0|_b$ . We show this on the basis of  $a^\dagger(t)a(t)$

$$\langle a^\dagger(t)a(t) \rangle \stackrel{\kappa \rightarrow \infty}{\cong} \langle 0|_b \langle \Psi_0 | \left( a_{adb}^\dagger(t) + \frac{2}{\kappa} \xi_1^\dagger(t) \right) \left( a_{adb}(t) + \frac{2}{\kappa} \xi_1(t) \right) | \Psi_0 \rangle | 0 \rangle_b \quad (4.31)$$

$$= \langle 0|_b \langle \Psi_0 | a_{adb}^\dagger(t) a_{adb}(t) | \Psi_0 \rangle | 0 \rangle_b, \quad (4.32)$$

where  $|\Psi_0\rangle$  is the initial system state and  $|0\rangle_b$  is the bath vacuum state. In the transition from the first to the second line, we used the fact that  $\xi_1(t)|0\rangle_b = 0$ . Here we want to note that this procedure works as well for larger products on cavity field operators. Let  $\Sigma$  be an arbitrary atom operator, for which we want to compute

$$\begin{aligned} \langle (a^\dagger)^n \Sigma(a)^m \rangle &\stackrel{\kappa \rightarrow \infty}{\cong} \langle a_{adb}^\dagger (a^\dagger)^{n-1} \Sigma(a)^{m-1} a_{adb} \rangle \\ &= \langle (a^\dagger)^{n-1} a_{adb}^\dagger \Sigma a_{adb} (a)^{m-1} \rangle \\ &\vdots \\ &= \langle (a_{adb}^\dagger)^n \Sigma(a_{adb})^m \rangle, \end{aligned} \quad (4.33)$$

where  $n$  and  $m$  are integers, in this derivation we immediately dropped the noise operators, since they act on the vacuum as in Eq. (4.32). Additionally, we used that  $a_{adb}^{(\dagger)}$  is an operator in the two-level subspace and therefore commutes with  $a^{(\dagger)}$ . If we use normal ordered operators we see that it is applicable to use

$$a(t) = a_{adb}(t), \quad (4.34)$$

which is in principle the same expression as we used during the whole chapter.

But this opens a brand-new question, if the noise operators drop out in the Langevin approach, why did we obtain a mismatch between adiabatic elimination and numerics for  $g^{(2)}(0)$  seen in Fig. A.1. If one does not use  $\kappa \rightarrow \infty$ , the formal solution of Eq. (4.29) will have a contribution to  $a^\dagger a$  in the form of

$$\int_0^t \int_0^t d\tau' d\tau a_{adb}^\dagger(t-\tau) a_{adb}(t-\tau') e^{-\frac{\kappa}{2}(\tau+\tau')}. \quad (4.35)$$

#### 4. Adiabatic Elimination

See that in the adiabatic elimination we would use

$$a_{adb}^\dagger(t)a_{adb}(t), \tag{4.36}$$

as a representation of  $a^\dagger a$ . But from the exact result, we obtained an integral in which also past times are taking effects. Therefore, the adiabatic elimination can also fail for steady state expectation values, for which one would apply the limit  $t \rightarrow \infty$ .

To summarize, in the Langevin approach commutation relations, hold so that we can either use normal ordering or not, both are valid options. However under the formal limit of  $\kappa \rightarrow \infty$ , when using normal ordering we can drop the noise terms, which gives us an expression of the cavity field operator that coincides with Eq. (4.4). Therefore we conclude that the adiabatic elimination is a reasonable approximation if one uses normal ordered operators and a large cavity dissipation rate  $\kappa$ .

## 5. Prodiabatic Elimination

This section introduces the *prodiabatic elimination*, a technique developed to address the limitations of the adiabatic elimination. As a concrete application, we aim to achieve a more accurate approximation of the  $g^{(2)}$ -function. To this end, we first derive a new expression for the cavity field operator  $a$ . Using this expression, we propose a novel approach to solving the two-level dynamics, resulting in a significant improvement over the adiabatic elimination. In this chapter, we restrict our analysis to the case of a resonant drive  $\Delta_c = \Delta_d = 0$ .

### 5.1. General Procedure of the Prodiabatic Elimination

#### 5.1.1. Obtaining the Cavity Field Operator

To start things off we formally solve Eq. (4.1), which we rewrite to

$$\dot{a} = -\frac{\kappa}{2}(a - a_{adb}), \quad (5.1)$$

where  $a_{adb} = -2i/\kappa(g\sigma - \epsilon\sqrt{\kappa})$  is defined by the two-level system operators, here we want to note that  $\sigma(t)$  is not given by Eq. (4.11), but is so to be determined further on. Formally solving Eq. (5.1) will lead to

$$a(t) = e^{-\frac{\kappa t}{2}} a(0) + \int_0^t d\tau \frac{\kappa}{2} a_{adb}(\tau) e^{\frac{\kappa(\tau-t)}{2}}. \quad (5.2)$$

Notice that Eq. (5.2) is dependent on an integral involving  $a_{adb}(\tau)$ , which is a problem since one would need to solve the other non-linearly coupled two-level system differential equation to evaluate it. To make further progress we substitute  $\tau' = t - \tau$  in the integral of Eq. (5.2)

$$a(t) = e^{-\frac{\kappa t}{2}} a(0) + \int_0^t d\tau' \frac{\kappa}{2} a_{adb}(t - \tau') e^{-\frac{\kappa \tau'}{2}}. \quad (5.3)$$

Next, we will apply a Taylor expansion in  $\tau'$  around  $\tau' = 0$  on  $a_{adb}(t - \tau')$ , leading to

$$a_{adb}(t - \tau') = a_{adb}(t) - \dot{a}_{adb}(t)\tau' + \frac{d_t^2 a_{adb}(t)}{2} \tau'^2 + \mathcal{O}(\tau'^3), \quad (5.4)$$

with  $d_t$  indicating a total derivative with respect to  $t$ . Note that this expansion needs  $\sigma(t)$  to be an analytic function, otherwise, the expansion in the form of a Taylor series is not justified. But in the presence of noise  $\dot{\sigma} \propto \hat{\xi}_1$  and since  $\hat{\xi}_1$  is a stochastic operator we cannot differentiate it. This becomes a problem as soon as we want to include terms like  $d_t^2 a_{adb}$ , as there is the second derivative of  $\sigma(t)$  involved, for which we would need  $d_t \hat{\xi}_1$ , which does not exist. But in our case, we are not dealing with any noise terms so the expansion should be justified. In the presence of noise, one needs an argument as to why the noise is negligible, similar to what we did in Sec. 4.4, once the noise is argued away the same steps as further on can be taken.

The Taylor expansion is a crucial step as it allows us to pull  $a_{adb}(t)$  and its derivatives out of the integral of Eq. (5.3), which removes the need to find an expression of the two-level dynamics and makes the integral solvable in a straight forward manner. Next, we want to truncate the expansion because we argue that the neglected terms are of higher order in  $1/\kappa$ . This can be seen

## 5. Prodiabatic Elimination

by the first substituting the Taylor expansion of Eq. (5.4) into the formal solution of Eq. (5.3) leading to

$$\begin{aligned}
a(t) = & a(0)e^{-\frac{\kappa t}{2}} \\
& + a_{adb}(t) \left(1 - e^{-\frac{\kappa t}{2}}\right) \\
& + \frac{1}{\kappa} \dot{a}_{adb}(t) \left(-2 + e^{-\frac{\kappa t}{2}}(2 + \kappa t)\right) \\
& + \frac{1}{4\kappa^2} d_t^2 a_{adb}(t) \left(8 - e^{-\frac{\kappa t}{2}}((\kappa t + 2)^2 + 4)\right) \\
& + \mathcal{O}(1/\kappa^3),
\end{aligned} \tag{5.5}$$

where we will be now neglecting the term proportional to  $d_t^2 a_{adb}(t)$  as it involves higher orders in  $1/\kappa$ , with the same reasoning we also drop the  $\mathcal{O}(1/\kappa^3)$  part. Note that we cannot truncate the expansion at Eq. (5.4), as  $\tau'$  might be a large parameter, but since  $1/\kappa$  is generally very small, truncating the series at this point is justified. This results in our approximation being

$$a_{pdb}(t) = a(0)e^{-\frac{\kappa t}{2}} + a_{adb}(t) \left(1 - e^{-\frac{\kappa t}{2}}\right) + \frac{1}{\kappa} \dot{a}_{adb}(t) \left(-2 + e^{-\frac{\kappa t}{2}}(2 + \kappa t)\right), \tag{5.6}$$

which is equivalent to

$$a_{pdb}(t) = a(0)e^{-\frac{\kappa t}{2}} - \frac{2i}{\kappa} (g\sigma(t) - \epsilon\sqrt{\kappa}) (1 - e^{-\frac{\kappa t}{2}}) - \frac{2ig}{\kappa^2} \dot{\sigma}(t) \left(-2 + e^{-\frac{\kappa t}{2}}(2 + \kappa t)\right), \tag{5.7}$$

so we can again approximate the cavity operator based on the two-level dynamics. This new expression of  $a(t)$  will be labeled by *pdb*, standing for *prodiabatic*.

In the limit of  $t \rightarrow \infty$  we obtain

$$\lim_{t \rightarrow \infty} a_{pdb}(t) = \lim_{t \rightarrow \infty} a_{adb}(t), \tag{5.8}$$

where we assumed that the derivative of  $\sigma$  vanishes for long times. This result is nice since we know that  $a_{adb}$  will yield satisfying results in the long time limit. But one problem still remains; we do not have an expression for  $a_{adb}(t)$ . One could think we could use the result obtained in Chap. 4, but this will not work, since the adiabatic elimination is not suited for approximating  $\dot{\sigma}$  at early times, therefore leading to a significant error in  $\dot{a}_{adb}$ . We outlined this further in the discussion of Fig. 5.6. Additionally, we would restrict the validity of our solution again to the limitations of the adiabatic elimination. Therefore we will propose a new method to obtain the two-level dynamics.

### 5.1.2. Obtaining the Two-Level Dynamics

This section will show how we obtain an expression of  $a_{adb}(t)$ , for this we start by assuming that we may replace  $a(t)$  by

$$a(t) \approx a_{adb}(t) - \frac{2}{\kappa} \dot{a}_{adb}(t) = -\frac{2i}{\kappa} (g\sigma(t) - \epsilon\sqrt{\kappa}) + \frac{4ig}{\kappa^2} \dot{\sigma}(t), \tag{5.9}$$

which one obtains by assuming  $\kappa t \gg 1$  therefore all the exponential functions of Eq. (5.6) decay to zero, leading to the above. The assumption remains that the two-level dynamics are the slow ones and the cavity is quickly adapting to these changes, which is reasonable if  $\kappa$  is large. Notice that  $a(t)$  of Eq. (5.9) is only in the two-level subspace, similar to the adiabatic elimination, as outlined in Chap. 4. In contrast to that, our expression is also dependent on a derivative; this is a consequence of going one order beyond the adiabatic elimination. To solve the two-level

## 5. Prodiabatic Elimination

dynamics we will use Eq. (5.9) and based on it we can find an approximation of  $\sigma(t)$ . Once we found an expression of  $\sigma(t)$  we also get an expression on  $\dot{\sigma}(t)$ , which then gives us all the parts of  $a_{pdb}$ , see Eq. (5.7).

We start with the equation of motion of  $\sigma(t)$ , by inserting Eq. (5.9) we obtain

$$\begin{aligned}\dot{\sigma} &= -\frac{\gamma}{2}\sigma + ig\sigma_z a \\ &= -\frac{\gamma}{2}\sigma + ig\sigma_z \left( a_{adb}(t) - \frac{2}{\kappa}\dot{a}_{adb}(t) \right) \\ &= -\left( \frac{\gamma}{2} + \frac{2g^2}{\kappa} \right) \sigma - \frac{2g\epsilon\sqrt{\kappa}}{\kappa}\sigma_z - \frac{4g^2}{\kappa^2}\sigma_z\dot{\sigma},\end{aligned}\tag{5.10}$$

which is equivalent to

$$\left( 1 + \frac{4g^2}{\kappa^2}\sigma_z \right) \dot{\sigma} = -\left( \frac{\gamma}{2} + \frac{2g^2}{\kappa} \right) \sigma - \frac{2g\epsilon\sqrt{\kappa}}{\kappa}\sigma_z.\tag{5.11}$$

To treat the  $\left( 1 + \frac{4g^2}{\kappa^2}\sigma_z \right)$  correctly we propose a simple inversion of it. For this notice

$$\left( 1 + \frac{4g^2}{\kappa^2}\sigma_z \right)^{-1} = \frac{\kappa^2}{\kappa^4 - 16g^4} (\kappa^2 - 4g^2\sigma_z),\tag{5.12}$$

where we obtained this by first writing everything in matrix form and inverting the matrix

$$\left( 1 + \frac{4g^2}{\kappa^2}\sigma_z \right)^{-1} = \begin{pmatrix} 1 + \frac{4g^2}{\kappa^2} & 0 \\ 0 & 1 - \frac{4g^2}{\kappa^2} \end{pmatrix}^{-1} = \begin{pmatrix} \frac{\kappa^2}{\kappa^2 + 4g^2} & 0 \\ 0 & \frac{\kappa^2}{\kappa^2 - 4g^2} \end{pmatrix},\tag{5.13}$$

by then representing this matrix by  $\sigma_z$  and  $\mathbb{1}$  you will obtain Eq. (5.12). This allows us to remove the  $\left( 1 + \frac{4g^2}{\kappa^2}\sigma_z \right)$  by multiplying its inverse from the left

$$\begin{aligned}\dot{\sigma} &= \frac{\kappa^2}{\kappa^4 - 16g^4} (\kappa^2 - 4g^2\sigma_z) \left( -\left( \frac{\gamma}{2} + \frac{2g^2}{\kappa} \right) \sigma - \frac{2g\epsilon\sqrt{\kappa}}{\kappa}\sigma_z \right) \\ &= -\frac{\kappa(\gamma\kappa + 4g^2)}{2\kappa^2 - 8g^2}\sigma - \frac{2g\epsilon\sqrt{\kappa}\kappa^3}{\kappa^4 - 16g^4}\sigma_z + \frac{8g^3\epsilon\sqrt{\kappa}\kappa}{\kappa^4 - 16g^4},\end{aligned}\tag{5.14}$$

now since we have an expression of  $\dot{\sigma}$  we can use this in Eq. (5.9), such that now this representation of  $a$  has no derivatives anymore, but is only a linear combination of two-level operators. Notice that there is an underlying assumption in Eq. (5.14), since for  $\kappa = 2g$  we would divide by zero further if  $\kappa < 2g$  we will obtain a positive decay rate, meaning exponential growth in  $\sigma(t)$ , which would not only contradict the existence of a steady state but would also make  $|\langle\sigma\rangle| > 1$  possible which is impossible for normalized states. Therefore we will generally assume  $\kappa > 2g$ , as this leads to the wanted decay.

Next, we find a linearized differential equation of  $\dot{\sigma}_z$  this is accomplished by again replacing  $a(t)$  by Eq. (5.9) and by replacing  $\dot{\sigma}$  by Eq. (5.14), thus we will obtain

$$\begin{aligned}\dot{\sigma}_z &= -2ig \left( \sigma^\dagger a - a^\dagger \sigma \right) - \gamma(\sigma_z + 1) \\ &= -2ig \left( \sigma^\dagger a_{adb} - a^\dagger_{adb}\sigma - \frac{2}{\kappa} \left( \sigma^\dagger \dot{a}_{adb} - \dot{a}^\dagger_{adb}\sigma \right) \right) - \gamma(\sigma_z + 1) \\ &= -\frac{\kappa(\gamma\kappa + 4g^2)}{\kappa^2 - 4g^2}(\sigma_z + 1) - \frac{4g\epsilon\sqrt{\kappa}\kappa}{4g^2 - \kappa^2}(\sigma + \sigma^\dagger).\end{aligned}\tag{5.15}$$

## 5. Prodiabatic Elimination

Similar to Chap. 4, with the differential equations of  $\dot{\sigma}$  and  $\dot{\sigma}^\dagger$ , we obtain a linear system of equations of the form  $\dot{x} = Ax$ , which is easily solved by an exponential matrix ansatz. For this we define the matrix

$$A = \begin{pmatrix} -\frac{\kappa(\gamma\kappa+4g^2)}{2\kappa^2-8g^2} & 0 & -\frac{2g\epsilon\sqrt{\kappa}\kappa^3}{\kappa^4-16g^4} & \frac{8g^3\epsilon\sqrt{\kappa}\kappa}{\kappa^4-16g^4} \\ 0 & -\frac{\kappa(\gamma\kappa+4g^2)}{2\kappa^2-8g^2} & -\frac{2g\epsilon\sqrt{\kappa}\kappa^3}{\kappa^4-16g^4} & \frac{8g^3\epsilon\sqrt{\kappa}\kappa}{\kappa^4-16g^4} \\ \frac{4g\epsilon\sqrt{\kappa}\kappa}{\kappa^2-4g^2} & \frac{4g\epsilon\sqrt{\kappa}\kappa}{\kappa^2-4g^2} & -\frac{\kappa(\gamma\kappa+4g^2)}{\kappa^2-4g^2} & -\frac{\kappa(\gamma\kappa+4g^2)}{\kappa^2-4g^2} \\ 0 & 0 & 0 & 0 \end{pmatrix}, \quad (5.16)$$

which solves the system of equations by

$$\begin{pmatrix} \sigma(t) \\ \sigma^\dagger(t) \\ \sigma_z(t) \\ 1 \end{pmatrix} = e^{At} \begin{pmatrix} \sigma(0) \\ \sigma^\dagger(0) \\ \sigma_z(0) \\ 1 \end{pmatrix}. \quad (5.17)$$

By expanding Eq. (5.16) in orders up to  $1/\kappa$  the leading order terms will result in Eq. (4.9), again displaying the connection to the adiabatic elimination and showing our inclusion of higher order effects. This concludes the main steps of the prodiabatic elimination. We obtained a simple representation of  $a_{adb}$  and  $\dot{a}_{adb}$ , inserting these expressions into Eq. (5.6) will give the full expression of for  $a_{pdb}(t)$ . We say this is an improvement to the adiabatic elimination since it does not only include  $a_{adb}$  but also includes derivative terms as  $\dot{a}_{adb}$ . A notable improvement over the adiabatic elimination can be observed, for instance, in Fig. 5.1.

We want to end this section by giving a brief overview of all the steps we took to end up with a new approximation of the cavity field operator, a list of them can be seen below.

Steps to Perform Prodiabatic Elimination	
1:	Formally solve $\dot{a}$
2:	Taylor expand $a_{adb}(t - \tau)$ in $\tau$ around $\tau = 0$
3:	Assume $\kappa t \gg 1$ to simplify $a_{pdb}(t)$
4:	Replace each $a$ by simplified $a_{pdb}(t)$ in equations of motions of two-level system
5:	Linearize the equations by inverting $\left(1 + \frac{4g^2}{\kappa^2}\sigma_z\right)$
6:	Solve two-level dynamics by an exponential matrix ansatz
7:	Use two-level solution to obtain full $a_{pdb}(t)$

## 5.2. Two-Level System

### 5.2.1. Effective Lindblad Master Equation

As done in Chap. 4 we would like to represent the equations of motion of the two-level system by a Lindblad master equation (LME) since an LME will give a lot of insight into what happens effectively in the two-level system. It turns out that it is possible to find a master equation (ME) such that it reproduces Eqs. (5.14) and (5.15). Finding this ME is not a trivial task, we provide a derivation in App. A.4. Here we only present the full ME, which reproduces the results of the prodiabatic elimination and expand it in terms of  $1/\kappa$  and low drive strengths  $\epsilon$ .

## 5. Prodiabatic Elimination

Both expansions yield Lindblad-form master equations, as all rates remain positive, ensuring trace preservation and complete positivity. In contrast, the full ME includes a negative rate, violating these properties.

We start by outlining the full ME, for this we display the rates

$$\gamma_{1,2} = \frac{\gamma (1 + F_p)(1 + \frac{\gamma}{\kappa} F_p) \pm \sqrt{\frac{8\epsilon^2 \gamma F_p^3}{\kappa^2} + (1 + F_p)^2 (1 + \frac{\gamma}{\kappa} F_p)^2}}{2 \left( 1 - (\frac{\gamma}{\kappa} F_p)^2 \right)}, \quad (5.18)$$

based on this, the total master ME is given by

$$\dot{\rho} = -i[H, \rho] + \sum_{i=1,2} \frac{\gamma_i}{1 + 2\epsilon^2 \kappa \frac{\frac{\gamma_i^3 F_p^3}{\kappa^3}}{(1 - \frac{\gamma_i^2 F_p^2}{\kappa^2})^2 \gamma_i^2}} \mathcal{D} \left[ \sigma + \frac{2 \left( \frac{\gamma_i}{\kappa} F_p \right) g \epsilon}{\left( (1 - (\frac{\gamma_i}{\kappa} F_p)^2 \right) \kappa^{1/2} \gamma_i \right)} \sigma_z \right] \rho. \quad (5.19)$$

with the Hamiltonian

$$H = -\frac{ig\epsilon}{\sqrt{\kappa}} \frac{2 + \frac{\gamma}{\kappa} F_p}{1 - (\frac{\gamma}{\kappa} F_p)^2} (\sigma - \sigma^\dagger). \quad (5.20)$$

Now we want to roughly interpret this master equation. Notice that the numerator of the rates  $\gamma_{1,2}$  is of the form  $x \pm \sqrt{y + x^2}$ , where both  $x$  and  $y$  are positive variables, therefore  $\gamma_2$  will always be negative. Further on we can interpret the rates  $\gamma_{1,2}$ , first of all, we want to know when the negative rate is comparably big, this is once  $\frac{\epsilon^2 \gamma F_p^3}{\kappa^2} = \frac{64g^6 \epsilon^2}{\gamma^2 \kappa^5}$  becomes a large quantity. This could be achieved by having a large coupling  $g$ , small rates  $\gamma$  and  $\kappa$ , while using a big drive strength  $\epsilon$ . Usually, we can assume large coupling and small dissipation rate  $\gamma$ , but having a large drive while simultaneously using a low cavity dissipation rate is not considered; we want the cavity dissipation rate  $\kappa$  to stabilize the cavity field implying a large dissipation and a low drive  $\epsilon$ . Further  $\kappa$  is limited by the condition  $\kappa > 2g$ , which we need to avoid divergences, so we can not consider an arbitrary low  $\kappa$  within this theory anyway. Therefore we will typically have  $\frac{\epsilon^2 \gamma F_p^3}{\kappa^2} \ll 1$  this implies  $\gamma_2 = 0$ , therefore we conclude that the negative rate is typically close to 0 and is not affecting the overall dynamics too much. By assuming the same on  $\gamma_1$  we obtain

$$\gamma_1 = \gamma \frac{1 + F_p}{1 - \frac{\gamma}{\kappa} F_p}, \quad (5.21)$$

which closely resembles the results of the adiabatic elimination.

Next, we have to discuss the new dissipator. We would expect the dissipation to be solely in  $\sigma$ , but surprisingly in the ME of Eq. (5.19) we also have a part that is proportional to  $\sigma_z$ . First, notice that the dissipation is still dominated by  $\sigma$ , the part proportional to  $\sigma_z$  is a small disturbance to it. In Eq. (5.25) one can see the expansion for low  $\epsilon$ , where under typical system values this prefactor of the  $\sigma_z$  term in the dissipation is a small parameter. We can further interpret this by having a look at the dissipator in the more simple form  $\mathcal{D}[\sigma + \xi \sigma_z]$ , where in our case  $\xi$  is a real-valued and typically small parameter. The jump associated with this operator on the pure state  $|1\rangle\langle 1|$  is

$$(\sigma + \xi \sigma_z) |1\rangle\langle 1| (\sigma^\dagger + \xi \sigma_z) = |0\rangle\langle 0| + \xi^2 |1\rangle\langle 1| + \xi (|1\rangle\langle 0| + |0\rangle\langle 1|), \quad (5.22)$$

where we can represent this state by the unnormalized Bloch vector  $(2\xi, 0, \xi^2 - 1) = (x, y, z)$ . Notice that under the assumption of a small  $\xi$ , this implies our state did not get fully mapped to the ground state  $|0\rangle$ , corresponding to the Bloch vector  $(0, 0, -1)$  and we also have a small  $x$ -component of the state. We speculate that this is due to the following; the two-level system

## 5. Prodiabatic Elimination

emits a photon into the cavity, which alters the cavity field and this change in the cavity field subsequently influences the two-level system again. This leads to the two-level system not fully decaying into the ground state, but this interpretation is purely speculative and we are unsure if that is the right way to think about the dissipator. Note that in the last two paragraphs, we argued that the proportionality of  $\sigma_z$  of the dissipator, is a small effect, so one might think it is acceptable to neglect it. But this is not the case, as this is part of the improvement compared to the adiabatic elimination, as will be seen further on.

Expanding the LME in the limit of large  $\kappa$ , we can verify that we obtained a result beyond the adiabatic elimination. Expanding all terms up to  $\mathcal{O}(1/\kappa^2)$  we obtain

$$H = -\frac{2ig\epsilon}{\sqrt{\kappa}}(\sigma - \sigma^\dagger), \quad (5.23)$$

and the master equation

$$\dot{\rho} = -i[H, \rho] + \gamma \left(1 + F_p + \frac{\gamma}{\kappa} F_p\right) \mathcal{D}[\sigma] \rho. \quad (5.24)$$

These results align with Eq. (4.13) but go one order beyond them with the decay rate enhanced further than in the adiabatic elimination. The general structure is the same as the adiabatic case, therefore the interpretation is the same as the LME of the adiabatic elimination, for the interpretation of this LME we refer to Sec. 4.2.1.

Since the drive is typically small, we aim to further also expand the master equation in orders of  $\epsilon$ . This is achieved by expanding the prefactors of the dissipators as well as the jump operators of the dissipator of Eq. (5.19). It is important to note that this expansion is not strictly rigorous, as it includes terms up to order  $\epsilon^2$  in the dissipator, while our overall expansion is limited to order  $\epsilon$ . However, given the assumption of a relatively small drive, we argue that the effect of the  $\epsilon^2$  terms is minimal. The reason for avoiding a fully rigorous expansion is that it would result in additional terms that cannot be expressed in the standard Lindblad master equation form. These terms would go beyond the typical unitary or dissipative contributions. Expanding in this manner, we find that the Hamiltonian is linear in  $\epsilon$ , meaning the expansion does not alter its form. Consequently, the Hamiltonian remains as given in Eq. (5.20). While it is still a driving term, its amplitude is more complex than in the adiabatic elimination or the simple  $1/\kappa$  expansion. The total LME reads

$$\dot{\rho} = -i[H, \rho] + \gamma \frac{1 + F_p}{1 - \frac{\gamma}{\kappa} F_p} \mathcal{D} \left[ \sigma + \frac{2g\epsilon\sqrt{\kappa}F_p}{\kappa^2(1 + F_p)(1 + \frac{\gamma}{\kappa}F_p)} \sigma_z \right] \rho, \quad (5.25)$$

With  $F_p$  given by Eq. (3.1), we observe that for large  $\kappa$ , the results of the adiabatic elimination are recovered, for example, see that if  $F_p\gamma/\kappa \ll 1$ , the decay rate matches that of the adiabatic elimination. We also want to highlight the prefactor of  $\sigma_z$  in the dissipator, as the primary effect remains the dissipation in  $\sigma$ . The  $\sigma_z$  component of the dissipator is scaled by  $1/\kappa^{3/2}$  as well as by  $\epsilon$ , suggesting that this prefactor is small for typical system parameters; however, its effect is non-negligible as we will show in the discussion of Fig. 5.1.

Next, we compare the previously derived master equations with numerical results as well as the outcomes of the adiabatic and prodiabatic eliminations. Since the LMEs are valid only within the two-level system, we need to use a slightly different initial state than usual. Specifically, we obtain the photon-reduced steady state from Eq. (4.17) using numerical methods and then trace out the cavity, resulting in a state defined solely within the two-level system.

## 5. Prodiabatic Elimination

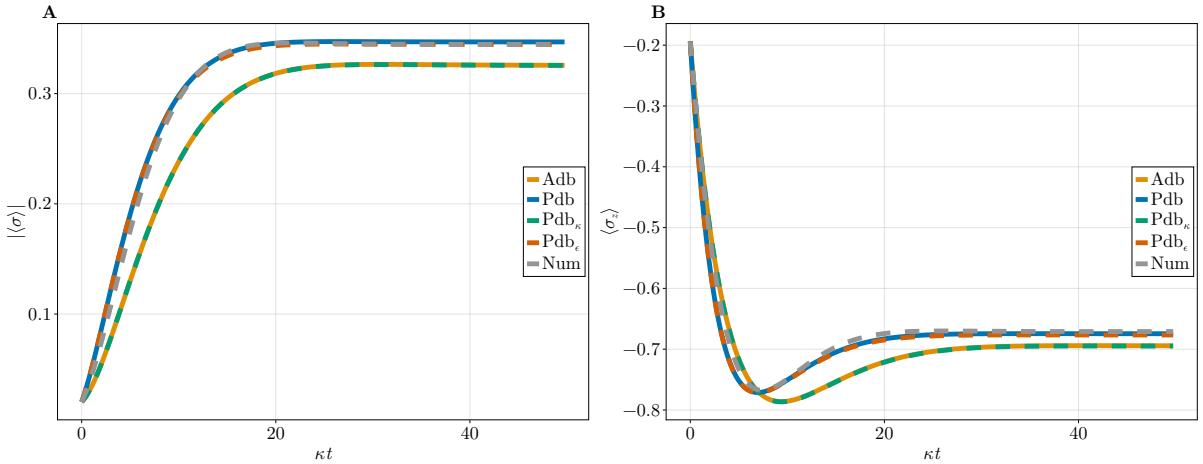


Figure 5.1.: Comparison between the different LMEs of each approximation, in **A**  $|\langle\sigma_x\rangle|$  and in **B**  $\langle\sigma_z\rangle$ . In orange the adiabatic elimination, in blue the full prodiabatic elimination, in green the prodiabatic elimination but expanded up to order  $1/\kappa^2$  given by Eq. (5.24), in red the expansion in  $\epsilon$  given by Eq. (5.25) and in gray the numerics. For the initial state, we chose the partial traced photon reduced state for all two-level LMEs and the full photon reduced state for the numerics, given by Eq. (4.17). System values are chosen as  $\gamma/\kappa = 1/800$ ,  $g/\kappa = 1/4$  and  $\epsilon/\sqrt{\kappa} = 1/6\sqrt{2}$ , the coherent decay factor equates to  $F_p = 200$ .

In Fig. 5.1, we observe the main differences between the approximations. First, the expansion in the drive closely matches the result of the prodiabatic elimination, with only small, barely noticeable differences. Secondly, the expansion in orders of  $1/\kappa$  in Eq. (5.24) matches well with the result of the adiabatic elimination. This agreement is expected, as  $F_p$  is large in this case and  $\gamma/\kappa$  small, therefore the second order correction has no big effect. Additionally, note that terms like  $F_p$  are of order  $1/\kappa$  so they have to be small otherwise truncating the expansion is not justified. But in our case,  $F_p$  is a large quantity, therefore we are not justified to truncate the expansion in  $1/\kappa$ . But if  $1/\kappa$  is so large that the expansion is justified there is no difference between adiabatic or prodiabatic elimination.

We can also observe the impact of including a term proportional to  $\sigma_z$  in the dissipator. In the example shown in Fig. 5.1, we use  $\frac{\gamma}{\kappa}F_p = \frac{1}{4}$ , which is relatively small. Consequently, the rates of the  $\epsilon$  expanded and  $1/\kappa$  expanded LMEs do not differ significantly. However, they employ different dissipators, and the inclusion of the  $\sigma_z$  term appears to yield significantly improved results. This improvement is notable, as the  $\sigma_z$  contribution represents only a small fraction of the total dissipation. Finally, we emphasize that the simulations were performed under a comparably high drive, which can be seen by  $\epsilon/\sqrt{\kappa} = 1/6\sqrt{2}$ , while the bad cavity limit would require  $\epsilon/\sqrt{\kappa} \ll 1$ . This supports the validity of the  $\epsilon$  expansion, even for relatively high drive values.

To observe a breakdown of the prodiabatic elimination and the  $\epsilon$  expansion of the full ME we need to consider an even larger driving strength  $\epsilon$  and  $\kappa$  close to  $2g$ . This can be seen in Fig. 5.2, where we observe the  $\epsilon$  expansion LME breaking down, which means it no longer aligns with the results of the prodiabatic elimination, which is to be expected for larger driving strengths. Additionally, the prodiabatic elimination is also failing, as it is no longer able to predict the numerical two-level system dynamics adequately.

## 5. Prodiabatic Elimination

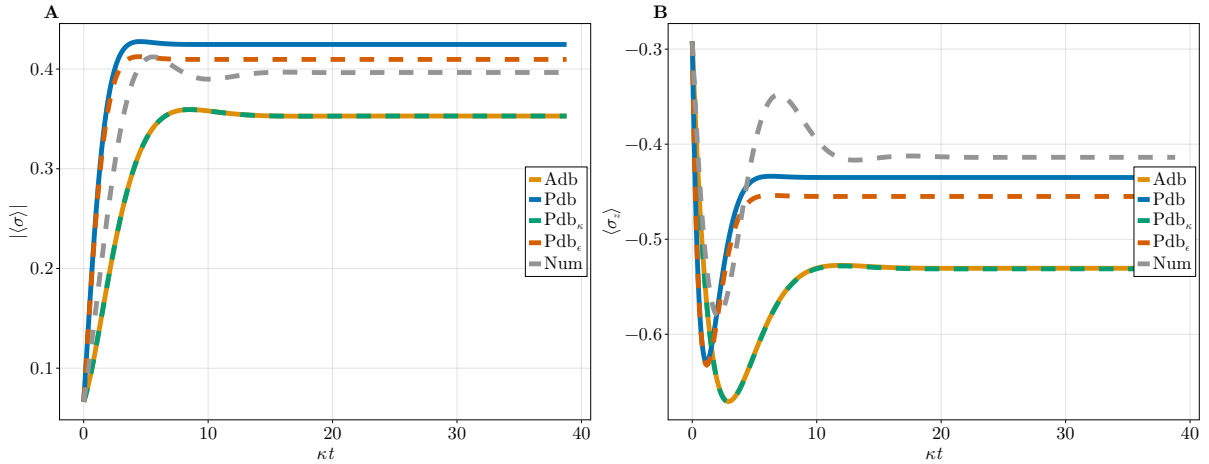


Figure 5.2.: Comparison between the different LMEs of each approximation, in **A**  $|\langle\sigma\rangle|$  and in **B**  $\langle\sigma_z\rangle$ . In orange the adiabatic elimination, in blue the full prodiabatic elimination, in green the prodiabatic elimination but expanded up to order  $1/\kappa^2$  given by Eq. (5.24), in red the expansion in  $\epsilon$  given by Eq. (5.25) and in gray the numerics. For the initial state, we chose the partial traced photon reduced state for all two-level LMEs and the full photon reduced state for the numerics, given by Eq. (4.17). System values are chosen as  $\gamma/\kappa = 1/800$ ,  $g/\kappa = 3/8$  and  $\epsilon/\sqrt{\kappa} = 1/4$ , the coherent decay factor equates to  $F_p = 450$ . By decreasing  $\kappa$ , while simultaneously increasing  $\epsilon$  the prodiabatic elimination fails and additionally is not coinciding with the  $\epsilon$  expanded LME anymore.

### 5.2.2. Steady State

The prodiabatic elimination also gives us a way of obtaining the steady state values, by simply taking the limit of  $t \rightarrow \infty$ . To do this we diagonalize the matrix  $A$  of Eq. (5.16) and see that all eigenvalues have a real part  $\leq 0$ , if  $2g < \kappa$ . Next, we find a transition matrix  $S$  such that

$$S^{-1}AS = A_{diag}, \quad (5.26)$$

where  $A_{diag}$  is the diagonal form of the matrix  $A$ , with the eigenvalues on its diagonal. Therefore, the calculation is simplified by seeing that in the long time limit, we obtain

$$\lim_{t \rightarrow \infty} e^{At} = \lim_{t \rightarrow \infty} S e^{A_{diag}t} S^{-1} = S \left( \lim_{t \rightarrow \infty} e^{A_{diag}t} \right) S^{-1}, \quad (5.27)$$

where in this limit all elements go to zero except for the one with the zero eigenvalue, which is the constant part. This is to be expected, since otherwise we would find that the steady-state values depend on the initial values, but this cannot be the case since we have a unique steady state. Another way to obtain the steady-state expectation values of the two-level system is by setting the derivatives in Eqs. (5.14) and (5.15) to zero and solving the resulting linear system of equations. Further, we can also compare this result directly to the adiabatic elimination, a comparison of the two-level steady state expectation values can be seen in Fig. 5.3. For the

## 5. Prodiabatic Elimination

prodiabatic elimination we obtain

$$\langle \sigma \rangle_{ss} = \frac{4g\sqrt{\kappa}\epsilon (4g^2 + \kappa^2) (\gamma\kappa + 4g^2)}{(4g^2 + \kappa^2) (\gamma\kappa + 4g^2)^2 + 32g^2\kappa^3\epsilon^2} \quad (5.28)$$

$$\langle \sigma_z \rangle_{ss} = -1 + \frac{32g^2\kappa\epsilon^2 (4g^2 + \kappa^2)}{(4g^2 + \kappa^2) (\gamma\kappa + 4g^2)^2 + 32g^2\kappa^3\epsilon^2}. \quad (5.29)$$

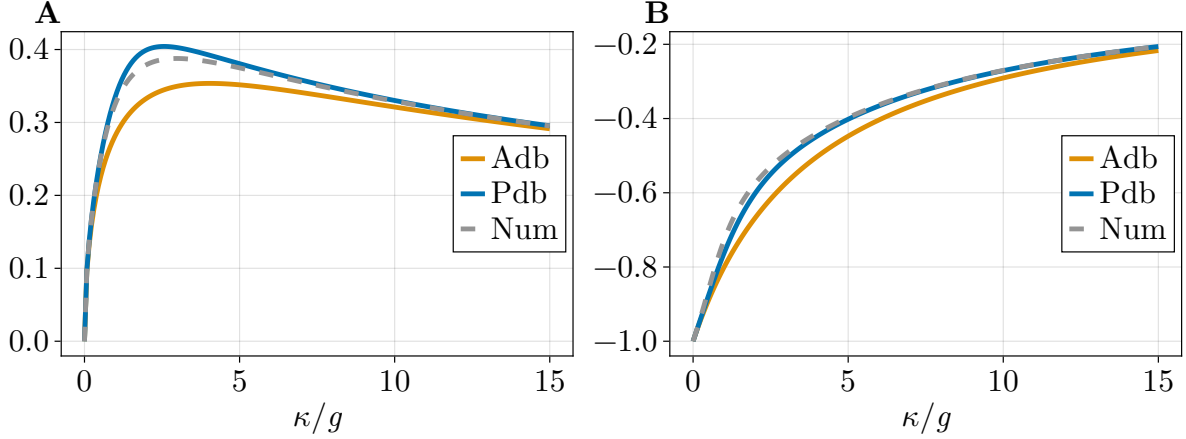


Figure 5.3.: Comparison between the different estimations of the steady state value of  $|\langle \sigma \rangle_{ss}|$  in **A** and  $\langle \sigma_z \rangle_{ss}$  in **B** as a function of the dissipation rate  $\kappa$ . In orange adiabatic elimination, in blue prodiabatic elimination and in gray the numerical results. System values are chosen as  $\gamma/g = 1/200$  and  $\epsilon/\sqrt{g} = 1/2\sqrt{2}$ .

It is important to note that in Fig. 5.3 we used a relatively high drive, the reason for this is simply that just then the discrepancies in the higher order terms become relevant, as can be seen in for example Fig. 5.4 where for increasing  $\epsilon$  the adiabatic elimination seemed to underestimate  $\langle \sigma_z \rangle_{ss}$ . We again notice a strict improvement of the prodiabatic elimination compared to adiabatic elimination. One might ask why in panel **B** for  $\kappa = 0$  we obtain  $\langle \sigma_z \rangle_{ss} = -1$ , in this case, there is no cavity dissipation so it seems counterintuitive that the atom will have the vacuum state  $|0\rangle$  as steady state. The reason for this is that the total drive strength is  $\epsilon\sqrt{\kappa} = 0$  at this point, but the dissipation rate  $\gamma$  of the two-level system is still present, because of this we expect to empty both cavity and two-level system at this point.

Next, we want to expand the atom expectation values for small drives, giving us a qualitative insight into how this new approach compares to the adiabatic elimination. Expanding  $\langle \sigma \rangle_{ss}$  and  $\langle \sigma_z \rangle_{ss}$  in both approximations leads to

Prodiabatic elimination	Adiabatic elimination
$\langle \sigma \rangle_{ss} = \frac{4g\sqrt{\kappa}\epsilon}{\gamma\kappa + 4g^2} - \frac{128\epsilon^3(g^3\kappa^{7/2})}{(4g^2 + \kappa^2)(\gamma\kappa + 4g^2)^3} + \mathcal{O}(\epsilon^5)$	$\frac{4g\sqrt{\kappa}\epsilon}{\gamma\kappa + 4g^2} - \frac{128\epsilon^3(g^3\kappa^{3/2})}{(\gamma\kappa + 4g^2)^3} + \mathcal{O}(\epsilon^5)$
$\langle \sigma_z \rangle_{ss} = -1 + \frac{32g^2\kappa\epsilon^2}{(\gamma\kappa + 4g^2)^2} - \frac{1024\epsilon^4(g^4\kappa^4)}{(4g^2 + \kappa^2)(\gamma\kappa + 4g^2)^4} + \mathcal{O}(\epsilon^5)$	$-1 + \frac{32g^2\kappa\epsilon^2}{(\gamma\kappa + 4g^2)^2} - \frac{1024\epsilon^4(g^4\kappa^2)}{(\gamma\kappa + 4g^2)^4} + \mathcal{O}(\epsilon^5)$

## 5. Prodiabatic Elimination

where we see, that the prodiabatic elimination aligns with the adiabatic elimination up to order  $\mathcal{O}(\epsilon^2)$  but in the higher order terms we obtain a difference. This discrepancy is scaled by  $1/\kappa$  which is a small parameter in the context of the bad cavity limit, however, those terms become relevant as soon as this assumption is relaxed.

### 5.2.3. Analyzing the Two-Level System Dynamics

Here we want to know if we can find a similar expression for the condition of oscillations as in Chap. 4. For this, we first find the eigenvalues of the matrix  $A$  of Eq. (5.16)

$$E_1 = 0 \quad (5.30)$$

$$E_2 = -\frac{\kappa(\gamma\kappa + 4g^2)}{2\kappa^2 - 8g^2} \quad (5.31)$$

$$E_3, E_4 = -3\kappa \frac{\gamma\kappa + 4g^2}{4(\kappa^2 - 4g^2)} \mp \kappa \frac{\sqrt{(4g^2 + \kappa^2) \left( (4g^2 + \kappa^2)(\gamma\kappa + 4g^2)^2 - 256g^2\kappa^3\epsilon^2 \right)}}{4(\kappa^4 - 16g^4)}, \quad (5.32)$$

$E_3, E_4$  can have imaginary parts if the part under the square root becomes negative. This is the case if the drive strength fulfills

$$\frac{\epsilon}{\sqrt{\kappa}} > \frac{g}{4\kappa\beta} \sqrt{\frac{\gamma}{\kappa} \frac{\beta}{1-\beta} + 1}, \quad (5.33)$$

where  $\beta$  is given by Eq. (3.4), this expression allows us to define a critical drive strength

$$\epsilon_c = \frac{g\sqrt{\kappa}}{4\kappa\beta} \sqrt{\frac{\gamma}{\kappa} \frac{\beta}{1-\beta} + 1}. \quad (5.34)$$

In Chap. 4 we obtained very similar results given by Eqs. (4.14) and (4.15). We notice that for  $\gamma/\kappa \rightarrow 0$  we recover the results of the adiabatic elimination. In contrast, our solution is always bigger than the one obtained from the adiabatic elimination, but since we are searching for a lower bound this does not mean the old result is wrong, it just hints that there exist even tighter bounds, for which we found one example. A comparison for different drive strengths can be seen in Fig. 5.4, where we can see the presence of oscillations when exceeding the critical drive strength.

## 5. Prodiabatic Elimination

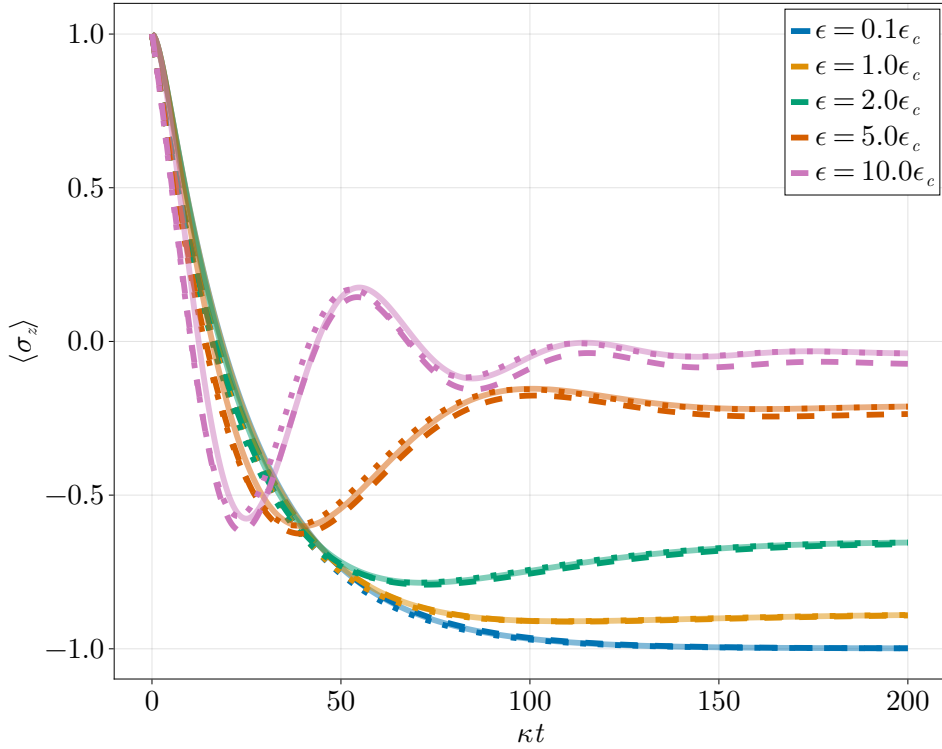


Figure 5.4.: Plot of the expectation value of  $\langle \sigma_z \rangle$  for multiples of  $\epsilon_c$ , given by Eq. (5.34), dashed adiabatic elimination, dotted prodiabatic elimination, and in solid full numerics of the model. The evolution starts in the vacuum state of the cavity  $|0\rangle$  and a single excitation  $|1\rangle$  in the two-level system. System values are chosen as  $g/\kappa = 1/10$  and  $\gamma/\kappa = 1/2000$ .

In Fig. 5.4 we see an increased drive strength will be able to result in oscillations in the expectation values of  $\sigma_z$ . The presence of oscillation is already observable by the eye at twice the critical drive strength, this can be seen as the green line is below its final value at around  $\kappa t \approx 60$ . We also notice that the prodiabatic elimination results in a more robust approximation for higher drives than the adiabatic elimination, as it is still able to obtain reasonable results for  $\epsilon = 5\epsilon_c$  and  $\epsilon = 10\epsilon_c$ , whereas the adiabatic elimination seems to slowly break down at this point.

### 5.2.4. Numerical Comparisons

In this section, we compare the results obtained from the prodiabatic elimination to the results from the adiabatic elimination as well as to full numerical simulations. Since we again use a long time limit it is interesting to check the dependence on the initial state. The two contenders of initial states are the vacuum state and the photon-reduced steady state of Eq. (4.17). In the case of the photon-reduced steady state, we use the numerics to obtain the initial conditions for the adiabatic and the prodiabatic elimination.

## 5. Prodiabatic Elimination

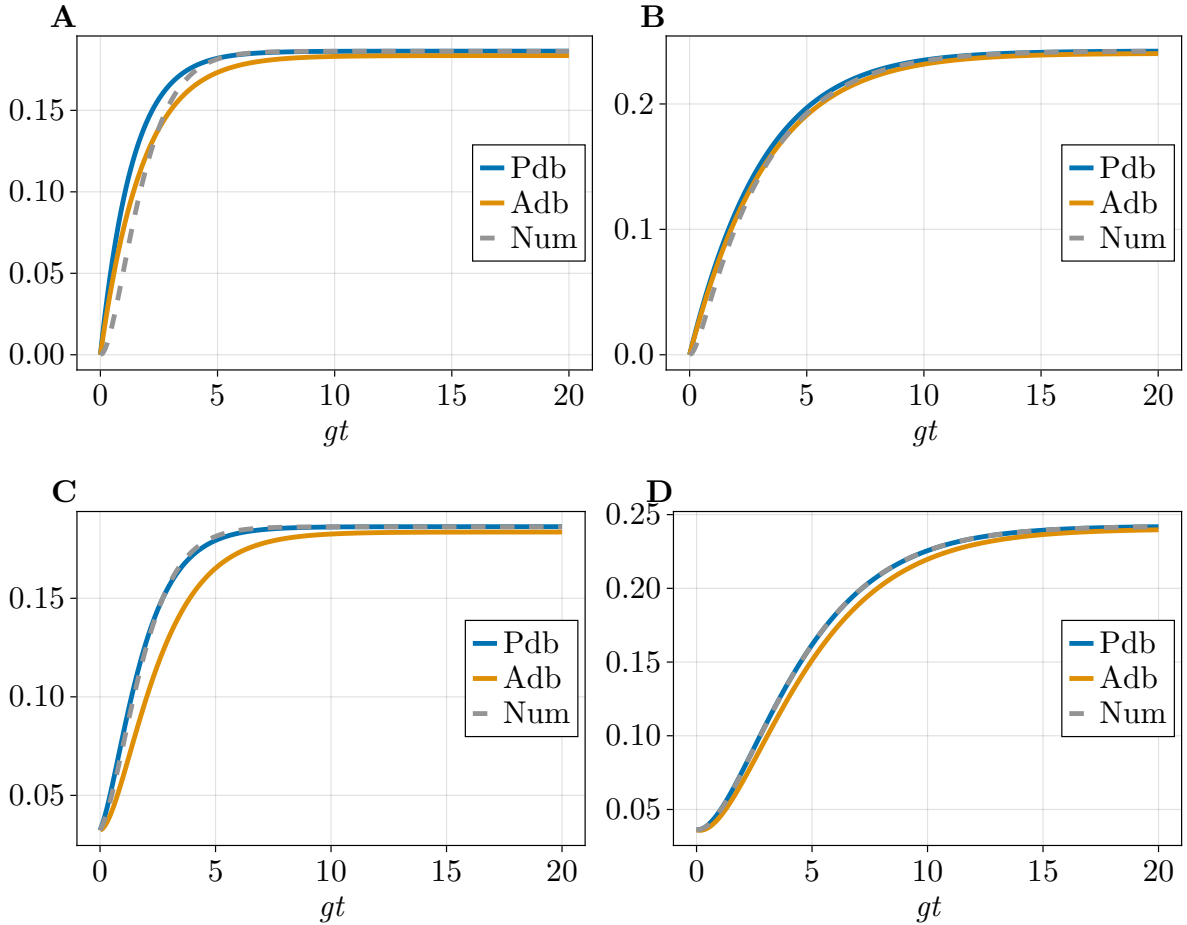


Figure 5.5.: Plot of  $|\langle\sigma\rangle|$  for varying  $\kappa$ , in orange adiabatic elimination, blue prodiabatic elimination and in gray the full numerics. **A**, **B** start in the vacuum state  $|0\rangle|0\rangle$  and **C**, **D** start in photon reduced state of Eq. (4.17). System values are  $\kappa/g = 4$  for **A**, **C** and  $\kappa/g = 8$  for **B**, **D**, the others are chosen as  $\epsilon/\sqrt{g} = 1/10$  and  $\gamma/g = 1/100$ .

By assuming an initial state that is related to the steady state we can enhance the accuracy of the approximation, as can be seen in Fig. 5.5 panels **C**, **D**, while using one that is not we decrease it, see panel **A**, **B**. Additionally increasing  $\kappa$  has the same effect as in the adiabatic elimination, with a definitive improvement visible in both the photon reduced as well we the vacuum case.

At this point we can explain why we did not use the adiabatic elimination to approximate  $a_{adb}(t)$  and  $\dot{a}_{adb}(t)$  of the prodiabatic approach. In principle Eq. (4.7) provides an expression of  $\dot{a}_{adb}(t)$  solely based on the two-level dynamics, which we are able to obtain from the adiabatic elimination. Further Eq. (4.11) gives us an expression of  $a_{adb}(t)$ . Therefore we would be able to find the full expression of  $a_{pdb}$  of Eq. (5.7) in the framework of the adiabatic elimination. We can already guess why we did not use this approach from panel **C**, **D** in Fig 5.5, since for early times the adiabatic elimination seems to stay too long at too low values, therefore underestimating the derivative. The opposite can be said for long times, where it is still growing when the numerics have stabilized to a certain value. We show that it would not be smart to use the adiabatic elimination in this way for the prodiabatic elimination by a qualitative comparison of  $\dot{\sigma}$  of the different approximations and numerics. For the expressions of  $\dot{\sigma}$  we will use Eqs. (4.7), (5.14)

## 5. Prodiabatic Elimination

and (4.2), where the first two can be obtained from their respective approximation and the last one from full numerics. The comparison can be seen in Fig. 5.6, where we again assumed the initial state to be the photon-reduced one since it is directly related to the  $g^{(2)}$ -function.

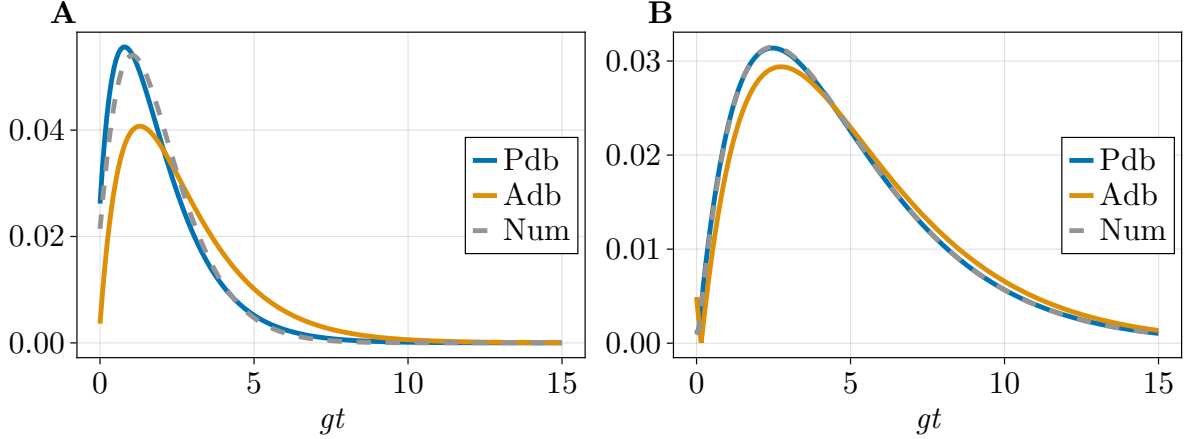


Figure 5.6.: Plot of  $|\langle \dot{\sigma} \rangle|$  for varying  $\kappa$ , orange adiabatic elimination, blue prodiabatic elimination and in gray full numerics. Evolution starting in the in photon reduced state of Eq. (4.17). System values are  $\kappa/g = 4$  for **A** and  $\kappa/g = 8$  for **B**, others chosen as  $\epsilon/\sqrt{g} = 1/10$  and  $\gamma/g = 1/100$ .

In Fig. 5.6 panel **A** we notice that the results of the adiabatic elimination are not well suited for an approximation of  $\dot{\sigma}$ , as there is a big mismatch at early times. Using the adiabatic elimination to directly approximate  $\dot{a}_{adb} \propto \dot{\sigma}$  would lead to a decrease in the accuracy of the cavity field approximation of the prodiabatic result. This is since early timescales will be affected very much by this mismatch. This can be seen by the scaling of how  $a_{adb}$  and  $\dot{a}_{adb}$  enter into the total expression of  $a_{pdb}$ , given by Eq. (5.6). Assuming  $\kappa$  is large,  $1 - \exp(-\kappa t/2)$  will quickly decay into 1, while  $-2 + \exp(-\kappa t/2)(2 + \kappa t)$  will decay to  $-2$ , therefore it is crucial to get a good estimation of the derivative at early times, otherwise it could decrease the overall accuracy of the approximation.

## 5.3. Cavity Dynamics

### 5.3.1. Steady State

In this section, we want to show how we compute steady-state expectation values involving the cavity field operator. For the steady state the assumption of  $\kappa t \gg 1$  has to hold therefore we will use Eq. (5.9) as an approximation of  $a$ . For expectation values involving multiple  $a$  we just replace each of them and use the two-level commutation relations. We demonstrate how to do this based on  $\langle a^\dagger a \rangle_{ss}$

$$\begin{aligned} \langle a^\dagger a \rangle_{ss} &= \left\langle \left( a_{adb}^\dagger - \frac{2}{\kappa} \dot{a}_{adb}^\dagger \right) \left( a_{adb} - \frac{2}{\kappa} \dot{a}_{adb} \right) \right\rangle_{ss} \\ &= \langle a_{adb}^\dagger a_{adb} \rangle_{ss} + \frac{4}{\kappa^2} \langle \dot{a}_{adb}^\dagger \dot{a}_{adb} \rangle_{ss} - \frac{2}{\kappa} \langle \dot{a}_{adb}^\dagger a_{adb} + a_{adb}^\dagger \dot{a}_{adb} \rangle_{ss}, \end{aligned} \quad (5.35)$$

since  $a_{adb}$  and  $\dot{a}_{adb}$  are in the two-level subspace, we can use the commutation relations in order to simplify this to a form where we are only left with expectation values involving  $\langle \sigma_i \rangle_{ss}$ . We

## 5. Prodiabatic Elimination

show how to do this on  $\langle \dot{a}_{adb}^\dagger a_{adb} \rangle_{ss}$

$$\begin{aligned}
 \langle \dot{a}_{adb}^\dagger a_{adb} \rangle_{ss} &= \frac{4g}{\kappa^2} \left\langle \left( -\frac{\kappa(\gamma\kappa + 4g^2)}{2\kappa^2 - 8g^2} \sigma - \frac{2g\epsilon\sqrt{\kappa}\kappa^3}{\kappa^4 - 16g^4} \sigma_z + \frac{8g^3\epsilon\sqrt{\kappa}\kappa}{\kappa^4 - 16g^4} \right) (g\sigma - \epsilon\sqrt{\kappa}) \right\rangle_{ss} \\
 &= \frac{2g\epsilon(\gamma\kappa + 8g^2)}{\sqrt{\kappa}(\kappa^2 - 4g^2)} \langle \sigma \rangle_{ss} \\
 &\quad - \frac{g^2((4g^2 + \kappa^2)(\gamma\kappa + 4g^2) - 8\kappa^3\epsilon^2)}{\kappa(\kappa^4 - 16g^4)} (\langle \sigma_z \rangle_{ss} + 1) \\
 &\quad - \frac{8g^2\epsilon^2}{\kappa^2 - 4g^2},
 \end{aligned} \tag{5.36}$$

where we used  $\langle \sigma \rangle_{ss} = \langle \sigma^\dagger \rangle_{ss}$ , which is the case as can be seen from Eq. (5.28). By plugging in the results of  $\langle \sigma \rangle_{ss}$  and  $\langle \sigma_z \rangle_{ss}$  from Sec. 5.2.2 we will obtain the final result. Applying the same steps to the other parts of Eq. (5.35) will result in

$$\langle a^\dagger a \rangle_{ss} = \frac{4\kappa\epsilon^2(\gamma^2(\kappa^2 - 4g^2)(4g^2 + \kappa^2)^2 + 32g^2\kappa^5\epsilon^2)}{(\kappa^4 - 16g^4)((4g^2 + \kappa^2)(\gamma\kappa + 4g^2)^2 + 32g^2\kappa^3\epsilon^2)}, \tag{5.37}$$

which additionally gives us the normalization of the  $g^{(2)}$ -function, so we have a practical need to know this expression.

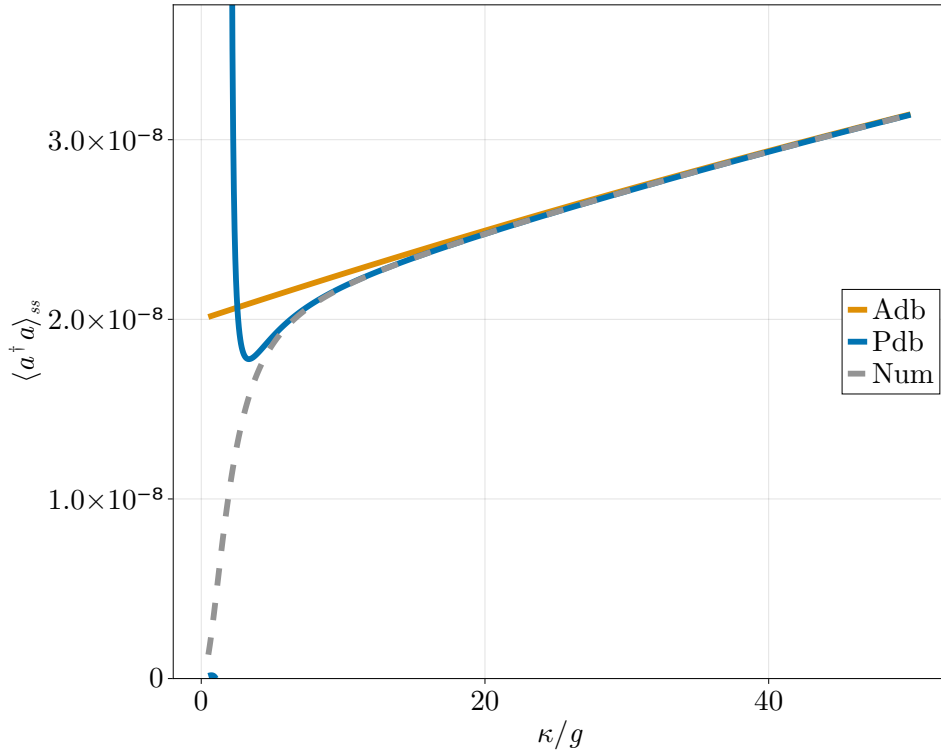


Figure 5.7.: Comparison between  $\langle a^\dagger a \rangle_{ss}$  of the different approximations for varying  $\kappa$ , in orange adiabatic elimination, in blue prodiabatic elimination and in gray numerics. System values are chosen as  $\epsilon/\sqrt{g} = 1/100\sqrt{2}$  and  $\gamma/g = 1/200$ .

In Fig. 5.7 we can see a qualitative comparison between the estimations of  $\langle a^\dagger a \rangle_{ss}$ . One thing we notice is the initial mismatch between prodiabatic elimination and numerics for low  $\kappa$ . This

## 5. Prodiabatic Elimination

tail comes from the fact that at this point  $\kappa \approx 2g$ , which means we divide by 0 in Eq. (5.37), for values of  $\kappa < 2g$  the prodiabatic elimination can also predict a negative photon number, which is unphysical. Therefore this mismatch was to be expected and we should restrict our conclusion to the part of  $\kappa > 2g$ . In this region, we notice that the prodiabatic elimination converges faster to the numerics than the adiabatic elimination.

Steady state expectation values involving more cavity operators are computed in the same manner, first we replace each  $a$  by Eq. (5.9), then use the fact that we can write this operator as one that is just in the two-level system and use the commutation relations of the two-level system. Now this expression should just depend on  $\langle \sigma_i \rangle_{ss}$  for which we found expressions already in Sec. 5.2.2, plugging these values in will conclude the calculation.

Here we also want to outline how we compute expectation values involving both cavity and two-level operators. In the case of the adiabatic elimination we used normal ordered operators, so all creation operators are to the left and all annihilation operators to the right, but with no ordering in the respective group. This was enough since

$$[\sigma, a_{adb}] = 0, \quad (5.38)$$

but for the prodiabatic elimination in the long time limit, we notice that Eq. (5.9) has a term proportional to  $\sigma_z$ , therefore it makes a difference if  $\sigma$  is to the left or the right of  $a_{pdb}$ . Following [17], for any two-level operator  $\Sigma$  we use the ordering

$$\left\langle (a_{pdb}^\dagger)^n \Sigma (a_{pdb})^m \right\rangle_{ss}, \quad (5.39)$$

where  $n$  and  $m$  are some natural numbers, so we put the atom expectation values in the middle and the cavity operators to the outside, notice that the overall structure remains normal ordered. This ordering also makes sense since one can use the same argument as in Sec. 4.4 Eq. (4.33) to drop the noise operators.

### 5.3.2. Average Cavity Field $\langle a(t) \rangle$

For the cavity field, two things come to mind; first, we need to compare  $a_{adb}(t)$  to  $a_{pdb}(t)$  and secondly, we can also compare them by assuming  $\kappa t \gg 1$ , thus  $a_{pdb}(t)$  will be described by Eq. (5.9). This gives insight into how the prodiabatic elimination compares to the adiabatic elimination if one assumes large  $\kappa$ , which comes naturally for the adiabatic case but not in the prodiabatic one. The large  $\kappa$  aspect of the adiabatic elimination is outlined in Sec. 4.4. The full prodiabatic result is obtained through

$$\begin{aligned} \langle a_{pdb}(t) \rangle &= \langle a(0) \rangle e^{-\frac{\kappa t}{2}} \\ &\quad - \frac{2i}{\kappa} (g \langle \sigma(t) \rangle - \epsilon \sqrt{\kappa}) (1 - e^{-\frac{\kappa t}{2}}) \\ &\quad - \frac{2ig}{\kappa^2} \left( -\frac{\kappa(\gamma\kappa + 4g^2)}{2\kappa^2 - 8g^2} \langle \sigma(t) \rangle - \frac{2g\epsilon\sqrt{\kappa}\kappa^3}{\kappa^4 - 16g^4} \langle \sigma_z(t) \rangle + \frac{8g^3\epsilon\sqrt{\kappa}\kappa}{\kappa^4 - 16g^4} \right) \left( -2 + e^{-\frac{\kappa t}{2}} (2 + \kappa t) \right), \end{aligned} \quad (5.40)$$

where  $\langle \sigma_i(t) \rangle$  is given by Eq. (5.17). This expression of  $a_{pdb}$  is obtained by plugging in Eq. (5.10) into Eq. (5.7).

Further on we want to compare this result to numerics and the adiabatic elimination, to do this we consider the photon-reduced steady state of Eq. (4.17), which we obtain from numerics and use for the initial conditions. A comparison between the different results on  $|\langle a(t) \rangle|$  is done in Fig. 5.8.

## 5. Prodiabatic Elimination

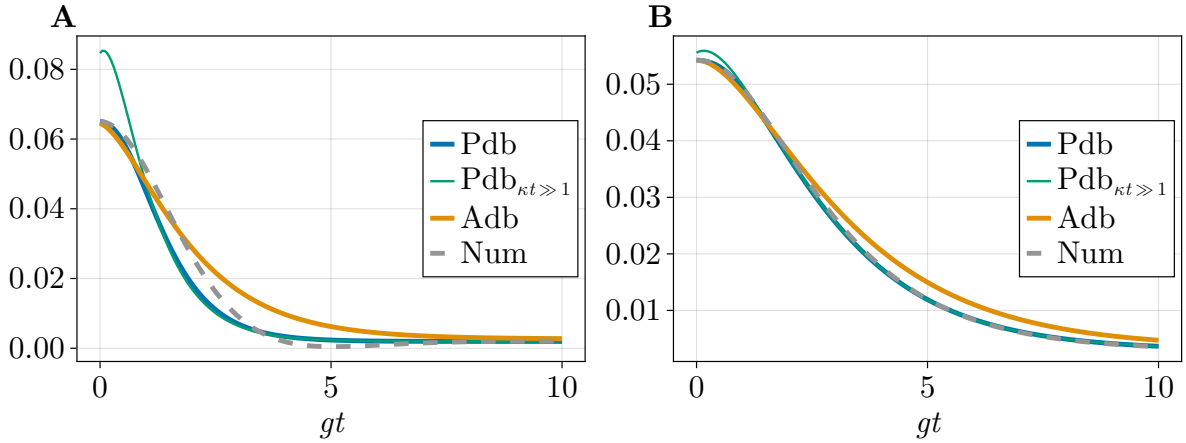


Figure 5.8.: Plot of  $|\langle a \rangle|$  as a function of time for varying  $\kappa$ , orange adiabatic elimination, blue prodiabatic elimination, green prodiabatic elimination assuming  $\kappa t \gg 1$  (Eq. (5.9)) and in gray full numerics. Evolution starting in the photon reduced state, see Eq. (4.17). System values are  $\kappa/g = 3$  for **A** and  $\kappa/g = 5$  for **B**, other values are chosen as  $\epsilon/\sqrt{g} = 1/10\sqrt{2}$  and  $\gamma/g = 1/200$ .

In Fig. 5.8 we see how well each of the approximations performs and compare them qualitatively. While all of them seem to work fairly well for larger  $\kappa$  (panel **B**), we can see a big difference for lower  $\kappa$  (panel **A**). We first notice that the prodiabatic elimination, for  $\kappa t \gg 1$ , is far away from the initial conditions, this makes sense since the assumption of  $\kappa t \gg 1$  has to fail for  $t = 0$ . Another way to understand this is that we know the adiabatic elimination works fairly well to get steady state expectation values of  $\langle a \rangle$ , but for  $t = 0$  we will be shifted away from the adiabatic result by the derivative of  $\dot{a}_{adb}$ , therefore leading to this mismatch. Further, we observe that both prodiabatic elimination approximations converge faster to the results of the numerics than the adiabatic elimination, this being visible in both panels.

Next, we can discuss the effect of choosing the vacuum as the initial state, remembering that the adiabatic elimination needed some time in order to match the numerics, as can be seen in Fig. 4.1.

## 5. Prodiabatic Elimination

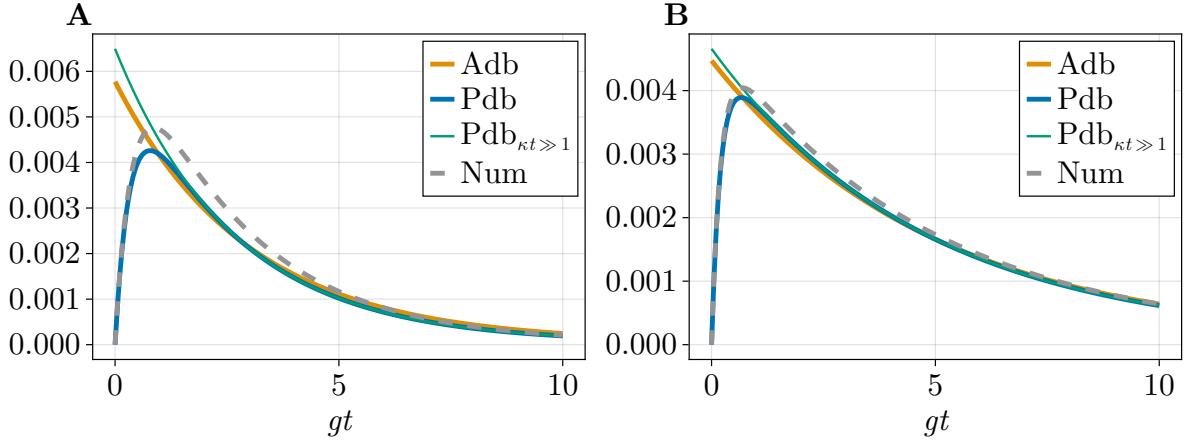


Figure 5.9.: Plot of  $|\langle a \rangle|$  as a function of time for varying  $\kappa$ , orange adiabatic elimination, blue prodiabatic elimination, green prodiabatic elimination assuming  $\kappa t \gg 1$  (Eq. (5.9)) and in gray full numerics. Evolution starting in the vacuum  $|0\rangle|0\rangle$ . System values are  $\kappa/g = 6$  for **A** and  $\kappa/g = 10$  for **B**, other values are chosen as  $\epsilon/\sqrt{g} = 1/100\sqrt{2}$  and  $\gamma/g = 1/200$ .

In Fig. 4.1 we can see nicely the effect of incorporating the initial conditions as the prodiabatic result matches well at early times. For later times it seems to converge quickly to similar values as the adiabatic elimination, this effect is visible for both the full prodiabatic elimination and the long time limit of the prodiabatic elimination. Additionally, we notice that an increase in  $\kappa$  increases the accuracy of all approximations, as panel **B** displays a better fit than panel **A**.

### 5.3.3. Obtaining the $g^{(2)}(t)$ -Function

In order to obtain the  $g^{(2)}$ -function we need to compute  $\langle a^\dagger(0)a^\dagger(\tau)a(\tau)a(0) \rangle$ . This calculation is rather straightforward but ends with a big expression. Here we will again show the solution if one assumes  $\kappa t \gg 1$  and use Eq. (5.9) for  $a$  since this will result in a more simple and understandable expression, but obtaining the full expression is done in the same manner. We again start by finding  $a^\dagger a$  for  $\kappa t \gg 1$ , this results in

$$\begin{aligned}
 a_{pdb}^\dagger(t)a_{pdb}(t) = & -\frac{4g\kappa^{3/2}\epsilon(\gamma+\kappa)}{(\kappa^2-4g^2)^2}(\sigma(t)+\sigma^\dagger(t)) \\
 & +\frac{2g^2\left((\gamma+\kappa)^2(4g^2+\kappa^2)^2-16\kappa^5\epsilon^2\right)}{(\kappa^4-16g^4)^2}(\sigma_z(t)+1) \\
 & +\frac{4\kappa^3\epsilon^2}{(\kappa^2-4g^2)^2},
 \end{aligned} \tag{5.41}$$

where once again we will assume  $\kappa > 2g$  and that we can use the commutation relations of the two-level system operators at equal times. As outlined in Sec. 5.1.2, the time-dependent operators are obtainable within our approximation. Notice that by expanding the prefactors of Eq. (5.41) up to order of  $1/\kappa^2$  one will reobtain Eq. (4.19), so we can again see the similarities to the adiabatic elimination.

## 5. Prodiabatic Elimination

We find the full  $g^{(2)}$ -function by using similar steps as in Sec. 4.3.2. We again use the quantum regression theorem to find

$$\begin{pmatrix} \langle a^\dagger(0)\sigma(t)a(0) \rangle \\ \langle a^\dagger(0)\sigma^\dagger(t)a(0) \rangle \\ \langle a^\dagger(0)\sigma_z(t)a(0) \rangle \\ \langle a^\dagger(0)a(0) \rangle \end{pmatrix} = e^{At} \begin{pmatrix} \langle a^\dagger\sigma a \rangle_{ss} \\ \langle a^\dagger\sigma^\dagger a \rangle_{ss} \\ \langle a^\dagger\sigma_z a \rangle_{ss} \\ \langle a^\dagger a \rangle_{ss} \end{pmatrix}, \quad (5.42)$$

where the matrix  $A$  is given by Eq. (5.16). Where all steady-state expectation values are obtainable from within the theory as was outlined in Sec. 5.3.1. Combining these results with Eq. (5.41) we obtain

$$\begin{aligned} \langle a^\dagger(0)a_{pdb}^\dagger(\tau)a_{pdb}(\tau)a(0) \rangle &= -\frac{4g\kappa^{3/2}\epsilon(\gamma+\kappa)}{(\kappa^2-4g^2)^2} \left( \langle a^\dagger(0)\sigma(\tau)a(0) \rangle + \langle a^\dagger(0)\sigma^\dagger(\tau)a(0) \rangle \right) \\ &+ \frac{2g^2 \left( (\gamma+\kappa)^2 (4g^2+\kappa^2)^2 - 16\kappa^5\epsilon^2 \right)}{(\kappa^4-16g^4)^2} \left( \langle a^\dagger(0)\sigma_z(\tau)a(0) \rangle + \langle a^\dagger(0)a(0) \rangle \right) \\ &+ \frac{4\kappa^3\epsilon^2}{(\kappa^2-4g^2)^2} \langle a^\dagger(0)a(0) \rangle, \end{aligned} \quad (5.43)$$

which is the numerator of the  $g^{(2)}$ -function, combining this with the normalization, given by Eq. (5.37), we obtain an expression of the  $g^{(2)}$ -function, in the long time limit by

$$g^{(2)}(\tau) = \frac{\langle a^\dagger(0)a_{pdb}^\dagger(\tau)a_{pdb}(\tau)a(0) \rangle}{\langle a^\dagger a \rangle_{ss}^2}. \quad (5.44)$$

In Fig. 5.10 this solution is identified by  $g_{\kappa t \gg 1}^{(2)}(\tau)$ . The same steps can be applied to the full prodiabatic elimination, but the expression for  $a^\dagger a$  already is much larger, due to the time-dependent prefactors of the operators as for example the  $(1 - e^{-\frac{\kappa t}{2}})$  prefactor of  $a_{adb}(t)$ , see Eq. (5.6).

We again want to compare these results to numerical simulations, as earlier we will obtain the photon reduced steady-state Eq. (4.17) from numerics, the comparison between them can be seen in Fig. 5.10.

## 5. Prodiabatic Elimination

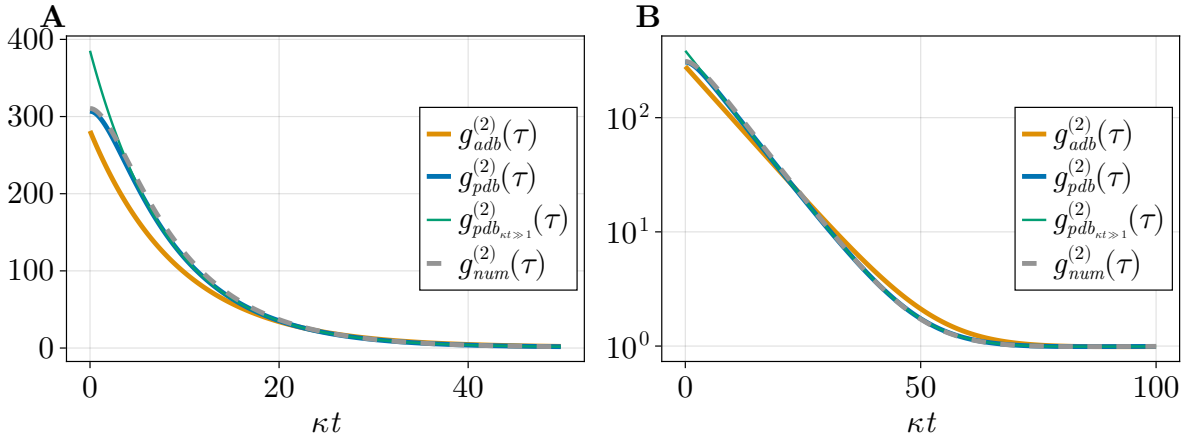


Figure 5.10.: Comparison between the  $g^{(2)}$ -functions of the different approximations orange adiabatic elimination, blue the full prodiabatic, green prodiabatic for  $\kappa t \gg 1$  based on Eq. (5.41) and in gray the numerics. System values are chosen as  $\kappa/g = 6$ ,  $\gamma/g = 1/200$  and  $\epsilon/\sqrt{g} = 1/10\sqrt{2}$ . With **A** having a linear y-scale and **B** a  $\log_{10}$  scale.

In Fig. 5.10 we see a comparison of those methods again a strict outperformance of the prodiabatic elimination in comparison to the adiabatic elimination can be observed, where Eq. (5.41) converges quickly to the prodiabatic result, which outperforms the adiabatic elimination at all times. We also notice that the full prodiabatic elimination can capture the overall shape of the  $g^{(2)}$ -function with disagreements being minor. One question raised by panel **A** is, why does it look like at  $t = 0$  we have a disagreement between full prodiabatic elimination and numerics? Since in principle the prodiabatic elimination should incorporate the initial condition, therefore this seems to be wrong. However, the reason for this initial mismatch is that the normalization constant of the prodiabatic elimination overestimates the photon number in the steady state, giving rise to this shift.

As in Chap. 4 we also want to show a simple expression of the  $g^{(2)}$ -function in the low drive limit. For this, we assume  $\kappa t \gg 1$  and calculate the  $g^{(2)}(\tau)$ -function in the manner as outlined at the beginning of this section. This final result we expand in orders of  $\epsilon$  to obtain

$$g^{(2)}(\tau) = \left( 1 - F_p^2 \frac{1 - (\frac{\gamma}{\kappa})^2}{1 - (\frac{\gamma}{\kappa})^2 F_p^2} e^{-\frac{\gamma}{2} \frac{F_p+1}{1 - \frac{\gamma}{\kappa} F_p} \tau} \right)^2 + \mathcal{O}(\epsilon^2), \quad (5.45)$$

where  $F_p$  is given by Eq. (3.1). Notice that for a low drive, the bad cavity limit is fulfilled if  $\gamma/\kappa \ll 1$ . In the limit of  $\gamma/\kappa \rightarrow 0$  we notice Eq. (5.45) will become Eq. (4.25), again displaying that we go beyond the adiabatic elimination and have more relaxed conditions on the system values. But if we go to the bad cavity limit we retrieve the results of the adiabatic elimination, which are exact in this limit.

Based on this we are also able to obtain a simple expression of the  $g^{(2)}(0)$  for low drives by

$$g^{(2)}(0) = \frac{(1 - 2\beta)^2}{\left( (\frac{\gamma}{\kappa}\beta)^2 - (\beta - 1)^2 \right)^2} + \mathcal{O}(\epsilon^2), \quad (5.46)$$

where  $\beta$  is given by Eq. (3.4). In Eq. (4.26) we presented the same quantity  $g^{(2)}(0)$  but using the adiabatic elimination. Similar to the adiabatic elimination, the prodiabatic elimination predicts

## 5. Prodiabatic Elimination

perfect photon antibunching for  $\beta = 1/2$ . However, the two methods differ in their predictions for perfect photon bunching; the prodiabatic elimination predicts it at  $\beta = \frac{1}{1+\frac{\gamma}{\kappa}}$ , while the adiabatic elimination predicts it at  $\beta = 1$ . Assuming that neither  $\kappa$  nor  $\gamma$  is zero,  $\beta = 1$  is not achievable by a finite coupling, which is in contrast to the prodiabatic elimination, which expects a value of  $\beta$  achievable by a finite coupling between the cavity and the two-level system.

## 6. Method of Multiple Scales

In this chapter we want to employ a standard singular perturbation technique on the problem, giving a ground to compare the adiabatic and the prodiabatic elimination to standard techniques. The chosen technique is the method of multiple scales, also known as the two-timing method when applied with two time scales. To illustrate its mechanics, this chapter begins with a simple test example, further on we outline how the method is applied to our specific problem and conclude with an explanation of why the approach was ultimately deemed unsuitable.

Rather than delving deeply into the details of the calculations, we aim to provide an overview of the chosen method, the principles behind its application, and the reasons for ultimately abandoning this ansatz. The primary references for this approach are [31–33].

### 6.1. Minimal Example of the Method of Multiple Scales

Let us start with an example of how the multiple time-scale method works for the second-order differential equation

$$\ddot{y} + \epsilon \dot{y} + y = 0, \quad (6.1)$$

where we assume  $\epsilon \ll 1$ . We note that this is the differential equation of a damped harmonic oscillator, which can be solved exactly. Having an exact solution to this problem is good since in the end we can compare the perturbative result of the method of multiple scales to it, which gives insight into which behavior the method can capture and how well it performs on this problem.

The technique begins by introducing two or more time scales; in our case, the *fast* time scale  $t$  and the *slow* time scale  $\tau = \epsilon t$ . Since  $\epsilon$  is assumed to be very small, it follows that  $\tau \ll t$ , indicating that the timescale  $\tau$  evolves much slower than  $t$ , justifying the designating of  $\tau$  as the slow variable. Furthermore, we treat  $t$  and  $\tau$  as *independent* parameters of  $y(t, \tau)$ , even though they are inherently related through  $t$ . The idea is that the short-term (fast) behavior can effectively decouple from the long-term (slow) behavior, allowing them to be considered independent [31]. In the case of the damped harmonic oscillator, the fast time scale captures the oscillatory behavior, while the slow time scale accounts for the damping. The assumption of independence between  $t$  and  $\tau$  in  $y(t, \tau)$  leads to

$$\begin{aligned} \dot{y} &= \frac{\partial y}{\partial t} + \frac{\partial y}{\partial \tau} \frac{\partial \tau}{\partial t} \\ &= \frac{\partial y}{\partial t} + \epsilon \frac{\partial y}{\partial \tau}, \end{aligned} \quad (6.2)$$

and

$$\begin{aligned} \ddot{y} &= \frac{\partial}{\partial t} \left( \frac{\partial y}{\partial t} + \epsilon \frac{\partial y}{\partial \tau} \right) + \epsilon \frac{\partial}{\partial \tau} \left( \frac{\partial y}{\partial t} + \epsilon \frac{\partial y}{\partial \tau} \right) \\ &= y_{tt} + 2\epsilon y_{t\tau} + \epsilon^2 y_{\tau\tau}, \end{aligned} \quad (6.3)$$

where we introduced small subscripts indicating a derivative.

Next, we expand  $y(t, \tau)$  in orders of  $\epsilon$

$$y = y_0 + \epsilon y_1 + \mathcal{O}(\epsilon^2), \quad (6.4)$$

## 6. Method of Multiple Scales

where from now on we disregard terms of order  $\epsilon^2$  and higher, thus the differential equation simplifies to

$$(y_0)_{tt} + \epsilon(y_1)_{tt} + 2\epsilon(y_0)_{t\tau} + \epsilon(y_0)_t + y_0 + \epsilon y_1 = 0. \quad (6.5)$$

To solve this equation we first sort it in orders of  $\epsilon$

$$\begin{aligned} \mathcal{O}(1) : & \quad (y_0)_{tt} = -y_0 \\ \mathcal{O}(\epsilon) : & \quad (y_1)_{tt} + 2(y_0)_{t\tau} + (y_0)_t = -y_1, \end{aligned}$$

and then solve each order independently. From the  $\mathcal{O}(1)$  equation it is simple to find

$$y_0(t, \tau) = A(\tau)e^{it} + A^*(\tau)e^{-it}, \quad (6.6)$$

as it is the differential equation of a usual harmonic oscillator. Here it is important to note that the amplitude function  $A(\tau)$  may depend on the slow timescale, this is because the  $\mathcal{O}(1)$ -equation is a partial differential equation only in the fast timescale. Plugging the result of Eq. (6.6) into the  $\mathcal{O}(\epsilon)$  equation we obtain

$$(y_1)_{tt} + y_1 = -(2A_\tau + A)ie^{it} + \text{conj.}, \quad (6.7)$$

where the conj. is the first part  $-(2A_\tau + A)ie^{it}$  complex conjugated. We will use conj. in the same way further on. The method of multiple scales is designed to systematically eliminate secular terms. In our context, secular terms refer to those that prevent the solution from converging to a fixed value, often leading to divergence or unbounded growth over time.

Applying this condition on our equation we demand  $2A_\tau + A = 0$ , which is solved by  $A = A(0)e^{-\tau/2}$ . This term is problematic since Eq. (6.7) describes a driven harmonic oscillator, if the driving force is for example on resonance the amplitude of the oscillations would increase in time, leading to a secularity. By removing this term with the mentioned condition we obtain

$$y_0(t) = A(0)e^{-\frac{1}{2}\epsilon t}e^{it} + \text{conj.}. \quad (6.8)$$

Where  $A(0)$  can be determined from the initial conditions of  $y$ . In this expression, we also see how the slow time scale  $\tau = \epsilon t$  captures the damping and the fast time scale  $t$  accounts for the oscillations.

Since we chose a pretty simple example we can compare Eq. (6.8) to the exact solution

$$y_{\text{exact}}(t) = c_1 e^{-\frac{1}{2}\epsilon t} e^{\frac{t}{2}\sqrt{\epsilon^2 - 4}} + \text{conj.}, \quad (6.9)$$

where  $c_1$ , equivalently to  $A(0)$ , is a constant to be determined by the initial conditions. The exact result of Eq. (6.9) bears a lot of similarities to the solution of the method of multiple scales of Eq. (6.8). Notice we assumed  $\epsilon \ll 1$ , otherwise truncating the expansion in orders of  $\epsilon$  would not be justified, because of this  $\sqrt{\epsilon^2 - 4} \approx 2i$  and thus the exact solution is equal to the result of the method of multiple scales Eq. (6.8) in the limit of  $\epsilon \rightarrow 0$ .

### 6.2. Application to the Cavity-Atom System

First, we need to explain why out of all perturbation methods we chose the method of multiple scales. We were inspired by the adiabatic elimination which assumes that the fast timescale is the cavity and the atom is the slow one. We assumed that by incorporating the fast time scale, instead of eliminating it, we would end up with an improvement compared to the adiabatic elimination. Further, we will show why this does not give a satisfactory result in comparison to the adiabatic or prodiabatic elimination.

## 6. Method of Multiple Scales

To remind ourselves we have the objective of applying the method of multiple scales to Eqs. (4.1), (4.2) and (4.3), where we assume the drive to be on resonance  $\Delta_c = \Delta_d = 0$ . To start this calculation we need to first obtain a perturbation parameter as well as the different timescales, in principle one can define any number of different timescales, but we will stick to two. The idea is that one timescale describes the cavity and the other one the two-level system. The perturbation parameter of our choice is  $1/\kappa$  for the simple reason that  $\kappa$  is a big parameter in the context of the bad cavity limit and the adiabatic elimination [17], which we try to orient ourself on. Since we will be expanding in orders of  $1/\kappa$ , we also need to modify the drive. Previously, the drive had a strength of  $\epsilon\sqrt{\kappa}$ , but to ensure a straightforward expansion, we assume that the drive is *independent* of the dissipation rate  $\kappa$ . To achieve this, we make the replacement

$$\epsilon\sqrt{\kappa} \rightarrow E, \quad (6.10)$$

where  $E$  is independent of  $\kappa$ . This picture can be interpreted as the drive and dissipation being on different sides of the cavity. The equations of motion will take the form

$$\dot{a} = -\frac{\kappa}{2}a - ig\sigma + iE \quad (6.11)$$

$$\dot{\sigma} = -\frac{\gamma}{2}\sigma + igZa \quad (6.12)$$

$$\dot{Z} = -2ig(\sigma^\dagger a - a^\dagger \sigma) - \gamma(Z + 1), \quad (6.13)$$

where we use  $\sigma_z = Z$ , to avoid indices getting crowded.

Next we introduce the timescales we want to work with, one might first consider the timescales  $t$  and  $t/\kappa$  as done in the example problem of Sec. 6.1, but those scales would have different units, which we try to avoid. Motivated by the dissipative processes governed by  $\gamma$  and  $\kappa$ , we introduce the dimensionless timescales

$$t_f = \kappa t \quad (6.14) \quad t_s = \gamma t, \quad (6.15)$$

since they are dimensionless the name timescale is misleading, but we will use the name anyway. After the approximation, we will always end up plugging in the  $t$  for which then the normal interpretation of being a time always remains the same. The reasoning behind those timescales is that  $t_f$  should capture the fast timescale, coming from the adapting cavity field, and  $t_s$  being the slow one, stemming from the two-level system. Moving on, we compute the first derivative of an arbitrary function  $A(t_s, t_f)$  leading to

$$\dot{A} = \frac{d}{dt}A = \frac{\partial t_f}{\partial t} \partial_{t_f} A + \frac{\partial t_s}{\partial t} \partial_{t_s} A = \kappa \partial_{t_f} A + \gamma \partial_{t_s} A, \quad (6.16)$$

where we used the short version  $\partial_{t_i} = \frac{\partial}{\partial t_i}$ , this notation will be common in this chapter since we will be dealing with a few partial derivatives.

Next, we assume all operators to be expandable in orders of  $1/\kappa$ , as well as being functions of both timescales

$$a(t_s, t_f) \approx a_0(t_s, t_f) + \frac{1}{\kappa} a_1(t_s, t_f) + \frac{1}{\kappa^2} a_2(t_s, t_f) + \mathcal{O}(1/\kappa^3) \quad (6.17)$$

$$\sigma(t_s, t_f) \approx \sigma_0(t_s, t_f) + \frac{1}{\kappa} \sigma_1(t_s, t_f) + \frac{1}{\kappa^2} \sigma_2(t_s, t_f) + \mathcal{O}(1/\kappa^3) \quad (6.18)$$

$$Z(t_s, t_f) \approx Z_0(t_s, t_f) + \frac{1}{\kappa} Z_1(t_s, t_f) + \frac{1}{\kappa^2} Z_2(t_s, t_f) + \mathcal{O}(1/\kappa^3), \quad (6.19)$$

where we want to note that the order  $n$  operators as for example  $a_n$  are not dimensionless anymore, but have units of energy <sup>$n$</sup> , this is the case because our perturbation parameter  $1/\kappa$

## 6. Method of Multiple Scales

has units of 1/energy. The expanded operator representations can be plugged into the equation of motions Eqs. (6.11), (6.12) and (6.13)) and sorted in orders of  $1/\kappa$ . We will show how to do this for the cavity operator  $a$ . Inserting the expanded expressions of the operators into the equation of motion will lead to

$$\begin{aligned} & \frac{1}{\kappa} \left( \gamma \left( \partial_{t_s} a_0 + \frac{1}{\kappa} \partial_{t_s} a_1 \right) + \kappa \left( \partial_{t_f} a_0 + \frac{1}{\kappa} \partial_{t_f} a_1 \right) \right) \\ &= -\frac{1}{2} \left( a_0 + \frac{1}{\kappa} a_1 \right) - \frac{ig}{\kappa} \left( \sigma_0 + \frac{1}{\kappa} \sigma_1 \right) + i \frac{E}{\kappa}, \end{aligned} \quad (6.20)$$

sorting them in orders of  $1/\kappa$  results in

$$\begin{aligned} \mathcal{O}(1) : \quad & \partial_{t_f} a_0 = -\frac{1}{2} a_0 \\ \mathcal{O}\left(\frac{1}{\kappa}\right) : \quad & \gamma \partial_{t_s} a_0 + \partial_{t_f} a_1 = -\frac{1}{2} a_1 - ig \sigma_0 + iE \quad . \end{aligned}$$

Applying the same steps on  $\sigma$  we obtain

$$\begin{aligned} \mathcal{O}(1) : \quad & \partial_{t_f} \sigma_0 = 0 \\ \mathcal{O}\left(\frac{1}{\kappa}\right) : \quad & \gamma \partial_{t_s} \sigma_0 + \partial_{t_f} \sigma_1 = -\frac{\gamma}{2} \sigma_0 - ig Z_0 a_0 \quad , \end{aligned}$$

and for  $Z$

$$\begin{aligned} \mathcal{O}(1) : \quad & \partial_{t_f} Z_0 = 0 \\ \mathcal{O}\left(\frac{1}{\kappa}\right) : \quad & \gamma \partial_{t_s} Z_0 + \partial_{t_f} Z_1 = -\gamma (Z_0 + 1) - 2ig \left( \sigma_0^\dagger a_0 - a_0^\dagger \sigma_0 \right) \quad , \end{aligned}$$

now one has to apply the same steps as outlined in Sec. 6.1, while being very careful about what might be a secular term. First, we find  $a_0$  from the  $\mathcal{O}(1)$  equation of  $a$

$$a_0(t_s, t_f) = A_0(t_s) e^{-\frac{t_f}{2}}, \quad (6.21)$$

as in Sec. 6.1 the amplitude  $A_0$  can still be a function of the slow timescale. Now use the solution of  $\mathcal{O}(1)$  in the  $\mathcal{O}(1/\kappa)$  equation of  $a$  to see

$$\begin{aligned} \partial_{t_f} a_1 &= -\frac{1}{2} a_1 - \gamma \partial_{t_s} a_0 - ig \sigma_0 + iE \\ &= -\frac{1}{2} a_1 - \gamma e^{-\frac{t_f}{2}} \partial_{t_s} A_0(t_s) - ig \sigma_0 + iE, \end{aligned} \quad (6.22)$$

notice that from  $\mathcal{O}(1)$  of  $\sigma$  we know that  $\sigma_0(t_s)$  is only a function dependent on the slow timescale, therefore Eq. (6.22) can be solved by using the method of variation of parameters

$$a_1(t_s, t_f) = -\gamma (\partial_{t_s} A_0) t_f e^{-\frac{t_f}{2}} - 2i (g \sigma_0(t_s) - E) + A_1(t_s) e^{-\frac{t_f}{2}}, \quad (6.23)$$

where  $A_1(t_s)$  comes from the integration constant. Understanding which terms may be secular is not easy, here we will follow the definition of [33]. Secular terms are now found by the following condition: if they can become larger than a lower-order term, during the time evolution, they are secular and therefore should be eliminated. For this purpose, notice that in the solution of the  $\mathcal{O}(1/\kappa)$  Eq. (6.23) of  $a$  exists a term that is  $\propto t_f e^{-\frac{t_f}{2}}$ , which at some point might outweigh the simple decay given in the  $\mathcal{O}(1)$  part of Eq. (6.21), therefore we will have to remove this term by the condition

$$\partial_{t_s} A_0 = 0 \Leftrightarrow A_0(t_s) = a_0(0), \quad (6.24)$$

## 6. Method of Multiple Scales

where we already applied the initial conditions. With this, one obtains a full expression of the  $\mathcal{O}(1)$  solution of the cavity field operator

$$a_0(t) = a_0(0)e^{-\frac{\kappa}{2}t}. \quad (6.25)$$

If we wanted to obtain a full expression for the  $1/\kappa$ -term we would have to include a term of order  $1/\kappa^2$  in  $a$ . This will then give rise to secular terms, which determine the  $\mathcal{O}(1/\kappa)$  solution and therefore give an expression of  $A_1(t_s)$ . In general, the next higher-order term provides the necessary conditions to fully determine the term of the preceding order, therefore to obtain an approximation up to order  $1/\kappa^n$ , one must include terms up to order  $1/\kappa^{n+1}$ .

For higher-order terms, the equations of the two-level system and the cavity field become increasingly intertwined, increasing the complexity of following those steps and making them high in labor cost. But this is not the only reason why we discarded this technique in the end. One is the expansion in  $1/\kappa$  is only possible if  $\kappa$  is by far the largest value, but this is not necessarily the case, for example, terms like  $F_p$  of Eq. (3.1) are of order  $1/\kappa$  but might still be bigger than 1. Therefore, the underlying condition to truncate the expansion is not reasonable, as higher-order terms can be as relevant as lower-order terms.

In this chapter we only displayed how to solve the first order of  $a$ , we didn't display the result up to and including the order  $1/\kappa^2$  terms. The result of this is rather large and we do not want to outline it here, but we can have a look at the result in the long time limit, here as in the prodiabatic elimination we will assume  $\kappa t = t_f \gg 1$ . When we apply this long time limit to the expression of  $a$  up to and including the order  $1/\kappa^2$  we obtain

$$a = -\frac{2i}{\kappa} \left[ g \left( \left( 1 - \frac{\gamma}{\kappa} \right) \sigma_0(t_s) + \frac{1}{\kappa} \sigma_1(t_s) \right) - E \right], \quad (6.26)$$

notice that under the assumption of  $\gamma/\kappa \ll 1$  this expression would be the adiabatically eliminated cavity operator expanded up to order  $1/\kappa^2$ . This seems to be promising, but in reality this approximation of  $\sigma = \sigma_0 + \frac{1}{\kappa}\sigma_1$  is too low order in  $1/\kappa$  to capture the dynamics of the two-level system well, which will lead to errors happening quickly as soon as  $\kappa$  is not by far the largest parameter, as can be seen in Fig. 6.1.

## 6. Method of Multiple Scales

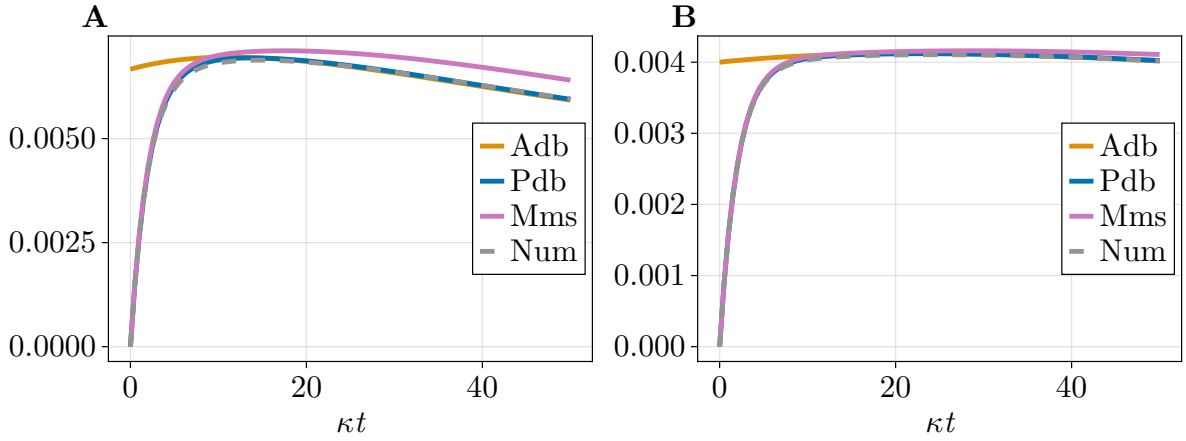


Figure 6.1.: Comparison between the different approximations on  $|\langle a \rangle|$ , the initial state is chosen to be the vacuum. In orange adiabatic elimination, blue prodiabatic elimination, pink method of multiple scales up to and including order  $1/\kappa^2$  (Mms) and in gray the full numerics. System values are chosen as  $\gamma/g = 1/2$  and  $E/g = 1/20$  and in **A**  $\kappa/g = 15$  and in **B**  $\kappa/g = 25$ .

In Fig. 6.1 we compare the method of multiple scales up to order  $1/\kappa^2$ , represented by the pink line, with the other approximations found in this thesis. For increasingly high  $\kappa$  it will align more with the numerics, but here we want to outline that we already use large  $\kappa$ . Since it is much more complicated and time-consuming to go through this sequence than it is to simply do the adiabatic or prodiabatic elimination, we do not consider this approach to have much merit. A possible way of improving this method is to consider more timescales and/or considering a different perturbation parameter.

## 7. Conclusion & Outlook

This thesis introduced the prodiabatic elimination, a novel method extending beyond the limitations of the adiabatic elimination in open quantum systems. By incorporating a systematic Taylor expansion, this approach allows for the inclusion of higher-order corrections and initial-state effects, providing an enhanced accuracy in the  $g^{(2)}$ -function and other observables. Compared to the adiabatic elimination, the prodiabatic elimination offers a more robust and versatile framework for solving the dynamics of a coupled cavity two-level system.

We introduced the prodiabatic elimination in Chap. 5, where we found that instead of using time-dependent operators, it is possible to find a master equation, describing the same dynamics. Further, for low drive strengths, it is possible to neglect the negative rate of the master equation, resulting in a simple Lindblad master equation that outperforms the adiabatic elimination and aligns well with the full prodiabatic elimination. Lastly, we found that the prodiabatic elimination outperformed the adiabatic elimination in describing the two-level dynamics, the cavity dynamics, steady-state values as well as the  $g^{(2)}(t)$ -function.

The method of multiple scales a standard singular perturbation method, seemed to offer similar capabilities as the prodiabatic elimination, but the complexity outweighs the advantages, as demonstrated in this works Chap. 6. In contrast, the prodiabatic elimination strikes a balance between computational simplicity and accuracy, making it a promising tool for future applications. We also explored alternative methods to approximate the dynamics, which are compiled and discussed in the appendix, see App. A.5.

While we successfully extended beyond the adiabatic elimination, several potential extensions to this work remain. Firstly, our results were tested on a single system. The adiabatic elimination is known for its general applicability, it is unclear whether the prodiabatic elimination will consistently outperform it in more complex systems. Testing the method on a broader range of systems with increased complexity represents a logical next step.

Additionally, incorporating higher-order terms into the prodiabatic elimination is currently not feasible in the same manner. Identifying the most efficient and generalizable method remains an open question.

Finally, comparing the prodiabatic elimination with real experimental measurements could provide valuable insights, since experimental data for the studied system already exists this should be a straightforward extension to this work [34].

# Bibliography

- [1] M. Aspelmeyer, T. J. Kippenberg, and F. Marquardt, “Cavity optomechanics,” *Rev. Mod. Phys.*, vol. 86, pp. 1391–1452, 4 Dec. 2014. [Online]. Available: <https://link.aps.org/doi/10.1103/RevModPhys.86.1391>.
- [2] A. Blais, A. L. Grimsmo, S. M. Girvin, and A. Wallraff, “Circuit quantum electrodynamics,” *Rev. Mod. Phys.*, vol. 93, p. 025 005, 2 May 2021. [Online]. Available: <https://link.aps.org/doi/10.1103/RevModPhys.93.025005>.
- [3] H. Mabuchi and A. Doherty, “Cavity quantum electrodynamics: Coherence in context,” *Science*, vol. 298, no. 5597, pp. 1372–1377, 2002.
- [4] P. Meystre, *Quantum Optics: Taming the Quantum*. Jan. 2021.
- [5] T. H. MAIMAN, “Stimulated optical radiation in ruby,” *Nature*, vol. 187, no. 4736, pp. 493–494, Aug. 1, 1960. [Online]. Available: <https://doi.org/10.1038/187493a0>.
- [6] A. L. Schawlow and C. H. Townes, “Infrared and optical masers,” *Phys. Rev.*, vol. 112, pp. 1940–1949, 6 Dec. 1958. [Online]. Available: <https://link.aps.org/doi/10.1103/PhysRev.112.1940>.
- [7] N. Tomm *et al.*, “A bright and fast source of coherent single photons,” *Nature Nanotechnology*, vol. 16, no. 4, pp. 399–403, 2021.
- [8] K. J. Vahala, “Optical microcavities,” *Nature*, vol. 424, no. 6950, pp. 839–846, Aug. 1, 2003. [Online]. Available: <https://doi.org/10.1038/nature01939>.
- [9] F. Vollmer and L. Yang, “Label-free detection with high-q microcavities: A review of biosensing mechanisms for integrated devices.” eng, *Nanophotonics*, vol. 1, no. 3-4, pp. 267–291, Dec. 1, 2012.
- [10] J. Zhu *et al.*, “On-chip single nanoparticle detection and sizing by mode splitting in an ultrahigh-q microresonator,” *Nature Photonics*, vol. 4, no. 1, pp. 46–49, Jan. 1, 2010. [Online]. Available: <https://doi.org/10.1038/nphoton.2009.237>.
- [11] R. J. Thompson, G. Rempe, and H. J. Kimble, “Observation of normal-mode splitting for an atom in an optical cavity,” *Phys. Rev. Lett.*, vol. 68, pp. 1132–1135, 8 Feb. 1992. [Online]. Available: <https://link.aps.org/doi/10.1103/PhysRevLett.68.1132>.
- [12] A. Wallraff *et al.*, “Strong coupling of a single photon to a superconducting qubit using circuit quantum electrodynamics,” *Nature*, vol. 431, no. 7005, pp. 162–167, Sep. 1, 2004. [Online]. Available: <https://doi.org/10.1038/nature02851>.
- [13] D. M. Meekhof, C. Monroe, B. E. King, W. M. Itano, and D. J. Wineland, “Generation of nonclassical motional states of a trapped atom,” *Phys. Rev. Lett.*, vol. 76, pp. 1796–1799, 11 Mar. 1996. [Online]. Available: <https://link.aps.org/doi/10.1103/PhysRevLett.76.1796>.
- [14] B.-W. Li *et al.*, “Observation of non-markovian spin dynamics in a jaynes-cummings-hubbard model using a trapped-ion quantum simulator,” *Phys. Rev. Lett.*, vol. 129, p. 140 501, 14 Sep. 2022. [Online]. Available: <https://link.aps.org/doi/10.1103/PhysRevLett.129.140501>.

## Bibliography

- [15] A. Dasgupta, “An analytically solvable time-dependent jaynes-cummings model,” *Journal of Optics B: Quantum and Semiclassical Optics*, vol. 1, no. 1, pp. 14–18, Jan. 1999. [Online]. Available: <http://dx.doi.org/10.1088/1464-4266/1/1/003>.
- [16] A. Pathak and A. Ghatak, “Classical light vs. nonclassical light: Characterizations and interesting applications,” *Journal of Electromagnetic Waves and Applications*, vol. 32, no. 2, pp. 229–264, Nov. 2017. [Online]. Available: <http://dx.doi.org/10.1080/09205071.2017.1398109>.
- [17] P. Rice and H. Carmichael, “Single-atom cavity-enhanced absorption. i. photon statistics in the bad-cavity limit,” *IEEE Journal of Quantum Electronics*, vol. 24, no. 7, pp. 1351–1366, 1988.
- [18] P. Meystre and M. SargentIII, *Elements of Quantum Optics*. Jan. 2007.
- [19] M. Fox, *Quantum Optics: An Introduction*. Oxford University Press, Apr. 2006. [Online]. Available: <https://doi.org/10.1093/oso/9780198566724.001.0001>.
- [20] B. W. Shore and P. L. Knight, “The jaynes-cummings model,” *Journal of Modern Optics*, vol. 40, no. 7, pp. 1195–1238, 1993. [Online]. Available: <https://doi.org/10.1080/09500349314551321>.
- [21] C.-H. Huang, Y.-H. Wen, and Y.-W. Liu, “Measuring the second order correlation function and the coherence time using random phase modulation,” *Opt. Express*, vol. 24, no. 4, pp. 4278–4288, Feb. 2016. [Online]. Available: <https://opg.optica.org/oe/abstract.cfm?URI=oe-24-4-4278>.
- [22] J. Bezanson, A. Edelman, S. Karpinski, and V. B. Shah, “Julia: A fresh approach to numerical computing,” *SIAM Review*, vol. 59, no. 1, pp. 65–98, 2017. [Online]. Available: <https://epubs.siam.org/doi/10.1137/141000671>.
- [23] S. Krämer, D. Plankensteiner, L. Ostermann, and H. Ritsch, “Quantumoptics.jl: A julia framework for simulating open quantum systems,” *Computer Physics Communications*, vol. 227, pp. 109–116, 2018.
- [24] S. Danisch and J. Krumbiegel, “Makie.jl: Flexible high-performance data visualization for Julia,” *Journal of Open Source Software*, vol. 6, no. 65, p. 3349, 2021. [Online]. Available: <https://doi.org/10.21105/joss.03349>.
- [25] B. Wong, “Points of view: Color blindness,” *Nature Methods*, vol. 8, no. 6, pp. 441–441, Jun. 1, 2011. [Online]. Available: <https://doi.org/10.1038/nmeth.1618>.
- [26] B. Wong, “Color coding,” *Nature Methods*, vol. 7, no. 8, pp. 573–573, Aug. 1, 2010. [Online]. Available: <https://doi.org/10.1038/nmeth0810-573>.
- [27] J. Feist and contributors, *QuantumAlgebra.jl*, version v1.1.0, Sep. 2021. [Online]. Available: <https://github.com/jfeist/QuantumAlgebra.jl>.
- [28] W. R. Inc., *Mathematica, Version 13.1*, Champaign, IL, 2024. [Online]. Available: <https://www.wolfram.com/mathematica>.
- [29] M. Sanz, E. Solano, and Í. L. Egusquiza, “Beyond adiabatic elimination: Effective hamiltonians and singular perturbation,” in *Applications + Practical Conceptualization + Mathematics = fruitful Innovation*, R. S. Anderssen *et al.*, Eds., Tokyo: Springer Japan, 2016, pp. 127–142.
- [30] S. Khan, B. K. Agarwalla, and S. Jain, “Quantum regression theorem for multi-time correlators: A detailed analysis in the heisenberg picture,” *Physical Review A*, vol. 106, no. 2, Aug. 2022. [Online]. Available: <http://dx.doi.org/10.1103/PhysRevA.106.022214>.

## Bibliography

- [31] S. H. Strogatz, *Nonlinear Dynamics and Chaos: With Applications to Physics, Biology, Chemistry and Engineering*. Westview Press, 2000.
- [32] C. M. Bender and S. A. Orszag, *Advanced Mathematical Methods for Scientists and Engineers*. McGraw-Hill, 1978.
- [33] A. H. Nayfeh, *Introduction to perturbation techniques* (Wiley classics library), eng. New York: J. Wiley & Sons, 1993.
- [34] N. Tomm *et al.*, “Realization of a coherent and efficient one-dimensional atom,” *Phys. Rev. Lett.*, vol. 133, p. 083 602, 8 Aug. 2024. [Online]. Available: <https://link.aps.org/doi/10.1103/PhysRevLett.133.083602>.
- [35] L. Ermann, G. G. Carlo, A. D. Chepelianskii, and D. L. Shepelyansky, “Jaynes-cummings model under monochromatic driving,” *Phys. Rev. A*, vol. 102, p. 033 729, 3 Sep. 2020. [Online]. Available: <https://link.aps.org/doi/10.1103/PhysRevA.102.033729>.
- [36] H.-P. Breuer and F. Petruccione, *The Theory of Open Quantum Systems*. Oxford University Press, Jan. 2007. [Online]. Available: <https://doi.org/10.1093/acprof:oso/9780199213900.001.0001>.

# A. Appendix

## A.1. Rotating Frame

In this section, we introduce the concept of moving into a rotating frame, a common technique used to simplify problems with time dependencies in the Hamiltonian. Usually one uses this technique to make a drive term time independent. The idea behind the rotating frame is to follow the time dependence by a reference frame that rotates at the same frequency as the drive. When we observe the system from this new perspective, the drive's time dependency is gone. This transformation simplifies our analysis, as it allows us to study the dynamics without the added complication of a time-dependent drive term. However, transitioning to a rotating frame involves more than just changing the state representation. Since we are viewing the system from a new reference frame, we must also adjust the Lindblad master equation to accurately describe the dynamics for this frame. For this consider the Lindblad master equation

$$\frac{d}{dt}\rho = -i[H, \rho] + \sum_i \kappa_i \mathcal{D}[L_i]\rho, \quad (\text{A.1})$$

where  $\rho$  is the state at question,  $H$  the Hamiltonian and  $L_i$  are some Lindblad jump operators with rate  $\kappa_i$ . Now we introduce a unitary operator  $R(t)$ , also named the rotating operator, which moves us into the rotating frame. In the rotating frame, the time dynamics are given by

$$\frac{d}{dt}(\rho') = \frac{d}{dt}(R\rho R^\dagger) = \dot{R}R^\dagger\rho' + \rho'R\dot{R}^\dagger - i[RHR^\dagger, \rho'] + \sum_i \kappa_i \mathcal{D}[RL_iR^\dagger]\rho', \quad (\text{A.2})$$

where we used the shorthand notation  $R(t) = R$  and used the unitarity of  $R$  multiple times. We also identified the density matrix in the rotating frame by  $\rho' = R\rho R^\dagger$ . In the context of the Jaynes-Cummings model, the rotating operator is given by

$$R(t) = e^{i\omega_d(a^\dagger a + \sigma^\dagger \sigma)t}, \quad (\text{A.3})$$

where  $\omega_d$  is the drive frequency. With this form of the rotating operator, notice that we obtain the identities

$$RaR^\dagger = ae^{-i\omega_d t} \quad (\text{A.4}) \quad R\sigma R^\dagger = \sigma e^{-i\omega_d t}. \quad (\text{A.5})$$

Using these identities, one can compute the new time dynamics in a simple fashion. The resulting master equation of this rotating frame is given by Eq. (3.16). More detailed information as well as the full derivation can be found in [35].

## A.2. Analysis of Exponential Matrix of Adiabatic Elimination

In this section, we want to further investigate the two-level dynamics of the adiabatic elimination. Assuming the drive to be on resonance  $\Delta_c = \Delta_d = 0$  we will take a look at the eigenvalues of the matrix  $A$ , where  $A$  is given by Eq. (4.9). The eigenvalues give us insight into the two-level

## A. Appendix

dynamics in the context of the adiabatic elimination since if  $A$  is diagonalizable by a transition matrix  $A_{diag} = S^{-1}AS$ , we can write the solution as

$$\vec{v}(t) = e^{At}\vec{v}(0) = Se^{S^{-1}Ast}S^{-1}\vec{v}(0) = Se^{A_{diag}t}S^{-1}\vec{v}(0). \quad (\text{A.6})$$

Given the eigenvalues of  $A$ , which are the diagonal components of  $A_{diag}$  we can therefore find important properties of the dynamics. The eigenvalues read

$$\lambda_0 = 0 \quad (\text{A.7})$$

$$\lambda_1 = -\frac{\gamma}{2} - \frac{2g^2}{\kappa} \quad (\text{A.8})$$

$$\lambda_{2,3} = -\frac{3\gamma\kappa + 12g^2 \pm \sqrt{(\gamma\kappa + 4g^2)^2 - 256g^2\kappa\epsilon^2}}{4\kappa}, \quad (\text{A.9})$$

where now the first eigenvalue  $\lambda_0$  just comes from the fact that we include the differential equation of the identity in the vector  $\vec{v}(0)$ , see Eq. (4.10) and any constant will not evolve in time.  $\lambda_1$  also has a rather straightforward interpretation as it is simply proportional to the enhanced decay rate of the two-level system. Further, we are interested in  $\lambda_3$ , which might become positive inducing exponential growth instead of decay, leading to an unphysical phenomenon. But the maximal value this term can take is

$$\lambda_3 = -\frac{\gamma\kappa + 4g^2}{2\kappa} = \lambda_1, \quad (\text{A.10})$$

which is always negative, achieving it is possible by  $\epsilon = 0$ . So we are always ensured to get a decay, which then gives us finite steady-state expectation values.

Another consideration is if our eigenvalues  $\lambda_{2,3}$  can have imaginary parts, which would mean that we end up with oscillations in the two-level operator expectation values. Achieving this is simple, one needs to adjust the drive to exceed a critical value defined by the inequality

$$\frac{\epsilon}{\sqrt{\kappa}} > \frac{\gamma\kappa + 4g^2}{16\kappa g}. \quad (\text{A.11})$$

### A.3. $g^{(2)}(0)$ -Function in the Adiabatic Elimination

For this section, we aim to find steady state representations of the  $g^{(2)}$ -function, which is equivalent to  $g^{(2)}(0)$ , by doing this we will also find a way to find general steady-state expectation values, in the framework of the adiabatic elimination. It is enough to look at the adiabatic eliminated equations of motion, given by Eqs. (4.7) and (4.8). For which we assume steady-state conditions, which eliminates all derivatives

$$0 = -\frac{2g\epsilon t_c}{\sqrt{\kappa}}\sigma_z - \left(\frac{2g^2 t_c}{\kappa} + \frac{\gamma}{2} + i\Delta_d\right)\sigma \quad (\text{A.12})$$

$$0 = -\left(\frac{4g^2}{\kappa} \text{Re}\{t_c\} + \gamma\right)(\sigma_z + \mathbb{1}) + \frac{4g\epsilon}{\sqrt{\kappa}}(t_c^*\sigma + t_c\sigma^\dagger), \quad (\text{A.13})$$

where this linear system of equations is solved by

$$\sigma_{ss} = \frac{4g\sqrt{\kappa}t_c\epsilon(4g^2 t_c^* + \kappa(\gamma - 2i\Delta_d))}{\kappa^2(\gamma^2 + 4\Delta_d^2) + 8g^2(2|t_c|^2(g^2 + 2\kappa\epsilon^2) + \kappa(2\Delta_d \text{Im}\{t_c\}) + \gamma \text{Re}\{t_c\})} \mathbb{1} \quad (\text{A.14})$$

$$\sigma_{z,ss} = -\frac{4g^2 t_c + \kappa(\gamma + 2i\Delta_d)}{4g\epsilon\sqrt{\kappa}t_c} \sigma_{ss}, \quad (\text{A.15})$$

## A. Appendix

where the subscript  $\bullet_{ss}$  indicated the steady state representation of the operator.

One could be confused as to why our operators became proportional to an identity, this is rather counterintuitive but makes sense. Remember for an operator  $A$  and an arbitrary state  $\rho$  we always have the condition

$$\text{tr}\{A_{ss}\rho\} = \langle A \rangle_{ss} . \quad (\text{A.16})$$

This property must be independent of the choice of  $\rho$  since we know that we will have a unique steady state independent of the initial conditions. Further, if  $A_{ss}$  is simply proportional to an identity operator  $c\mathbb{1}$ , where  $c$  is a constant

$$\langle A \rangle_{ss} = \text{tr}\{A_{ss}\rho\} = \text{tr}\{\rho\}c = c , \quad (\text{A.17})$$

and therefore  $A_{ss} = \langle A \rangle_{ss} \mathbb{1}$ . It is important to note, that this is not a proof of this property but makes the earlier result more understandable. The steady-state values may depend on the initial state, in those cases, this property cannot be true. Since this representation will always give the same steady-state expectations values, independent of the state  $\rho$ . In our case this is a true statement, therefore making the results reasonable.

For simplicity, we will now also assume the drive to be on resonance to the cavity and two-level system  $t_c = 1$  and  $\Delta_d = 0$ , which simplifies our steady state values to

$$\langle \sigma \rangle_{ss} = \frac{4g\sqrt{\kappa}\epsilon(4g^2 + \kappa\gamma)}{(\gamma\kappa + 4g^2)^2 + 32g^2\kappa\epsilon^2} \quad (\text{A.18})$$

$$\langle \sigma_z \rangle_{ss} = -1 + \frac{32g^2\kappa\epsilon^2}{(\gamma\kappa + 4g^2)^2 + 32g^2\kappa\epsilon^2} . \quad (\text{A.19})$$

Since our final goal is to find an expression for  $\langle a^\dagger a^\dagger a a \rangle_{ss}$  and  $\langle a^\dagger a \rangle_{ss}$  in the steady state case, we now replace each  $a$  by  $a_{adb}$  and use the known commutation relations of the two-level operators. This leads to

$$\langle a^\dagger a^\dagger a a \rangle_{ss} = \left(\frac{2}{\kappa}\right)^4 \left(2g^2\epsilon^2\kappa(\langle \sigma_z \rangle_{ss} + 1) - 2g\epsilon^3\kappa^{\frac{3}{2}}(\langle \sigma \rangle_{ss} + \langle \sigma^\dagger \rangle_{ss}) + \epsilon^4\kappa^2\right) \quad (\text{A.20})$$

$$\langle a^\dagger a \rangle_{ss} = \left(\frac{2}{\kappa}\right)^2 \left(\frac{g^2}{2}(\langle \sigma_z \rangle_{ss} + 1) - g\epsilon\sqrt{\kappa}(\langle \sigma \rangle_{ss} + \langle \sigma^\dagger \rangle_{ss}) + \epsilon^2\kappa\right) , \quad (\text{A.21})$$

which we can compute by simply plugging in the steady-state expressions of the two-level system operators

$$\langle a^\dagger a^\dagger a a \rangle_{ss} = \frac{16\epsilon^4}{\kappa^2} \left(\frac{(\gamma\kappa - 4g^2)^2 + 32g^2\kappa\epsilon^2}{(\gamma\kappa + 4g^2)^2 + 32g^2\kappa\epsilon^2}\right) \quad (\text{A.22})$$

$$\langle a^\dagger a \rangle_{ss} = \frac{4\epsilon^2(\gamma^2\kappa + 32g^2\epsilon^2)}{(\gamma\kappa + 4g^2)^2 + 32g^2\kappa\epsilon^2} , \quad (\text{A.23})$$

which one can already use in order to compare this result to numerical simulations of the system. One may ask why we are doing this, since until now it looks like we did not use any assumptions except for steady-state conditions, so it looks like we still have an exact expression, but this is not true. To obtain an expression of, for example,  $\langle a^\dagger a \rangle_{ss}$ , we assumed that it is correct to replace  $a$  by  $a_{adb}$ . But we know from Sec. 3.2 that  $a^\dagger(t)a(t) \neq (a^\dagger a)(t)$  which will also cause an inaccuracy for the steady state, we further outlined this behavior in Sec. 4.4. For the numerical comparison, we will be using the  $g^{(2)}$ -function at time 0, which means we want to evaluate

$$g^{(2)}(0) = \frac{\langle a^\dagger a^\dagger a a \rangle_{ss}}{\langle a^\dagger a \rangle_{ss}^2} , \quad (\text{A.24})$$

## A. Appendix

where we found an expression for all parts of this equation in Eqs. (A.22) and (A.23), plugging in these values equates to

$$g^{(2)}(0) = \frac{\left((\gamma\kappa - 4g^2)^2 + 32g^2\kappa\epsilon^2\right) \left((\gamma\kappa + 4g^2)^2 + 32g^2\kappa\epsilon^2\right)}{\kappa^2 (\gamma^2\kappa + 32g^2\epsilon^2)^2}. \quad (\text{A.25})$$

In Fig. A.1 we can see that the adiabatic elimination gives a very good estimation of the  $g^{(2)}$ -function at time 0, but we can also see that there is a mismatch for low values of  $\kappa$ . This mismatch was further explained in Sec. 4.4.

### A.3.1. Low Drive Expansions of $g^{(2)}(0)$ -Function

For this subsection, we focus on finding the earlier discussed  $g^{(2)}(0)$ , but we neglect terms of order  $\mathcal{O}(\epsilon^2)$  or higher, this will lead to a more simple expression of  $g^{(2)}(0)$ . We first find

$$\langle\sigma\rangle_{ss} = \frac{4g\sqrt{\kappa}\epsilon}{\gamma\kappa + 4g^2} + \mathcal{O}(\epsilon^3) \quad (\text{A.26})$$

$$\langle\sigma_z\rangle_{ss} = -1 + \frac{32g^2\kappa\epsilon^2}{(\gamma\kappa + 4g^2)^2} + \mathcal{O}(\epsilon^3), \quad (\text{A.27})$$

now using those expressions in Eqs. (A.20) and (A.21) we find a form of the  $g^{(2)}(0)$ -function in the low drive limit

$$g_{ss}^{(2)}(0) = \frac{(\gamma^2\kappa^2 - 16g^4)^2}{\gamma^4\kappa^4} = \frac{(1 - 2\beta)^2}{(1 - \beta)^4}, \quad (\text{A.28})$$

where we used the parameter  $\beta$ , given by Eq. (3.4).

## A. Appendix

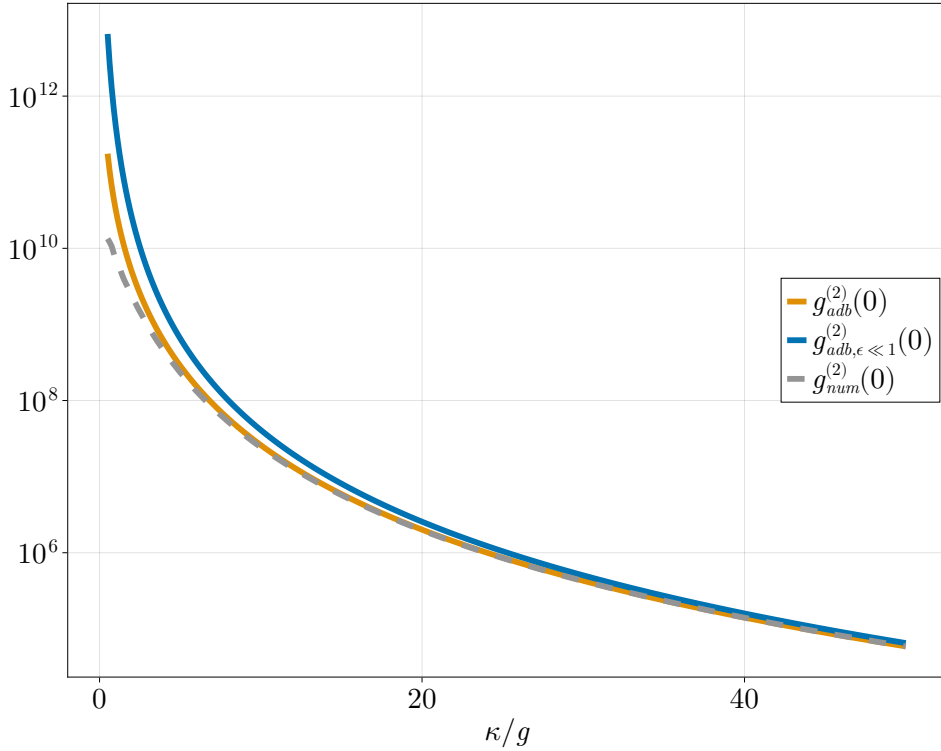


Figure A.1.: Comparison between exact numerical  $g^{(2)}(0)$  (dashed and gray) and the one obtained by the adiabatic elimination (orange) and the low drive expansion (blue) as a function of  $\kappa$  on a  $\log_{10}$ -scale. System values are chosen as  $\gamma/g = 1/200$  and  $\epsilon/\sqrt{g} = 2/1000\sqrt{2}$ .

In Fig. A.1 it is observable that for bigger  $\kappa$  the agreement between the approximations and the numerics is increased, hinting the fact that the approximation seems to get better if  $\kappa$  is big, which aligns with the results of [17].

### A.4. Derivation of the Master Equation for the Prodiabatic Elimination

For this section, we want to find an LME that will reproduce the dynamics given by Eqs. (5.14) and (5.15). In Chap. 4 it was possible to guess the master equation based on what we expect to happen in the two-level system. For us, it was not possible to guess an LME in the prodiabatic case, but one can still find a master equation (ME) as we will show in the following. Note that we found a ME not a LME, this is because one of the rates turns out to be negative. We will mostly rely on [36] for the whole derivation.

We start by defining a set of operators  $F_i$ , which are orthogonal with respect to the Hilbert-Schmidt inner product

$$\text{tr}\{F_i^\dagger F_j\} = \delta_{i,j}, \quad (\text{A.29})$$

which is done in our case by

$$F_1 = \sigma \quad (\text{A.30})$$

$$F_2 = \sigma^\dagger \quad (\text{A.31})$$

$$F_3 = \frac{1}{\sqrt{2}}\sigma_z, \quad (\text{A.32})$$

## A. Appendix

Next we define the general form of the generator

$$\dot{\rho} = -i[H, \rho] + \sum_{i,j=1}^3 c_{ij} \left( F_i \rho_S F_j^\dagger - \frac{1}{2} \{ F_j^\dagger F_i, \rho \} \right), \quad (\text{A.33})$$

where the Hamiltonian  $H$ , as well as the  $3 \times 3$  matrix  $c$ , are so far unknowns [36]. Using Eq. (A.33) we can derive an expression of  $\dot{A}$  for an arbitrary operator  $A$

$$\dot{A} = -i[A, H] + \sum_{i,j=1}^2 c_{ij} \left( F_j^\dagger A F_i - \frac{1}{2} \{ F_j^\dagger F_i, A \} \right), \quad (\text{A.34})$$

the derivation of this equation works in the same way as for Eq. (3.18). Based on this we derive the equations of motion of  $\sigma$  and  $\sigma_z$  and further set them equal to Eqs. (5.14) and (5.15). This step will eliminate a few unknowns, but because we have a total of 8 equations from this but 9 unknowns in  $c$  and a further 4 from  $H$  we do not expect a definite solution from this. By doing these steps we find

$$H = \begin{pmatrix} H_1 & \frac{2ig\kappa^{3/2}\epsilon(2g^2+\kappa^2)}{\kappa^4-16g^4} \\ -\frac{2ig\kappa^{3/2}\epsilon(2g^2+\kappa^2)}{\kappa^4-16g^4} & H_2 \end{pmatrix}, \quad (\text{A.35})$$

as well as

$$c = \begin{pmatrix} \frac{\kappa(\gamma\kappa+4g^2)}{\kappa^2-4g^2} & a_{12} & \frac{-8\sqrt{2}g^3\kappa^{3/2}\epsilon+a_{32}(\kappa^4-16g^4)}{16g^4-\kappa^4} \\ 0 & 0 & 0 \\ -\frac{8\sqrt{2}g^3\kappa^{3/2}\epsilon}{16g^4-\kappa^4} & a_{32} & -i(H_1 - H_2) \end{pmatrix}, \quad (\text{A.36})$$

but in order to arrive at a ME one requires that  $c$  is diagonalizable by a unitary  $U$  such that  $UcU^\dagger = c_{diag.}$ , where  $c_{diag.}$  the matrix with the eigenvalues  $\gamma_i$  of  $c$  on the diagonal [36]. From linear algebra, we know that a matrix is diagonalizable by a unitary if and only if it is normal, therefore we have to require that

$$cc^\dagger = c^\dagger c, \quad (\text{A.37})$$

which will result in  $H_1 = H_2$  and  $a_{12} = a_{32} = 0$ , but since  $H_1 = H_2$  is nothing but a constant shift to the Hamiltonian we set it to zero  $H_1 = H_2 = 0$ . Finding the unitary  $U$  is straightforward as this is just the matrix consisting of the normalized eigenvectors of  $c$  in each row. Now we will define a new set of operators  $A_i$  through

$$F_i = \sum_{k=1}^3 U_{ki} A_k, \quad (\text{A.38})$$

where the index indicates the  $k, i$  element of the matrix  $U$  [36]. It is important to note that this is not a normal matrix multiplication; instead, it will run over the column instead of the rows. This can be interpreted as applying the transposed matrix. By identifying the vectors

$$\vec{F} = (F_1, F_2, F_3) \quad (\text{A.39}) \quad \vec{A} = (A_1, A_2, A_3), \quad (\text{A.40})$$

we can derive a simple expression for the  $A_i$  operators by

$$\vec{A} = U^* \vec{F}, \quad (\text{A.41})$$

where  $U^*$  is the complex conjugated matrix  $U$ . Using  $A_i$  we can find the diagonal form of the ME by

$$\dot{\rho} = -i[H, \rho] + \sum_{i=1}^3 \gamma_i \left( A_i \rho_S A_i^\dagger - \frac{1}{2} \{ A_i^\dagger A_i, \rho \} \right) = -i[H, \rho] + \sum_{i=1}^3 \gamma_i \mathcal{D}[A_i] \rho, \quad (\text{A.42})$$

## A. Appendix

where  $\gamma_i$  is the corresponding eigenvalue of  $c$ .

Applying these steps we obtain the Hamiltonian

$$H = -\frac{ig\epsilon}{\sqrt{\kappa}} \left( \frac{2 + \frac{\gamma}{\kappa} F_p}{1 - \left(\frac{\gamma}{\kappa} F_p\right)^2} \right) (\sigma - \sigma^\dagger), \quad (\text{A.43})$$

and the rates

$$\gamma_{1,2} = \frac{\gamma(1 + F_p)(1 + \frac{\gamma}{\kappa} F_p) \pm \sqrt{\frac{8\epsilon^2 \gamma F_p^3}{\kappa^2} + (1 + F_p)^2 (1 + \frac{\gamma}{\kappa} F_p)^2}}{1 - \left(\frac{\gamma}{\kappa} F_p\right)^2}, \quad (\text{A.44})$$

where  $F_p$  is given by Eq. (3.1). There exists a third rate but since it is 0 it will not affect the dynamics and can be disregarded. Further, we define the variables

$$J_{1,2} = \frac{\left(1 - \left(\frac{\gamma}{\kappa} F_p\right)^2\right) \kappa^{1/2}}{2\sqrt{2} \left(\frac{\gamma}{\kappa} F_p\right) g\epsilon} \gamma_{1,2} \quad (\text{A.45})$$

$$1/N_{1,2} = \sqrt{1 + J_{1,2}^2}, \quad (\text{A.46})$$

which then gives us an expression of the  $A_i$  by

$$A_i = \frac{1}{N_i} \left( J_i \sigma + \frac{1}{\sqrt{2}} \sigma_z \right), \quad (\text{A.47})$$

putting everything together the ME reads

$$\dot{\rho} = -i[H, \rho] + \gamma_1 \mathcal{D} \left[ \frac{1}{N_1} \left( J_1 \sigma + \frac{1}{\sqrt{2}} \sigma_z \right) \right] \rho + \gamma_2 \mathcal{D} \left[ \frac{1}{N_2} \left( J_2 \sigma + \frac{1}{\sqrt{2}} \sigma_z \right) \right] \rho, \quad (\text{A.48})$$

which will reproduce the results obtained from the prodiabatic elimination. We can simplify this result by pulling out the constants of the dissipator and by further writing everything with respect to  $\gamma_{1,2}$  we obtain

$$\dot{\rho} = -i[H, \rho] + \sum_{i=1,2} \frac{\gamma_i}{1 + 2\epsilon^2 \kappa \frac{\frac{\gamma^3 F_p^3}{\kappa^3}}{(1 - \frac{\gamma^2 F_p^2}{\kappa^2})^2 \gamma_i^2}} \mathcal{D} \left[ \sigma + \frac{2 \left(\frac{\gamma}{\kappa} F_p\right) g\epsilon}{\left(1 - \left(\frac{\gamma}{\kappa} F_p\right)^2\right) \kappa^{1/2} \gamma_i} \sigma_z \right] \rho. \quad (\text{A.49})$$

It is important to note that  $\gamma_2$  is always negative (under  $\kappa > 2g$  assumption), this is because the numerator is of the form  $x - \sqrt{y + x^2}$ , where both  $x$  and  $y$  are positive. Because  $y$  is positive  $\sqrt{y + x^2}$  will be strictly bigger than  $x$ , making the rate always negative. Note that the denominator of  $\gamma_2$  is positive as long as  $\kappa > 2g$  holds. The negative rate implies that the ME does not model physical states, as well as resulting in a time evolution that is not trace-preserving or completely positive. Under the assumption that  $F_p$  is of order 1 in  $\kappa$ , the leading order term of  $\gamma_2$  is of order  $1/\kappa^2$ , therefore we conclude that the effect of this rate is minimal and it can be disregarded without a big loss of precision. Without assuming  $F_p$  to be of order 1 the leading order term is proportional to  $1/\kappa^5$ , leading to the same conclusion. For this term to have a significant effect, one would need  $\kappa$  to be close to  $2g$  as well as a large drive, both of which are far from the bad cavity limit, which we will usually not consider since then the whole point of having a fast adapting cavity breaks down, a more detailed discussion of the master equation can be found in Sec. 5.2.1.

## A.5. Additional Notable Methods

In this section, we aim to provide a brief overview of several alternative approaches explored during the development of this thesis. Rather than delving into detailed derivations, we focus on describing the core ideas behind these methods and offering a general understanding of their functionality.

### A.5.1. Low Photon Number Elimination

This technique is quite simple, here we will assume that the total photon number in the system is so small that we are able to approximate  $\sigma_z a \approx -a$ , this decouples Eqs. (4.1) and (4.2) to

$$\dot{a} = -\left(i\Delta_c + \frac{\kappa}{2}\right)a - ig\sigma + i\epsilon\sqrt{\kappa} \quad (\text{A.50})$$

$$\dot{\sigma} = -\left(i\Delta_d + \frac{\gamma}{2}\right)\sigma - iga \quad (\text{A.51})$$

therefore making a solution obtainable straightforwardly. The approximation of  $\sigma_z a = -a$  is very simple and is able to obtain good results as long as the drive is low compared to the dissipation, which makes the assumption of a low photon number reasonable. However, the condition of a low photon number is a bit restrictive.

Applying the same assumption to the prodiabatic elimination in Eq. (5.10), we replace the term proportional to  $\sigma_z a$  by  $-a$ . This eliminates the need to invert operators, as the equations of motion become immediately linearized. Under this assumption, the prodiabatic elimination can be computed to any desired order but is limited by the assumption of a low photon number.

### A.5.2. Boundary Layer Theory

In addition to the method of multiple scales, we also explored boundary layer theory, another approach within the framework of singular perturbation techniques. Boundary layer theory aims to bridge the long-time behavior, as described by the adiabatic elimination, with the short-time dynamics. The primary reference for this method is [32]. While boundary layer theory successfully incorporates the initial conditions into the solution, it is unable to extend beyond the results achieved through adiabatic elimination. The form of the cavity field operator results in

$$a(t) = a(0)e^{-\frac{\kappa}{2}t} + \frac{2i}{\kappa}(g\sigma(0) - E)e^{-\frac{\kappa}{2}t} - \frac{2i}{\kappa}(g\sigma(t) - E), \quad (\text{A.52})$$

where the  $\sigma(t)$  in the expression is given by the adiabatic elimination and again we replace the total drive strength by  $\epsilon\sqrt{\kappa} \rightarrow E$ . This approach gives rather nice results but has the problem of not going beyond the adiabatic elimination, it simply connects a solution in short-time behavior to the long-time one. Further if one would use something related to the steady state, for example, the photon reduces steady-state of Eq. (4.17), as the initial state, the method would expect that we can use the adiabatic elimination to approximate  $a(0)$  as  $a(0) = -\frac{2i}{\kappa}(g\sigma(0) - E)$ . But in this case, note that we would end up with  $a(t) = -\frac{2i}{\kappa}(g\sigma(t) - E)$ , which is the adiabatic elimination. So for an initial state related to the steady state, the method will give analogous results to the adiabatic elimination. Therefore it will not result in a different approximation of the  $g^{(2)}$ -function, which of course is a shortcoming if we want to go beyond adiabatic elimination.



## Erklärung zur wissenschaftlichen Redlichkeit und Veröffentlichung der Arbeit (beinhaltet Erklärung zu Plagiat und Betrug)

Titel der Arbeit: The Prodiabatic Elimination: A Method Beyond the Adiabatic Elimination

Name Beurteiler\*in: Patrick P. Potts

Name Student\*in: Jan Neuser

Matrikelnummer: 19-056-373

Ich bezeuge mit meiner Unterschrift, dass ich meine Arbeit selbständig ohne fremde Hilfe verfasst habe und meine Angaben über die bei der Abfassung meiner Arbeit benützten Quellen in jeder Hinsicht der Wahrheit entsprechen und vollständig sind. Alle Quellen, die wörtlich oder sinngemäss übernommen wurden, habe ich als solche gekennzeichnet.

Des Weiteren versichere ich, sämtliche Textpassagen, die unter Zuhilfenahme KI-gestützter Programme verfasst wurden, entsprechend gekennzeichnet sowie mit einem Hinweis auf das verwendete KI-gestützte Programm versehen zu haben.

Eine Überprüfung der Arbeit auf Plagiate und KI-gestützte Programme – unter Einsatz entsprechender Software – darf vorgenommen werden. Ich habe zur Kenntnis genommen, dass unlauteres Verhalten zu einer Bewertung der betroffenen Arbeit mit einer Note 1 oder mit «nicht bestanden» bzw. «fail» oder zum Ausschluss vom Studium führen kann.

Ort, Datum: Basel 28.02.25 Student\*in: Jan Neuser

Wird diese Arbeit oder Teile davon veröffentlicht?

Nein

Ja. Mit meiner Unterschrift bestätige ich, dass ich mit einer Veröffentlichung der Arbeit (print/digital) in der Bibliothek, auf der Forschungsdatenbank der Universität Basel und/oder auf dem Dokumentenserver des Departements / des Fachbereichs einverstanden bin. Ebenso bin ich mit dem bibliographischen Nachweis im Katalog SLSP (Swiss Library Service Platform) einverstanden. (nicht Zutreffendes streichen)

Veröffentlichung ab: 28.02.25

Ort, Datum: Basel 28.02.25 Student\*in: Jan Neuser

Ort, Datum: Basel 28.02.25 Beurteiler\*in: P. Potts

*Diese Erklärung ist in die Bachelor-, resp. Masterarbeit einzufügen.*